Quantum resonances in the valence bands of germanium. II. Cyclotron resonances in uniaxially stressed crystals

J. C. Hensel and K. Suzuki*
Bell Laboratories, Murray Hill, New Jersey 07974
(Received 17 July 1973)

As a consequence of the degeneracy of the Ge valence bands at $\vec{k} = 0$, the lowest Landau levels are anomalously spaced, so the cyclotron resonances of holes under "quantum" conditions, $\hbar\omega/k\Theta > 1$ (Θ being the temperature), give rise to complex line spectra. We report here measurements of these "quantum" spectra taken at 53 GHz and 1.2°K in samples of Ge subjected to uniaxial, compressive stresses which lower the cubic symmetry and remove the valence-band degeneracy. The effect of the stress T on the positions of the quantum lines permits their identification and also provides a direct measurement of the uniaxial deformation potentials: $D_u = 3.32 \pm 0.20$ eV and $D_u' = 3.81 \pm 0.25$ eV. At large stresses, as the energy surfaces assume ellipsoidal shape, the quantum lines arrange themselves into four line series identifiable by $M_J = \pm (1/2), \pm (3/2)$ for $T \parallel [001]$ and $T \parallel [111]$. With increasing stress the lines converge to two series limits corresponding to the "classical" effective masses of the two split bands, $|M_J| = (1/2), (3/2)$. For stress along each of the principal crystallographic directions—[001], [111], and [110]—the positions of two quantum lines, the "fundamental" transitions, are approximately invariant under stress and lie one at each series limit. From measurements of these extremely sharp lines in the geometry $\vec{H}_0 \parallel T$ we have determined the valence-band inverse-mass parameters to a "spectroscopic" precision: $\gamma_1 = 13.38 \pm 0.02$, $\gamma_2 = 4.24 \pm 0.03$, and $\gamma_3 = 5.69 \pm 0.02$. Less detailed but corroborative experiments were also done in the geometry $\vec{H}_0 \perp T$. From the measurements for $T \parallel [110]$ we read out directly the ratio of the deformation potentials, $D_u'/D_u = 1.15 \pm 0.02$. The strain interaction between the valence band edge and the spin-orbit–split-off valence-band results in a small linear shift of the fundamental transitions. Surprisingly, the deformation potentials, $D_w = 2.31 \pm 0.17$ eV and $D_w' = 2.81 \pm 0.20$ eV, measured from this interaction are significantly smaller than those given above which were measured directly from the gross strain decoupling of the valence bands. The difference is ascribed to the existence of *spin-dependent* deformation potentials which contribute differently to the two processes. The quantum-resonance line shapes are governed largely by strain and k_H broadening; however, for the narrowest lines, viz., the fundamental transitions, relaxation-time effects are in evidence and have been briefly investigated.

I. INTRODUCTION

The cyclotron resonance of holes in the degenerate valence band edge of Ge becomes anomalous at low temperatures and high magnetic fields. As pointed out by Luttinger and Kohn,[1,2] the spacings between Landau levels bearing low quantum numbers deviate considerably from the uniform intervals between the higher "classical" levels. Thus, when the anomalous lower states are preferentially populated under the above-defined "quantum" conditions, cyclotron-resonance spectra of exceptional complexity are observed,[3-6] whose interpretation presents a formidable challenge.[7-9]

In fact, our experience shows that it is virtually impossible to unravel spectra of this kind without having either a sure means to identify the lines or a precisely measured set of band parameters which would allow one to compute unambiguous theoretical fits to the spectra. The key, we find, to deciphering the quantum spectra[10] of Ge is the use of uniaxial stress applied to the crystal which can decouple the valence bands. In the preceding paper[11] we have sketched the requisite theoretical spectroscopy. In this paper we experimentally attack the problem from two directions: We study the behavior[12,13] of the quantum lines in Ge as a function of uniaxial stress in order to, first, identify the principal quantum lines and, second, determine the valence-band effective-mass parameters γ_1, γ_2, and γ_3 to high precision. With the benefit of these results (plus the g-factor parameters κ and q obtained in the next paper[14] of this series) it will be possible in a later paper[15] to analyze, in detail, the complex spectra of unstressed or "cubic" Ge. In addition, from these measurements we evaluate the constants F, G, H_1, and H_2, which represent the individual contributions to the hole effective masses from each of the four representations that are connected to the valence band edge by $\vec{k}\cdot\vec{p}$ interactions. These constants form a cornerstone in the construction of band theories.[16]

By lowering the cubic symmetry of the crystal, a uniaxial stress T splits[17,18] the fourfold (including spin) degenerate Γ_8^+ valence band edge of Ge into two Kramers doublets which, under certain conditions, may be conveniently identified in terms of the axial quantum numbers $M_J = \pm\frac{1}{2}, \pm\frac{3}{2}$. An earlier study[19] on silicon done at 9 GHz emphasized in the classical spirit the features of the energy surfaces of the two decoupled bands. From cyclotron reso-

nances of holes in these decoupled bands we measured the inverse-mass band parameters which characterize the shapes of the energy surfaces for *both* the stressed and unstressed valence bands.

In the present study on Ge our aims are much broader. Working at 53 GHz we shall examine in detail the consequences of the uniaxial stress on *individual* or quantum transitions between low-lying Landau levels belonging to both Kramers doublets, $M_J = \pm\frac{3}{2}, \pm\frac{1}{2}$, as they decouple. It will become apparent that a study of this kind offers an even greater abundance of information concerning the structure of the valence bands.

Uniaxial stress has a profound effect on the nature of the quantum spectra; both intensities and positions of the lines are changed in a major way. These characteristic stress effects make it possible for us to establish firm spectroscopic identifications of the individual resonance lines. Furthermore, from the unfolding of the quantum spectra we determine both magnitudes and signs of the valence-band uniaxial deformation-potential constants—these measurements[20] being the first obtained solely with the $J=\frac{3}{2}$ manifold. This spectroscopic method for measuring the deformation potentials is essentially a definitive one based upon the Luttinger-Kohn effective-mass description of the valence-band structure which has been experimentally well established by our cyclotron-resonance studies. No further assumptions are basically necessary.

As the bands decouple at large stresses the quantum cyclotron resonances arrange themselves into four line series which converge upon two series limits corresponding to the effective masses of the classical ellipsoidal energy surfaces of the respective split bands, $M_J = \pm\frac{3}{2}, \pm\frac{1}{2}$. Earlier attempts[21,22] at 9 GHz to determine the effective masses for the $M_J = \pm\frac{1}{2}$ band in Ge, along the lines of our original work in silicon,[19] were inconclusive. The hole resonances were observed[21] to be excessively broadened by the Hasegawa[23] mechanism, an inhomogeneous broadening arising from residual nonparabolicity due to incomplete decoupling of the bands. At 53 GHz we overcome this limitation present at lower frequencies by resolving the inhomogeneous resonances into their component lines from which the effective masses may be directly determined.

For this purpose two lines in these series are especially useful; they are the "fundamental" lines corresponding to the $n=0\rightarrow 1$ transitions for $M_J = -\frac{1}{2}$ and $-\frac{3}{2}$. These lines possess unique properties: in particular, they are very sharp; their positions, to lowest order, are invariant under stress; and, furthermore, they lie at the series limits, the effective masses of which are related to γ_1, γ_2, and γ_3 in an elementary way. Because of these properties the fundamental lines can be used to fix γ_1, γ_2, and γ_3 to an unprecedented precision. (The values thus obtained differ slightly, but not insignificantly, from the most accurate ones previously gotten from classical measurements[24] of the "light"- and "heavy"-hole resonances. In the Appendix we examine the systematic errors incumbent in the latter technique, which if taken into account, largely reconcile the differences.)

In connection with these measurements a small linear shift with stress is observed for the $M_J = -\frac{1}{2}$ fundamental lines. (The $M_J = -\frac{3}{2}$ lines do not shift.) This shift, analogous to one observed earlier in silicon,[19] results from the strain interaction[23] with the $J=\frac{1}{2}$ spin-orbit–split-off valence band and is, thus, proportional to a uniaxial deformation potential. Surprisingly, the values of the deformation potentials derived in this way are substantially *smaller* than those more directly measured, by the procedure mentioned earlier, within the $J=\frac{3}{2}$ multiplet. The resolution[20] of this apparent discrepancy lies in the existence, previously unrecognized, of spin-dependent deformation potentials which contribute in different ways, inside as compared to outside the $J=\frac{3}{2}$ manifold, from the spin-independent deformation potentials.

Our experiments clarify the confusion existing in earlier attempts[25] in unstressed Ge to locate and identify an important quantum transition (which turns into the $M_J = -\frac{1}{2}$ fundamental transition under [111] stress) between the two low-lying quaside-coupled $n=0$, 1 Landau levels for $\vec{H}_0 \parallel [111]$. ($\vec{H}_0$ is the external, static magnetic field.) The behavior of the spectrum under uniaxial stress confirms a conjecture suggested earlier[4] to the effect that the final state ($n=1$) is nearly degenerate with and, hence, strongly admixed (for $k_H \neq 0$) with two other states; so that a weak "fundamental triplet" appears in place of the strong single line anticipated.

The line shapes of the hole quantum cyclotron resonances are almost completely governed by k_H broadening[26]; only for the narrowest lines, e.g., the fundamental lines, are relaxation-time effects clearly in evidence. Although no systematic study of the cyclotron resonance scattering time τ has been undertaken, a few qualitative conclusions can be drawn. The scattering times at 53 GHz are *shorter* than at 9 GHz, and at the higher frequency they are substantially independent of temperature over the range 1.2 to 4.2 °K. This behavior is consistent with the "quantum" acoustic-phonon-scattering process of Meyer.[27]

Most of our measurements in this paper were made for $\vec{H}_0 \parallel T$. Because there exists a well-defined axis of quantization, the spectra for this case are most readily interpreted; and furthermore, the complete set of inverse-mass band parameters and deformation potentials can be deter-

mined by measurements in this geometry. However, some corroborative but less detailed measurements were undertaken for $\vec{H}_0 \perp T$. The results obtained were found to be wholly consistent with the values of γ_1, γ_2, γ_3, and D_u and D_u' determined from the $\vec{H}_0 \parallel T$ experiments.

II. VALENCE-BAND LANDAU LEVELS IN Ge

A general exposition of the theoretical spectroscopy of quantum cyclotron resonance has been given in Paper I. In this section we specialize the results apropos of our experiments in uniaxially stressed Ge.

A. In the absence of stress

We begin by considering the eigenstates of a hole in the Γ_8^+ valence band of Ge with an externally applied magnetic field $\vec{H}_0$ but without, for the moment, a uniaxial stress T. In the absence of stress and spin-orbit interactions the valence-band state at $\vec{k}=0$ is a sixfold degenerate (including spin) p multiplet characterized by the representation Γ_{25}^+ (or Γ_{25}'). Spin-orbit interaction splits this state by $\Delta = 0.29$ eV into a fourfold degenerate Γ_8^+ state (isomorphic to $J=\frac{3}{2}$) which forms the band edge and a twofold degenerate Γ_7^+ split-off state (isomorphic to $J=\frac{1}{2}$) as shown in Fig. 1(a). Ordinarily for cyclotron resonance in Ge at, say, 53 GHz it is sufficient for calculating energy levels to include interactions only within the upper $J=\frac{3}{2}$ manifold. (Interactions between $J=\frac{3}{2}$ and $J=\frac{1}{2}$ will be considered in Sec. II C). Within the $J=\frac{3}{2}$ manifold the dynamics of a hole in a magnetic field is described in the effective-mass formalism by the Luttinger[2] Hamiltonian [Eq. (I.29)],

$$\mathcal{H}_k = -\frac{\hbar^2}{m}\Big(\gamma_1\frac{k^2}{2} - \gamma_2[(J_x^2 - \tfrac{1}{3}J^2)k_x^2 + \text{c.p.}] - 2\gamma_3(\{J_xJ_y\}\{k_xk_y\} + \text{c.p.}) + \frac{e}{\hbar c}\kappa\vec{J}\cdot\vec{H}_0 + \frac{e}{\hbar c}q(J_x^3H_{0x} + \text{c.p.})\Big), \quad (1)$$

where

$$\vec{k} = (1/i)\nabla + (e/\hbar c)\vec{A}. \quad (2)$$

Here J_x, J_y, and J_z are the components of the angular momentum operator $\vec{J}(J=\frac{3}{2})$ referred to the cubic crystal axes; c.p. denotes cyclic permutation; the quantities $\{J_xJ_y\}$, etc., represent symmetrized products, i.e., $\{J_xJ_y\} = \frac{1}{2}(J_xJ_y + J_yJ_x)$; and $\vec{A}$ is the vector potential of the external magnetic field $\vec{H}_0$. In the first three terms of $\mathcal{H}_k$, which give the classical energy surfaces at zero magnetic field, the coefficients γ_1, γ_2, and γ_3 are Luttinger's valence-band inverse-mass parameters.[28] The last two terms, which vanish for $\vec{H}_0 = 0$, depend purely on "spin"; and their coefficients κ and q are related to the g factor of the free hole (see Paper III).

The component k_H of the wave vector in Eq. (2) along $\vec{H}_0$ commutes with $\mathcal{H}_k$ and, hence, is a constant of motion. Accordingly, the eigenvalues of $\mathcal{H}_k$ will depend parametrically upon k_H in a complicated fashion.[29] Peaks in the cyclotron-reso-

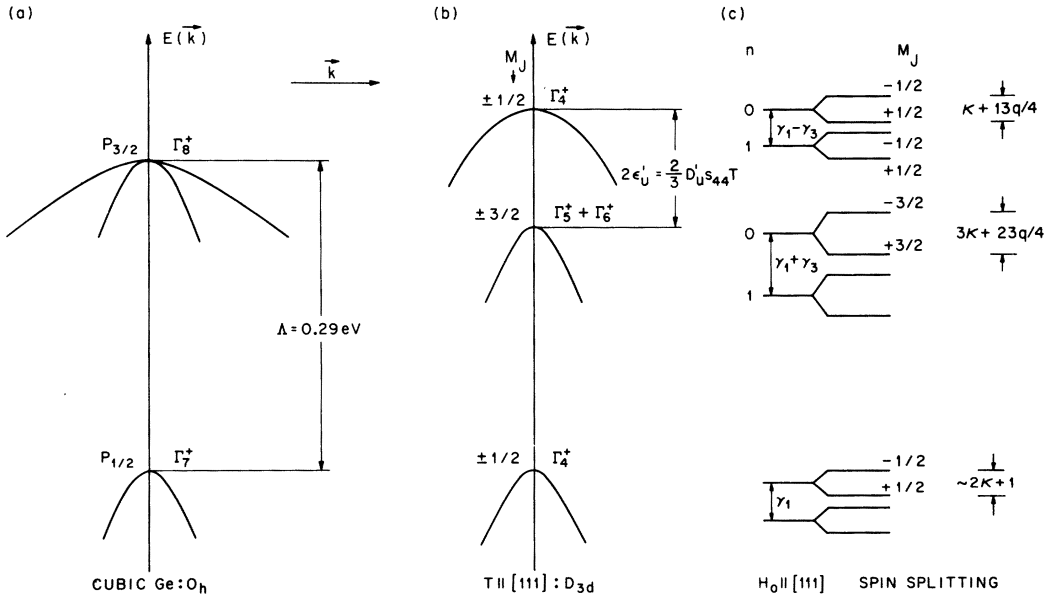

FIG. 1. Valence bands of Ge near $\vec{k}=0$ for (a) cubic symmetry (O_h) in absence of uniaxial stress and for (b) trigonal symmetry (D_{3d}) produced by a uniaxial, compressive stress along [111]. In (c) we schematically represent the Landau levels plus spin splitting of the bands in (b) for $\vec{H}_0 \parallel [111]$.

nance spectrum arise from critical points of the one-dimensional joint density of states defined by the condition

$$\left(\frac{\partial E_{st}}{\partial k_H}\right)^{-1} \to \infty, \tag{3}$$

where E_{st} is the energy difference between Landau levels s and t. By symmetry all allowed transitions have critical points at $k_H = 0$; but "noncentral" critical points occur at $k_H \neq 0$ as well and contribute importantly to the quantum spectra of "cubic" or unstressed Ge analyzed in Paper IV. However, for spectra taken under uniaxial stress, it will turn out to be usually sufficient (and certainly more convenient) to assume that $k_H = 0$, inasmuch as the strain-split bands take on an approximately ellipsoidal shape. This assumption is not justified for some transitions observed and will be removed when they are considered.

The diagonalization of the Hamiltonian $\mathcal{H}_k$ proceeds along the following lines. When a specific representation is introduced for $\vec{J}$, $\mathcal{H}_k$ becomes a 4×4 matrix Hamiltonian which generates a numerical secular matrix of infinite dimension. All eigenstates of $\mathcal{H}_k$, generally speaking, are coupled to one another to some order. As a result, the eigenvectors

$$\psi = \sum_n \sum_{M_J} a_n(M_J) u_n \left| M_J \right\rangle \tag{4}$$

are mixtures of all four Bloch states $|M_J\rangle$, where $M_J = \pm\frac{1}{2}, \pm\frac{3}{2}$; and the amplitude of each contains an infinite number of harmonic oscillator states u_n with $n = 0, 1, 2, 3, \ldots$. For $\vec{H}_0$ along a crystal axis of ν-fold rotational symmetry, the secular matrix decouples into ν submatrices (each of infinite dimension) and certain restrictions are placed on the values of n which appear in the eigenvectors of each matrix—a property which underlies the cyclotron-resonance selection rules. If we set $k_H = 0$ the secular submatrices further decouple into two. (Under special conditions[30] additional partitioning occurs.) To calculate the eigenvalues we must use a computer to diagonalize the ν (or 2ν) fully coupled but suitably truncated secular matrices retaining all terms in "warping"[31] $(\gamma_2 - \gamma_3)$ and k_H (where necessary).

The low-lying Landau levels (at $k_H = 0$) thus obtained are given in Fig. 2 for $\vec{H}_0$ along the principal

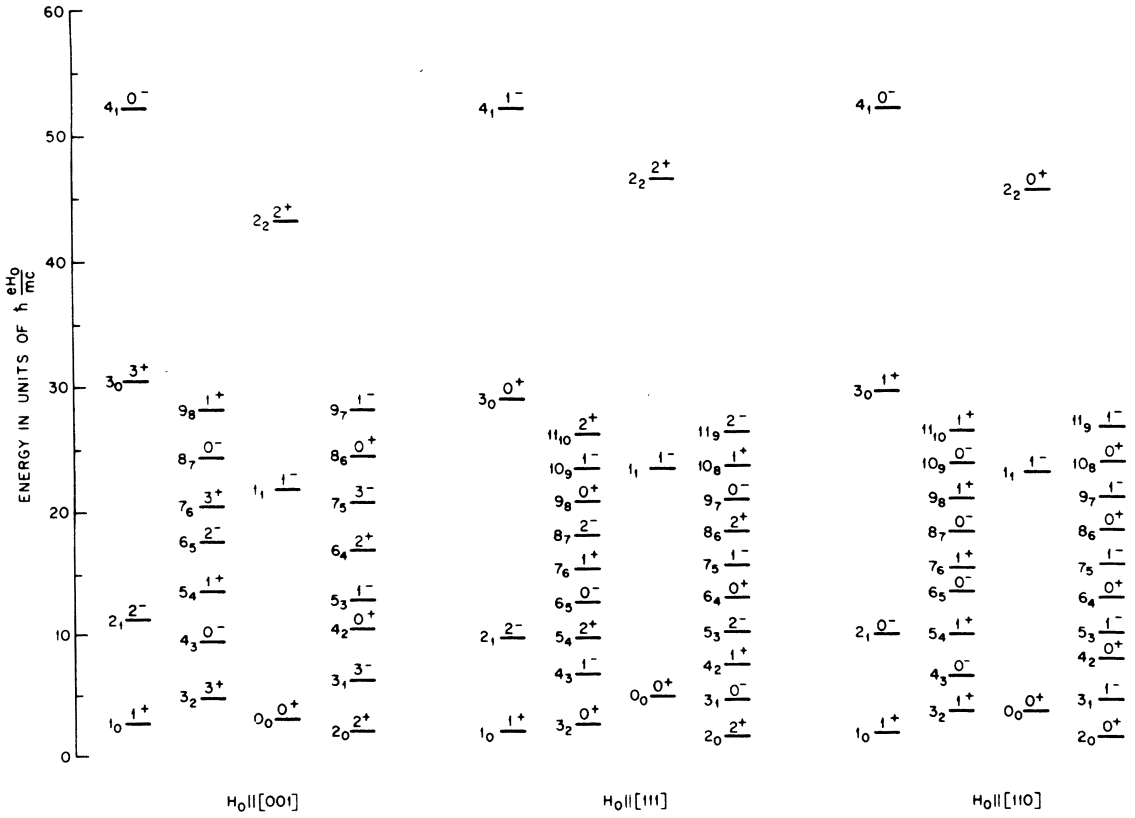

FIG. 2. Valence-band Landau levels in Ge calculated at $k_H = 0$. The values of the band parameters were $\gamma_1 = 13.38$, $\gamma_2 = 4.24$, $\gamma_3 = 5.69$, $\kappa = 3.41$, and $q = 0.06$. As is customary we invert the sign of the hole energy; so the levels are plotted in "ascending" order. The Landau levels are classified by (N_n, K^π).

crystallographic directions: [001], [111], and [110]. The secular matrices have been truncated at a total dimension[32] of approximately 80×80 which assures convergence of approximately the fifteen lowest eigenstates in each of the four Luttinger ladders. As customary we invert the sign of Eq. (1) so that the hole Landau levels are arrayed in ascending order; also the energies are given in dimensionless units of $\hbar eH_0/mc$.

In Fig. 2 we classify the Landau levels by the scheme (N_n, K^π) appropriate for "magnetic coupling" when $T=0$. Two quantum numbers are necessary to identify uniquely each eigenstate: N, the Landau quantum number for the envelope function, and its subscript n, which is required to distinguish the four states of the same N. Although n plays the role of an index, it has been chosen in such a way that we can ascribe to it a simple physical intepretation. It essentially identifies the principal harmonic-oscillator state[33] u_n present in the envelope function of N. (n corresponds to n_a in Paper I.) Noting that $n\leq N$, we generate in a natural way the array of levels

$$\begin{array}{cccc} \cdot & \cdot & \cdot & \cdot \\ 4_4 & 4_3 & 4_2 & 4_1 \\ 3_3 & 3_2 & 3_1 & 3_0 \\ 2_2 & 2_1 & 2_0 & \\ 1_1 & 1_0 & & \\ 0_0 & & & \end{array}$$

The quantum number $K(K=0, \ldots, \nu-1)$ embodies the ν-fold rotational symmetry of the crystal about the direction of $\vec{H}_0$. π is the parity of the envelope function. The magnetic quantum number M_J is connected with N, n and K by the relations

$$N=M_J+\tfrac{3}{2}+n, \quad K\equiv N \pmod{\nu} \ . \tag{5}$$

Using the quantum numbers (N_n, K^π) it is possible to express the cyclotron-resonance selection rules for $\vec{\mathcal{E}}_1\perp\vec{H}_0$, where $\vec{\mathcal{E}}_1$ is the microwave electric field, for $\vec{H}_0$ along any crystal orientation. If we symbolically categorize the successive symmetry breaking interactions

$$\mathcal{H}_0^{a}+\mathcal{H}_0^{na}+\mathcal{H}_1^{a}+\mathcal{H}_1^{na}$$

—where $\mathcal{H}_0^{a}$ is the axial Hamiltonian; $\mathcal{H}_0^{na}$ contains "warping" terms proportional to $\gamma_2-\gamma_3$; $\mathcal{H}_1^{a}$ represents the k_H terms; and $\mathcal{H}_1^{na}$ combines $\gamma_2-\gamma_3$ and k_H interactions—we get a hierarchy of selection rules as follows (see Table IV of Paper I):

$$\begin{array}{llll} M_0(\mathcal{H}_0^{a}) & \Delta N=\pm1, & \Delta\pi \text{ yes}, & \Delta K=\pm1, \\ M_1(\mathcal{H}_0^{na}) & & \Delta\pi \text{ yes}, & \Delta K=\pm1, \\ M_2(\mathcal{H}_1^{a}) & \Delta N=\pm1, & & \Delta K=\pm1, \\ M_3(\mathcal{H}_1^{na}) & & & \Delta K=\pm1 . \end{array}$$

In general, the selection rule[34] $\Delta K=\pm1$ [with the understanding that $\Delta K=\pm(\nu-1)$ is equivalent to $\Delta K=\mp1$] is the only strictly rigorous selection rule; the extent of the violation of the other selection rules depends upon the magnitude of the symmetry breaking terms in the Hamiltonian, i.e., the magnitudes of $\gamma_2-\gamma_3$ and k_H.

B. In the presence of stress

When the cubic symmetry is reduced by the application of a uniaxial stress, the $J=\frac{3}{2}$ state further splits [see Fig. 1(b)] into a pair of Kramers doublets which may be identified by the axial quantum number M_J under certain circumstances. The splitting of the $J=\frac{3}{2}$ states at $\vec{k}=0$ is given by the strain Hamiltonian[18] [Eq. (I. 30)]

$$\begin{aligned} \mathcal{H}_\epsilon &= D_d(\epsilon_{xx}+\epsilon_{yy}+\epsilon_{zz})+\tfrac{2}{3}D_u[(J_x^2-\tfrac{1}{3}J^2)\epsilon_{xx}+\text{c.p.}] \\ &\quad +\tfrac{2}{3}D_u'[2\{J_xJ_y\}\epsilon_{xy}+\text{c.p.}], \end{aligned} \tag{6}$$

where $\epsilon_{\mu\nu}$ are the components of the strain tensor. D_d, D_u, and D_u' are the Kleiner-Roth valence-band deformation potentials.[35] The dilatational component D_d shifts the entire Γ_{25}^+ multiplet without splitting the bands and may be ignored in the present work. D_u and D_u' are the "uniaxial" deformation potentials which describe the valence band splitting for uniaxial stresses along the [001] and [111] directions, respectively. For uniaxial stresses the Hamiltonian $\mathcal{H}_\epsilon$ can conveniently be rewritten in terms of the direction cosines (τ_x, τ_y, τ_z) of the stress T,

$$\begin{aligned} \mathcal{H}_\epsilon &= \epsilon_d+\epsilon_u[(J_x^2-\tfrac{1}{3}J^2)\tau_x^2+\text{c.p.}] \\ &\quad +\epsilon_u'[2\{J_xJ_y\}\tau_x\tau_y+\text{c.p.}], \end{aligned} \tag{7}$$

where

$$\begin{aligned} \epsilon_d &= (s_{11}+2s_{12})D_dT, \\ \epsilon_u &= \tfrac{2}{3}(s_{11}-s_{12})D_uT, \\ \epsilon_u' &= \tfrac{1}{3}s_{44}D_u'T, \end{aligned} \tag{8}$$

expressed in terms of the elastic compliance constants s_{11}, s_{12}, and s_{44}. Next, we specialize Eq. (7) (with the dilatational part ϵ_d omitted) for the three most important cases, T along [001], [111] and [110], and list the eigenvalues:

$T\parallel[001]$:

$$\begin{aligned} &\mathcal{H}_\epsilon=\epsilon_u(J_z^2-\tfrac{1}{3}J^2), \\ &\epsilon=+\epsilon_u \ \text{ for } M_J=\pm\tfrac{3}{2}, \\ &\quad=-\epsilon_u \ \text{ for } M_J=\pm\tfrac{1}{2}. \end{aligned} \tag{9}$$

$T\parallel[111]$:

$$\mathcal{H}_\epsilon=\tfrac{2}{3}\epsilon_u'[\{J_xJ_y\}+\text{c.p.}], \tag{10}$$

which transforms on taking $J_3\parallel[111]$ into

$$\mathcal{H}_\epsilon=\epsilon_u'(J_3^2-\tfrac{1}{3}J^2), \tag{11}$$

$$\epsilon = +\epsilon_u' \quad \text{for } M_J = \pm\tfrac{3}{2},$$

$$= -\epsilon_u' \quad \text{for } M_J = \pm\tfrac{1}{2}.$$

$T \parallel [110]$:

$$\mathcal{H}_e = -\tfrac{1}{2}\epsilon_u(J_x^2 - \tfrac{1}{3}J^2) + \epsilon_u'\{J_xJ_y\}, \tag{12}$$

which transforms on taking $J_3 \parallel [110]$, $J_\pm = 2^{-1/2} \times (J_1 \pm iJ_2)$ (the choice of the orthogonal axes 1 and 2 is immaterial) into

$$\mathcal{H}_e = \tfrac{1}{4}(\epsilon_u + 3\epsilon_u')(J_3^2 - \tfrac{1}{3}J^2) + \tfrac{1}{4}(\epsilon_u - \epsilon_u')(J_+^2 + J_-^2), \tag{13}$$

$$\epsilon = \pm\epsilon_u'' = \pm\tfrac{1}{2}(\epsilon_u^2 + 3\epsilon_u'^2)^{1/2}.$$

When $T \parallel [001]$ or $[111]$, $\mathcal{H}_e$ is simultaneously diagonal with $J_3 \parallel T$, so that M_J along T is a good quantum number. Otherwise, when the symmetry is less than threefold, the eigenstates are a linear combination of M_J states. One interesting exception to this statement occurs when $\epsilon_u = \epsilon_u'$. [Note that the last nondiagonal term in Eq. (13) then vanishes.] This can be easily seen if we separate the stress Hamiltonian (7) into isotropic and anisotropic parts

$$\mathcal{H}_e = \epsilon_d + \epsilon_u[(\vec{J}\cdot\vec{\tau})^2 - \tfrac{1}{3}J^2] + \epsilon_u(\beta - 1)[2\{J_xJ_y\}\tau_x\tau_y + \text{c.p.}], \tag{14}$$

where $\beta = \epsilon_u'/\epsilon_u$ is the "splitting anisotropy parameter." We note that if $\beta = 1$ ($\epsilon_u = \epsilon_u'$), first, $\mathcal{H}_e$ becomes rotationally invariant; so the strain splitting is isotropic with respect to the direction of T. Second, if in addition we choose the axis of quantization "3" along T, i.e., $\vec{J}\cdot\vec{\tau} \to J_3$, then $\mathcal{H}_e$ is diagonal and M_J becomes a good quantum number for any direction of T. In other words the condition $\beta = 1$ leads to "isotropic quantization." Although this special situation only roughly corresponds to the actual one in Ge, it is a useful limit for classification of states.

The Landau levels in uniaxially stressed Ge are

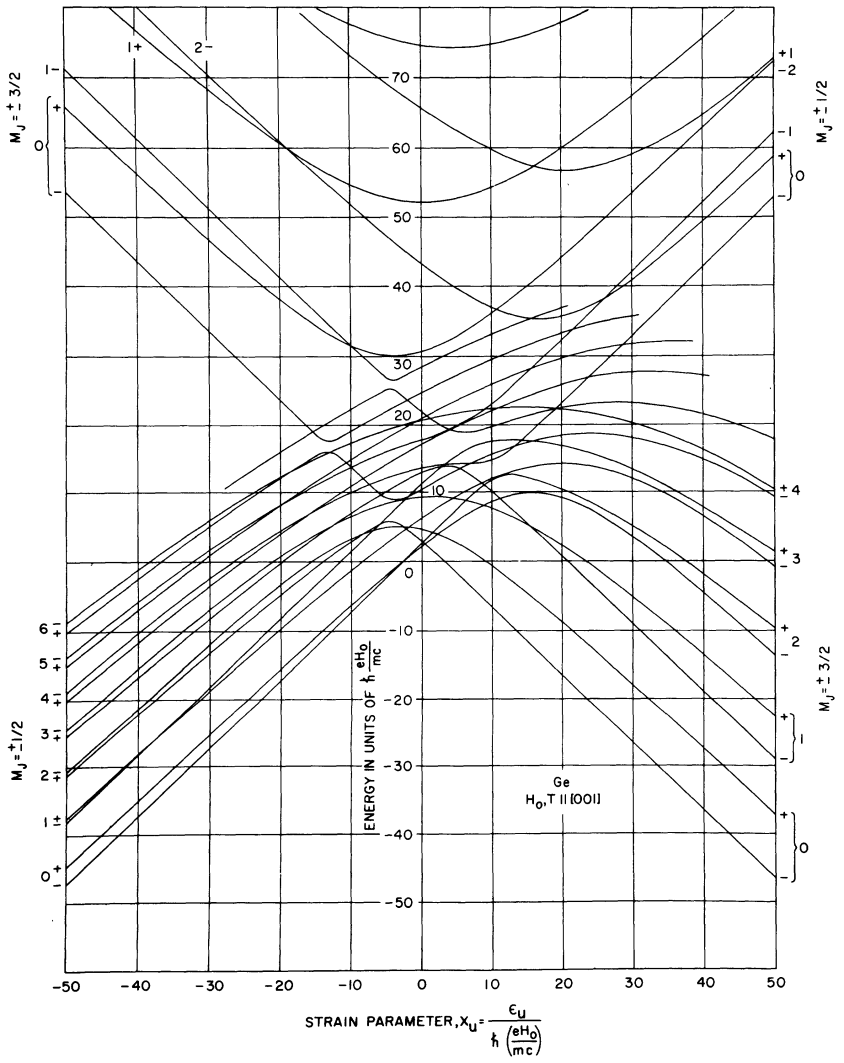

FIG. 3. Stress dependence of the $k_H = 0$ Landau levels for $\vec{H}_0$, $T \parallel [001]$ calculated as a function of the dimensionless "strain parameter" x_u. The values of the band parameters were the same as for Fig. 2. The levels may be identified at zero stress by referring to Fig. 2. At large stress the levels are labelled by the quantum numbers $(n, \pm M_J)$.

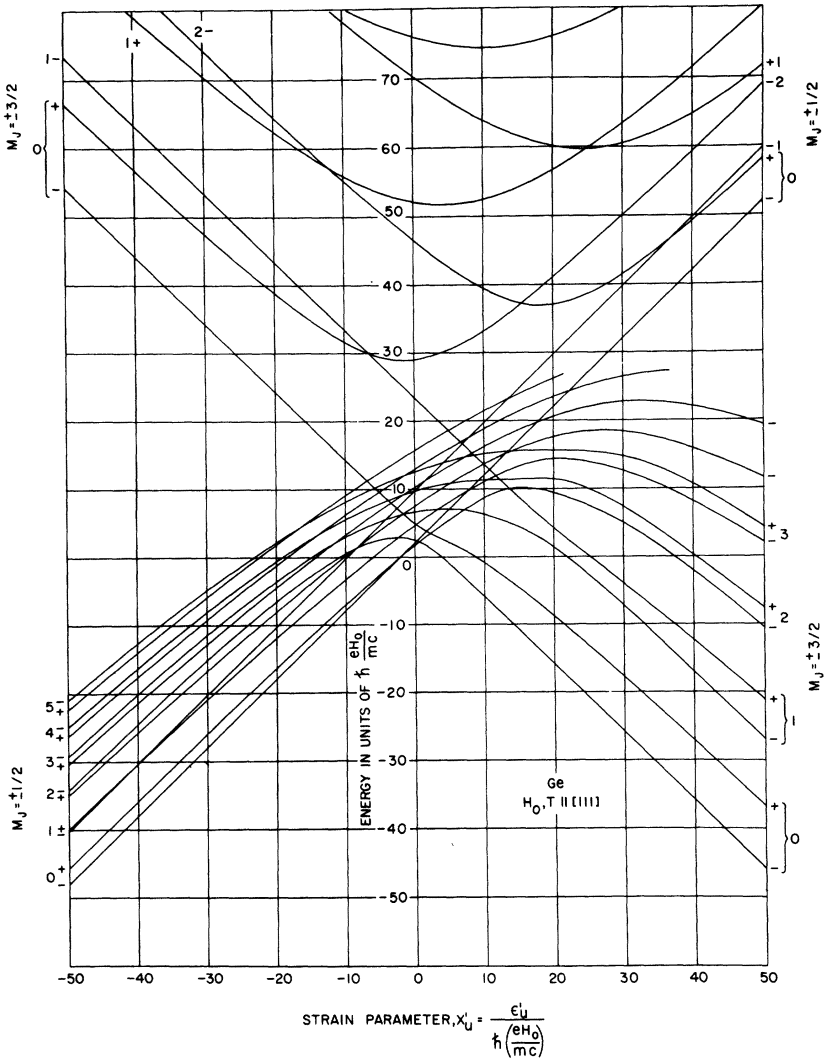

FIG. 4. Stress dependence of the $k_H = 0$ Landau levels for $\vec{H}_0$, $T \parallel [111]$ calculated as a function of the dimensionless "strain parameter" x'_u. See caption of Fig. 3.

obtained by diagonalizing the complete Hamiltonian $\mathcal{H}_k + \mathcal{H}_\epsilon$. The results for $\vec{H}_0$, $T \parallel [001]$ and $\vec{H}_0$, $T \parallel [111]$ at $k_H = 0$ are shown in Figs. 3 and 4, respectively. The energies of the Landau levels in Figs. 3 and 4 as in Fig. 2 are "inverted" and expressed in dimensionless units of $\hbar eH_0/mc$; it is natural to express the strain energies likewise as dimensionless "strain parameters"

$$x_u = \frac{\epsilon_u}{\hbar eH_0/mc}, \tag{15a}$$

$$x'_u = \frac{\epsilon'_u}{\hbar eH_0/mc}, \tag{15b}$$

$$x''_u = \frac{\epsilon''_u}{\hbar eH_0/mc} = \tfrac{1}{2}(x_u^2 + 3x_u'^2)^{1/2} \tag{15c}$$

(or generically just x). In Ge, D_u, $D'_u > 0$, so for our experiments which employ compressive stress ($T < 0$) this implies x_u, $x'_u < 0$, which restricts us to the left-half of these energy level diagrams. For clarity the Landau levels in Figs. 3 and 4 are not labeled at zero stress; the (N_n, K^τ) classifications can be readily made by comparing the levels at $x = 0$ with those in Fig. 2.

For $\vec{H}_0 \parallel T$ the symmetries of $\mathcal{H}_\epsilon$ and $\mathcal{H}_k$ are compatible; and the diagonalization, the quantum numbers and the selection rules discussed in Sec. II A are virtually unchanged as the strain is turned on. However, when the stress is large it is more convenient to classify the Landau levels in a "stress-coupling" scheme (n, M_J), n and M_J both being "good" quantum numbers for $\vec{H}_0$, $T \parallel [001]$ and $[111]$. Their connection with K in Eq. (5) remains valid always. The cyclotron resonance selection rules for $\vec{\mathcal{E}}_1 \perp \vec{H}_0$ are $\Delta n = \pm 1$ and $\Delta M_J = 0$ (which are, of necessity, consistent with $\Delta K = \pm 1$). For Ge, as can be seen from Figs. 3 and 4, the quantum number n has particular merit in that the identity of n for each level is preserved[36] in going from zero to large stress (with allowance made for the exchange of character in wave functions at

"level crossings"). For $\vec{H}_0$, $T \parallel [110]$ the (n, M_J) classification is useful only near $\beta = 1$.

The situation for $\vec{H}_0 \perp T$ is much more complex and is separately discussed in Sec. IV E.

We see in Figs. 3 and 4 that there are large changes in the positions of the Landau levels relative to one another as the bands are decoupled by uniaxial stress. Overall the array of Landau levels splits into two groups corresponding to the split band edges in Fig. 1(b); the $M_J = \pm\frac{3}{2}$ levels move "up" while the $M_J = \pm\frac{1}{2}$ levels move "down" for $x < 0$ (compressive stress) and *vice versa* for $x > 0$. At low stresses ($0 < |x| < 10$) where magnetic and strain energies are comparable, the relative positions of the levels are strong functions of x resulting in a complex and rapidly changing spectrum as stress is applied. At large x values we note that the Landau levels fall into regular sequences with uniform spacing characteristic of ellipsoidal energy surfaces. There are, in fact, four such series identifiable by $M_J = \pm\frac{1}{2}$ and $M_J = \pm\frac{3}{2}$ for $T \parallel [001]$ and $[111]$. In the limit $T \to \infty$ the "$\pm$" lines of each M_J asymptotically merge and approach the respective series limits $|M_J| = \frac{1}{2}, \frac{3}{2}$. Quite generally we can express the cyclotron-resonance effective masses of the two series limits by

$$\frac{m}{m_0^*} = \left(\frac{\beta_1^2 m^2}{m_2 m_3} + \frac{\beta_2^2 m^2}{m_1 m_3} + \frac{\beta_3^2 m^2}{m_1 m_2}\right)^{1/2}, \tag{16}$$

where m_1, m_2, and m_3 are given in terms of γ_1, γ_2, and γ_3 in Table I. Here $(\beta_1\beta_2\beta_3)$ are the direction cosines of $\vec{H}_0$ with respect to the "stress" coordinate systems defined in Table I. For the uniaxial cases, $T \parallel [001]$ and $[111]$, we have the following simplifications: $m_1 = m_2 = m_\perp$, $m_3 = m_\parallel$, $\beta_1^2 + \beta_2^2 = \sin^2\theta$, $\beta_3 = \cos\theta$, θ being the angle between $\vec{H}_0$ and T.

In principle, we could determine m_1, m_2, and m_3 and, in turn, γ_1, γ_2, and γ_3 by applying Eq. (16) to measurements of cyclotron resonances in the decoupled bands at the limit of large stress (strictly speaking, large x values). This essentially was the program undertaken in our earlier (classical) work[19] in Si. However, this "limit" is difficult to approach experimentally especially for the relatively large magnetic fields used in quantum spectroscopy. Fortunately, it is quite unnecessary to do this. In both Figs. 3 and 4 we note that the two lowest levels in the $M_J = -\frac{1}{2}$ and $M_J = -\frac{3}{2}$ ladders depend linearly on x and run approximately parallel to one another across the entire diagram. These behave as do decoupled or "pure" $M_J = -\frac{1}{2}$ or $-\frac{3}{2}$ states even at $x = 0$. Thus, the two transitions, $(0, -\frac{1}{2}) \to (1, -\frac{1}{2})$ and $(0, -\frac{3}{2}) \to (1, -\frac{3}{2})$, have a remarkable property—their positions (to lowest order) are stress invariant. We refer to these transitions as the "fundamental transitions"; they mark, respectively, the series limits which the rest of the $\pm\frac{1}{2}$ and $\pm\frac{3}{2}$ transitions approach asymptotically at large x. Thus, the high-stress limit can be, in fact, exactly simulated at low stress by measurements on the fundamental transitions.

The above is illustrated schematically in Fig. 1(c) which shows the lowest $M_J = \pm\frac{1}{2}$ and $\pm\frac{3}{2}$ Landau levels for $\vec{H}_0$, $T \parallel [111]$ in the limit $x'_u \to \infty$. The $-\frac{1}{2}$ and $-\frac{3}{2}$ fundamental transitions are seen to be complementary in that they give the effective masses $(\gamma_1 - \gamma_3)^{-1}$ and $(\gamma_1 + \gamma_3)^{-1}$, respectively; so measurements of both determine γ_1 and γ_3 independently. The case $\vec{H}_0$, $T \parallel [001]$ is the same with the simple replacement $\gamma_3 \to \gamma_2$ being made. All three band parameters γ_1, γ_2, and γ_3 can thus be fixed directly from the fundamental transitions.

TABLE I. Zeroth-order inverse effective-mass tensor components for the $M_J = \pm\frac{1}{2}$ and $\pm\frac{3}{2}$ series limits. For $T \parallel [110]$ the states are labeled by their character $\pm M_J$ at the uniaxial limit $\beta = 1$; also the effective masses are a function of η_1 and η_2 defined by $\eta_1 = (1 + 3\beta^2)^{-1/2}$ and $\eta_2 = \beta(1 + 3\beta^2)^{-1/2}$, where β is the strain anisotropy parameter. In the uniaxial cases [001] and [111], the parallel axes of the tensor are along T. For $T \parallel [110]$ we adopt the coordinate system $1 \parallel [1\bar{1}0]$, $2 \parallel [00\bar{1}]$, and $3 \parallel [110]$.

T	$M_J = \pm\frac{1}{2}$	$M_J = \pm\frac{3}{2}$
[001]	$m/m_\perp = \gamma_1 - \gamma_2$ $m/m_\parallel = \gamma_1 + 2\gamma_2$	$m/m_\perp = \gamma_1 + \gamma_2$ $m/m_\parallel = \gamma_1 - 2\gamma_2$
[111]	$m/m'_\perp = \gamma_1 - \gamma_3$ $m/m'_\parallel = \gamma_1 + 2\gamma_3$	$m/m'_\perp = \gamma_1 + \gamma_3$ $m/m'_\parallel = \gamma_1 - 2\gamma_3$
[110]	$m/m_1 = \gamma_1 + \gamma_2\eta_1 - 3\gamma_3\eta_2$ $m/m_2 = \gamma_1 - 2\gamma_2\eta_1$ $m/m_3 = \gamma_1 + \gamma_2\eta_1 + 3\gamma_3\eta_2$	$m/m_1 = \gamma_1 - \gamma_2\eta_1 + 3\gamma_3\eta_2$ $m/m_2 = \gamma_1 + 2\gamma_2\eta_1$ $m/m_3 = \gamma_1 - \gamma_2\eta_1 - 3\gamma_3\eta_2$

C. Interactions between the $J = \frac{3}{2}$ and $J = \frac{1}{2}$ manifolds

So far we have ignored the effects of the $J = \frac{1}{2}$ manifold on the positions of the Landau levels in $J = \frac{3}{2}$ which, in view of the large valence band spin-orbit splitting in Ge, $\Delta = 0.29$ eV, might be expected to be quite negligible. However, for the fundamental transitions which can be measured to high precision they become important and must be taken into account. Their origin can be traced quite easily.[37] We write the full 6×6 matrix Hamiltonian for the valence band (including strain) as

$$\begin{matrix} J = \frac{3}{2} & \frac{1}{2} \end{matrix}$$
$$\begin{bmatrix} \mathcal{H}_{11} & \mathcal{H}_{12} \\ \mathcal{H}_{21} & \mathcal{H}_{22} \end{bmatrix}, \tag{17}$$

where $\mathcal{H}_{12}$ is the 4×2 matrix connecting the $J = \frac{3}{2}$ and $J = \frac{1}{2}$ manifolds. The second-order energy correction from $\mathcal{H}_{12}$ to the $J = \frac{3}{2}$ multiplet $(1/\Delta)\mathcal{H}_{12}\mathcal{H}_{21}$ contains three types of interactions (ignoring the indices)

$$\mathcal{H}^{(2)}(J = \tfrac{3}{2}) = (1/\Delta)(\mathcal{H}_k^2 + 2\mathcal{H}_k\mathcal{H}_e + \mathcal{H}_e^2), \tag{18}$$

which cause, respectively, the magnetic-field-dependent effective-mass shift, the linear strain-

dependent effective-mass shift, and a second-order strain splitting. The last does not directly affect the effective masses and can be neglected.

1. Magnetic-field-dependent effective-mass shift

The first term in Eq. (18) shifts the cyclotron resonance lines even in the absence of stress. The shift of the inverse effective mass of the fundamental transition $(0, -\frac{1}{2}) \rightarrow (1, -\frac{1}{2})$ is

$$\Delta\left(\frac{m}{m^*}\right) = -\hbar\frac{eH_0}{mc}\frac{1}{\Lambda}[4\gamma_2^2 - 2\gamma_2(\kappa+1)]$$

for $\vec{H}_0 \parallel [001]$, (19)

$$\Delta\left(\frac{m}{m^*}\right) = -\hbar\frac{eH_0}{mc}\frac{1}{\Lambda}[4\gamma_3^2 - 2\gamma_3(\kappa+1) + 4(\gamma_3-\gamma_2)^2]$$

for $\vec{H}_0 \parallel [111]$ (20)

[cf. Eqs. (I. 147) and (I. 148) obtained for the spherical case]. A similar shift occurs for $M_J = -\frac{3}{2}$ transitions, but it is negligibly small at the lower magnetic fields where these resonances lie.

2. Linear strain-dependent effective-mass shift

For the axial cases, $T \parallel [001]$ and $T \parallel [111]$, the admixing of the eigenstates $J=\frac{3}{2}$ and $J=\frac{1}{2}$ by the second interaction in Eq. (18) obeys the selection rule $\Delta M_J = 0$. A linear stress-dependent effective-mass shift, then, is characteristic only for cyclotron resonances in $M_J = \pm\frac{1}{2}$ states, a fact which serves for their identification.

The theory of the strain-shifts for quantum cyclotron resonances in the $M_J = \pm\frac{1}{2}$ decoupled states has been developed[38] in Paper I; the results have a formal resemblance to Hasegawa's classical calculations[23] for silicon. However, owing to the larger spin-orbit coupling in Ge, one new ingredient must be added to the theory, namely, spin-dependent effects in the deformation potentials. When spin effects are included, the "mixing" deformation potentials D_w and D'_w in the strain matrix elements connecting $J=\frac{1}{2}$ and $J=\frac{3}{2}$ cease to be identical to the splitting deformation potentials, D_u and D'_u, which appear *within* the $J=\frac{3}{2}$ manifold. Accordingly, the inverse effective-mass shifts for the $M_J = \pm\frac{1}{2}$ series limits are (to first order in ϵ_w/Λ)

$T \parallel [001]$:

$$\Delta\left(\frac{m}{m_\perp^*}\right) = -\alpha_\perp T = \frac{4\epsilon_w}{\Lambda}\Gamma_2,$$
$$\Delta\left(\frac{m}{m_\parallel^*}\right) = -\alpha_\parallel T = \frac{-8\epsilon_w}{\Lambda}\Gamma_2; \quad (21)$$

$T \parallel [111]$:

$$\Delta\left(\frac{m}{m_\perp^*}\right) = -\alpha'_\perp T = \frac{4\epsilon'_w}{\Lambda}\Gamma_3,$$
$$\Delta\left(\frac{m}{m_\parallel^*}\right) = -\alpha'_\parallel T = \frac{-8\epsilon'_w}{\Lambda}\Gamma_3; \quad (22)$$

where

$$\epsilon_w = \tfrac{2}{3}(s_{11}-s_{12})D_w T, \quad (23)$$

$$\epsilon'_w = \tfrac{1}{3}s_{44}D'_w T. \quad (24)$$

[As an example of another, minor, spin effect, the band parameters Γ_2 and Γ_3 in Eqs. (21) and (22) in the matrix elements between $J=\frac{3}{2}$ and $J=\frac{1}{2}$ can, in principle, differ from γ_2 and γ_3, the band parameters within $J=\frac{3}{2}$. For Ge the distinction is probably unimportant.] For $T \parallel [110]$ the formulas for the shifts are more complicated; and having been given in Paper I [Eq. (I. 144)], they will not be repeated here.

In summary, the anisotropic cyclotron resonance effective masses in the strain-decoupled $M_J = \pm\frac{1}{2}$ bands (i.e., the quantum series limits) can, for the uniaxial cases $T \parallel [001]$ and [111], be written

$$m/m^*(\theta) = m/m_0^*(\theta) - \alpha(\theta)T \quad (25)$$

where $m_0^*(\theta)$ is given by Eq. (16) and $\alpha(\theta)$ is given by the expression[19]

$$\alpha(\theta) = \tfrac{1}{2}m_0^*(\theta)\left[\frac{2\alpha_\perp}{m_\perp}\cos^2\theta + \left(\frac{\alpha_\perp}{m_\parallel} + \frac{\alpha_\parallel}{m_\perp}\right)\sin^2\theta\right] \quad (26)$$

in terms of the components $\alpha_\perp$ and $\alpha_\parallel$ in Eqs. (21) and (22). When $\vec{H}_0 \parallel T$, the simplifications $m_0^* = m_\perp$ and $\alpha = \alpha_\perp$ are obtained. Equation (25) holds for the fundamental transitions $(0, -\frac{1}{2}) \rightarrow (1, -\frac{1}{2})$ at *finite* stresses[38] and will be used for their analysis in succeeding sections. Except for the αT term these transitions are virtually stress invariant. The αT shifts for other transitions are almost completely overshadowed by the much larger shifts due to strain interactions within $J=\frac{3}{2}$ and will not be of particular interest to us.

III. EXPERIMENTAL DETAILS

A. Microwave spectrometer

The cyclotron resonance measurements were done using millimeter waves at 53 GHz. The spectrometer, shown schematically by a block diagram in Fig. 5, is a balanced-bridge cavity type employing a superheterodyne detector, the sensitivity of which is vital to the detection of the weak quantum lines. Also essential is the ability of the superheterodyne scheme to operate at the low microwave power levels $P_0 \sim 10^{-8}$–10^{-9} W necessary to avoid saturation of the cyclotron resonances. Since much of the success of the present experiment owes to the sensitivity and reliable performance of this spectrometer, we briefly call attention to some of its important features. The millimeter-wave power sources, both signal and local oscillators, are low-power (~10 mW) backward-wave oscillators (BWO) (Bendix type TE-67). The signal BWO is frequency locked to a harmonic (usually sixth harmonic) of an X-band (9-GHz) LFE 814 ultrastable tunable signal source (which uses an invar

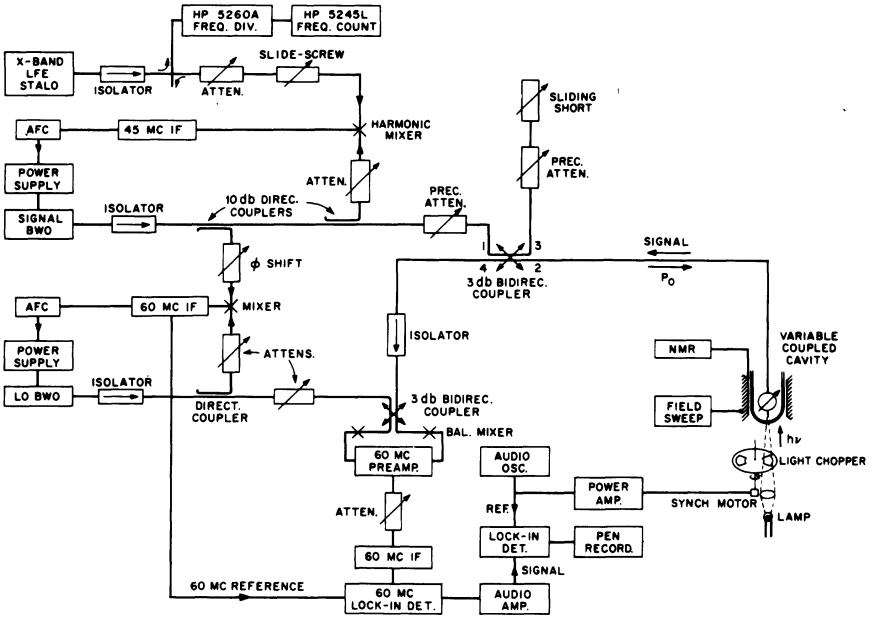

FIG. 5. Block diagram of the microwave spectrometer operating in the 50–60-GHz band.

cavity for reference). The local BWO, in turn, is locked to the signal BWO but shifted with a difference frequency $\Delta\nu = 60$ MHz equal to the signal i.f. frequency. The over-all frequency stability of the system holds to about 1 part in 10^6. The X-band reference frequency was monitored continuously by the Hewlett-Packard (HP) frequency-divider–frequency-counter combination.

The microwave bridge and balanced mixer make use of 3-dB bidirectional couplers rather than the conventional "magic" tee, since the former at millimeter wavelengths are usually better matched and have broader bandwidths. Two modes of balanced-bridge operation are possible. In the first, the bridge bucking elements are the attenuator and sliding-short in arm 3 of the bridge coupler. This mode suffers from the inherent drawback that the opposite arm (arm 2) of the bridge, the transmission line to the cavity, is electrically very long for millimeter waves and the inevitable thermal expansion changes and mechanical disturbances in it result in excessive drift and noise. These problems can be mitigated by operation in the second mode which was employed for most of our measurements. Here the bridge match was achieved *at the cavity* by adjustment of the spectrometer frequency and the cavity variable coupler (the attenuator in arm 3 having been set at ∞ for termination). Usually, we operated at exact match and the absorption component of the cyclotron-resonance signal was selected by varying the reference phase to the 60-MHz lock-in detector by means of "Φ shift." The detected absorption signal, modulated at 100 or 1000 Hz, is amplified and synchronously detected with a typical time constant of 0.1 or 0.25 sec. The output is displayed on a chart recorder.

The cyclotron-resonance spectrum is observed by slowly sweeping the magnetic field linearly in time by a sawtooth control signal fed to the magnet power supply. The magnetic field is measured by field markers on the recorder traces from proton-NMR signals. Usually the spectrum was traversed in both sweep directions, "up" field and "down" field, to eliminate any hysteresis effects due to finite time constants in the recorder or electronics.

The rectangular microwave cavity (see Fig. 6) operates in the TE_{101} mode. This mode was chosen to give linear polarization of the microwave electric field $\vec{\mathcal{E}}_1$, the orientation of which relative to $\vec{H}_0$ governs the cyclotron-resonance selection rules. The cavity is made in two $\frac{1}{4}\lambda$ sections, each "hubbed" from coin silver. Narrow slots to admit light were cut on the cavity bottom in a way that microwave currents were not broken.

B. Strain apparatus

The uniaxial stress is applied to the sample by means of the apparatus[39] pictured in Fig. 6. Rectangular samples of Ge of dimensions $2.2 \times 1.5 \times 0.2$ mm were positioned on their "flat" side spaced approximately 0.1 mm above the slotted cavity floor, well out of the maximum $\vec{\mathcal{E}}_1$ field at the center of the cavity, by a sheet of transparent Mylar. The sample was uniaxially stressed by force applied to it from the external loading on the split halves of the cavity. One half of the cavity was fixed, and the other half movable, pivoting about the top edge of the cavity split. The uniformity of loading on the sample ends was improved by placing between the sample ends and cavity wall

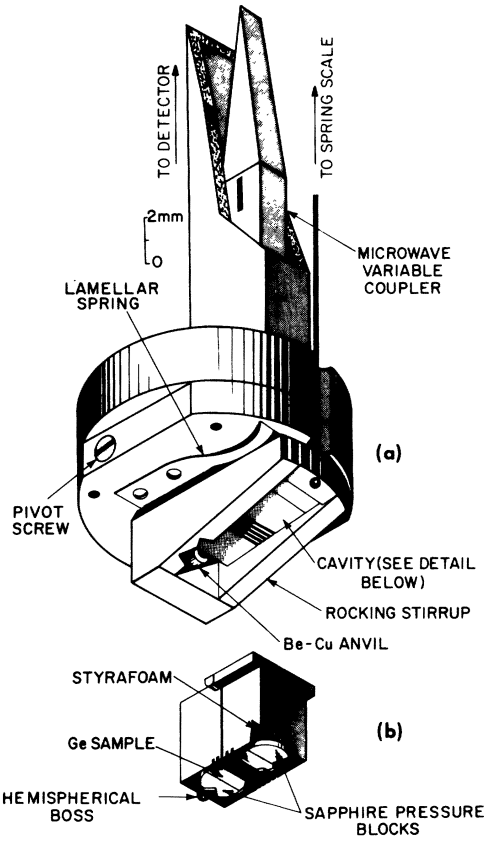

FIG. 6. Apparatus for application of a uniaxial stress to the Ge sample. The tension in the phosphorbronze wire, loaded by the spring scale, produces, by the lever action of the "rocking stirrup," a horizontal force against the hemispherical boss on the cavity. The rectangular cavity, shown in detail in (b), is made up in two sections, one fixed and the other free to pivot about a fulcrum axis along the upper edge of the split. The external force is thereby transmitted via the semicircular, sapphire pressure blocks to the ends of the Ge sample.

semicircular bearing sections cut from fused quartz or sapphire—plane faces against sample ends and "rounds" against cavity walls. Thin "vellum" paper pieces, 0.05 mm thick, were cemented to the plane faces of the bearing spacers to provide a "buffer" for the ends of the sample to prevent localized-strain-concentration points. The remainder of the cavity was filled with fine porosity Styrofoam to exclude as much liquid He as possible as well as to keep the sample and bearing sections firmly in place during assembly of the apparatus. The external force against the movable half of the cavity is supplied by a pivoted-lever mechanism actuated by a flexible phosphorus-bronze stranded wire running up the cryostat and tied to a calibrated spring balance at the top. This spring balance is located in a vacuum-tight Lucite chamber positioned above and connecting with the He cryostat; so it was not necessary that the transmission of force pass through a sylphon or grease vacuum seal, thereby eliminating an otherwise serious source of friction and stress hysteresis. The tension in the spring balance—and, hence, the stress in the sample—was adjustable externally by means of a screw shaft through an O-ring seal at the top of the chamber.

The geometry in the above apparatus was arranged so the stress is applied transverse to the Dewar axis, and therefore, in the plane of the dc magnetic field $\vec{H}_0$. Most runs were made with $\vec{H}_0 \parallel T$ and it necessarily follows (see Fig. 6) that $\vec{H}_0 \perp \vec{\mathcal{E}}_1$, as required for ordinary cyclotron resonance. (Measurements for the geometry $\vec{H}_0 \perp T$ require a different apparatus which is mentioned briefly in Sec. IV E.)

The strain apparatus was calibrated[40] in two ways: first, by calculation of the mechanical advantage of the system; and, second, by the determination of the actual force on the sample. We made this measurement by substituting a piezoresistance strain gauge in place of the sample within the cavity. The strain gauge, cut as an exact replica of the sample from a single crystal of n-type Ge (3×10^{15} Sb/cm^3) and orientated along a [111] axis, was in turn calibrated "on the bench" by direct loading with weights. The results of the two calibration methods agreed within a few percent. We calculated the strain in the sample from the stress (determined from the above load calibration and careful measurements of the sample dimensions) using the elastic compliance constants $s_{11} = 9.37\times10^{-7}$ cm^2/kg, $s_{12} = -2.57\times10^{-7}$ cm^2/kg, and $s_{44} = 14.3\times10^{-7}$ cm^2/kg, from McSkimin's[41] data extrapolated to 1 °K. It is estimated that the strain would be determined by this procedure to an over-all accuracy of about 5%. The uniformity of strain in the samples could be estimated from the broadening of certain cyclotron-resonance lines which shift rapidly with stress. Throughout the "active" central region of the sample illuminated by light we estimate in this way the maximum strain nonuniformity to be no more than 5% for a typical "good" run. At the ends of the sample where the force is applied, the strain homogeneity is undoubtedly poorer. In spite of the most elaborate precautions in assembly of the apparatus, "bad" runs were not infrequent; these were instantly recognized by the seriously broadened and distorted appearance of the cyclotron-resonance line shapes and were rejected outright.

C. Samples

All of the samples used in these experiments were cut from a single crystal[42] $nWLP$-33 of ultrapure Ge ($N_D \sim 5\times10^{12}$ cm^{-3}, $N_A \sim 4\times10^{12}$ cm^{-3}). This particular crystal was typical of a number of very pure crystals tested, all of which showed well resolved and nearly identical cyclotron-resonance quantum spectra. The crystallographic orientation

of the samples was determined, prior to cutting, to within ~0.3° using an x-ray goniometer; final orientation of the spectrometer magnetic field with respect to the crystal axes was accomplished *in situ* by observing the electron-cyclotron-resonance lines. The samples were cut to their rough dimensions and then lapped on all sides to approximately final dimensions except the length which was left oversize. Next, the sample was etched in *CP*-4 to reduce surface recombination. As a final operation the samples were mounted lengthwise through a rectangular slot in a flat lapping plate, which had been precision ground to a thickness exactly equalling the desired sample length; the slightly protruding ends of the sample were then lapped flush with the surface of the plate. This procedure assured accurate control of the length, exact parallelism of the end surfaces, and eliminated the rounded corners and edges which resulted from etching.

For our experiments the samples were in direct contact with liquid helium at all times; measurements were made at both 1.2 and 4.2 °K.

Free carriers, both holes and electrons, were generated in the sample by white light chopped at the modulation frequency. The sample was directly illuminated via the cavity light slots by a collimated (f/16) beam from a 6-V ribbon-filament lamp (GE 9*A*) focused through the unsilvered Pyrex walls of the Dewar tail. As the cyclotron-resonance lines, especially those for the electrons, are broadened by excessively strong illumination, we intentionally cut the light intensity by operating the lamp at 4 V (filament temperature ~1800 °C) and inserting in the optical path a neutral-density filter having 25% transmission.

It is difficult to ascertain absolute carrier densities in the samples; nevertheless even a very

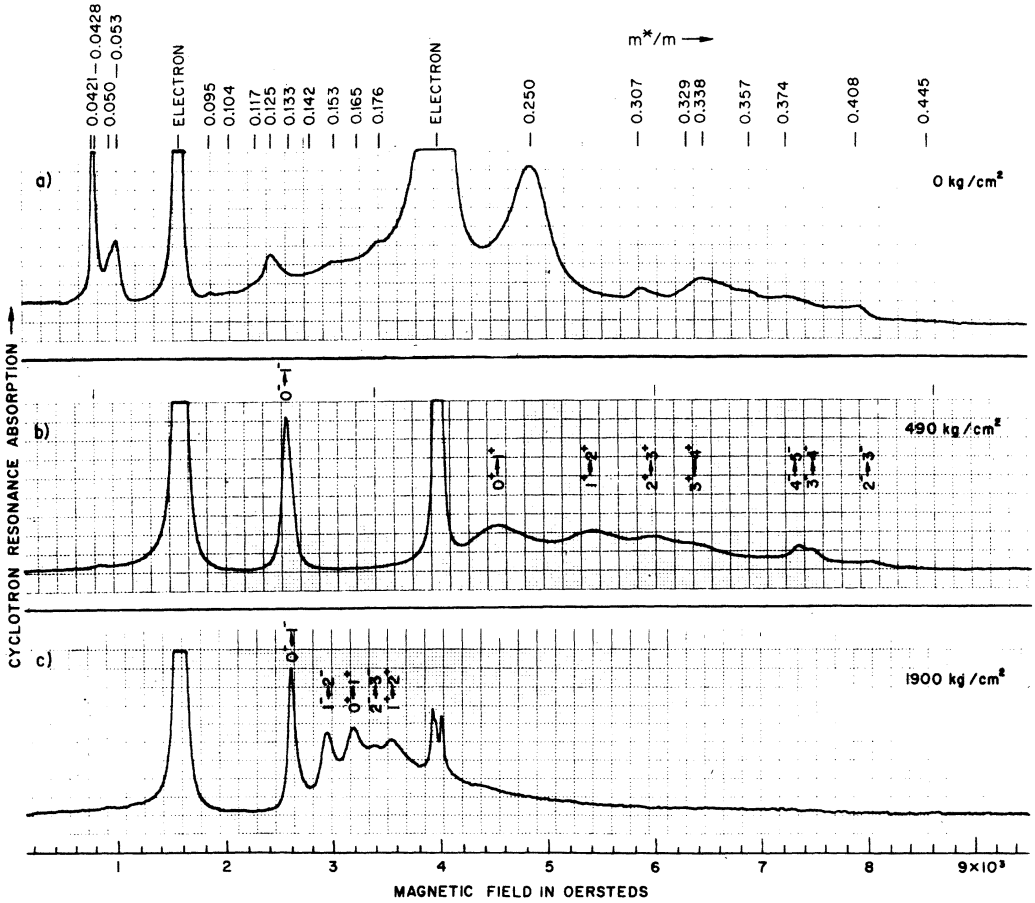

FIG. 7. Effect of uniaxial stress on the cyclotron resonance spectrum in Ge. The recorder traces were taken at 1.2 °K and 52.9 GHz with $\vec{H}_0 \| [111]$. The top trace (a) shows the quantum spectrum of holes in an unstrained crystal. The hole resonances are designated by their effective masses. Traces (b) and (c) were taken with a uniaxial, compressive stress applied along [111]. In these traces we label the hole lines by the $(n, \pm M_J)$ notation abbreviated to $n^{\pm}$ (all transition appearing here are $M_J = \pm\frac{1}{2}$). The slight splitting of the high-mass electron line seen in trace (c) is due to an ~0.3° misorientation of $\vec{H}_0$ from the [111] axis.

rough estimate would be worth knowing. Measurements of the intensity and spectral distribution of the source plus consideration of the layout of the optics leads to an estimate of ~10 μW for the "effective" optical input power, i.e., the fraction of the light flux which actually reaches the sample surface and has $h\nu_{optical} > E_g$ (the threshold for creation of free carriers). Assuming unity quantum efficiency and a hole lifetime of ~10^{-9} sec (see Sec. V D) we calculate the (steady-state) number of holes in the sample to be ~5×10^4, which represents a density of ~10^9 cm^{-3} within a volume determined by the hole diffusion length.

IV. EXPERIMENTAL RESULTS

A. Nature of the cyclotron-resonance spectra

As the degeneracy of the valence bands of Ge is lifted by uniaxial stress, the quantum cyclotron-resonance spectrum for holes undergoes striking changes. This is illustrated in Fig. 7 by recorder tracings of $\vec{H}_0 \| [111]$ spectra taken as a function of compressive stress applied to the [111] axis of the sample. Before tackling the data in detail, we pause to examine the general features of these spectra.

In the top trace [Fig. 7(a)] taken at zero stress is the "quantum" spectrum of hole resonance lines, designated by their effective mass values, together with the strong, sharp lines of the electron resonances. (The less prominent resonances show up more clearly at 4.2 °K or at higher gain.) The hole spectrum in unstressed Ge is complex; the lines do not fit into any obvious pattern. The analysis of this spectrum, in which k_H effects play an essential role, will be the topic of Paper IV. Broadly speaking, the lines above 4000 Oe ($m^*/m > 0.2$) derive from the "heavy"-hole Landau ladders (starting with states 3_2 and 2_0 in Fig. 2) while the lines below 1000 Oe ($m^*/m < 0.06$), derive from the "light"-hole ladders (starting with states 0_0 and 2_1). Most lines in the intermediate region are "harmonic" transitions from the heavy-hole ladders. The weak lines at $m^*/m = 0.117$ and 0.133 plus the stronger line at $m^*/m = 0.125$ constitute the "fundamental" triplet (all three transitions originate from the low-lying state 1_0 in Fig. 2).

The transformation of the hole spectrum by uniaxial stress, 490 kg/cm^2, is shown in the middle trace, Fig. 7(b). In the stressed spectrum the hole resonances fall into well-defined sequences or line series. The low-field resonances from the $M_J = \pm\frac{3}{2}$ bands have vanished because these bands move "up" (refer to Fig. 4) under compressive stress and depopulate. The high-field resonances evolve, without evidencing much change in intensity, into two line series, $M_J = +\frac{1}{2}$ and $M_J = -\frac{1}{2}$. (Identifications are explained in Sec. IV B.) The most prominent hole line in the spectrum is the "fundamental" transition $(0, -\frac{1}{2}) \rightarrow (1, -\frac{1}{2})$, the fixed line which marks the $T \rightarrow \infty$ series limit for both $M_J = +\frac{1}{2}$ and $M_J = -\frac{1}{2}$ series. Incidentally, this line does not develop, as it would seem, from the resonance at $m^*/m = 0.125$ in trace (a) but rather from a very weak line at $m^*/m = 0.133$. Trace (b) was recorded near the stress where the $(1, -\frac{1}{2})$ and $(2, -\frac{1}{2})$ levels cross (see Fig. 4), so the second line of the $M_J = -\frac{1}{2}$ series, $(1, -\frac{1}{2}) \rightarrow (2, -\frac{1}{2})$, is missing (i.e., $m^*/m \rightarrow \infty$).

A typical high-stress spectrum, taken at 1900 kg/cm^2, is shown in the bottom trace (c) of Fig. 7; we see that the $M_J = +\frac{1}{2}$ and $-\frac{1}{2}$ series have moved to lower fields and overlap one another as both converge upon the $T \rightarrow \infty$ series limit at the $(0, -\frac{1}{2}) \rightarrow (1, -\frac{1}{2})$ line. This line, we note, in both traces (b) and (c) in Fig. 7 is much the narrowest of the hole lines; for it is relatively insensitive to strain and k_H effects which broaden the others.

At very low stresses, several weak lines of the $M_J = -\frac{3}{2}$ series can be detected. These are shown in a trace in Fig. 8 taken at ~50 kg/cm^2 with $\vec{H}_0$, $T \| [111]$. The initial line $(0, -\frac{3}{2}) \rightarrow (1, -\frac{3}{2})$ is a stress-independent transition (a "fundamental" transition) which marks the $M_J = \pm\frac{3}{2}$ series limit. The next line $(1, -\frac{3}{2}) \rightarrow (2, -\frac{3}{2})$ is just perceptible under these experimental conditions. A "classical" light-hole resonance also appears in the spectrum as 50 kg/cm^2 is insufficient to uncouple the deeper Landau levels.

The positions of the electron lines in Figs. 7 and 8 are unaffected by uniaxial stress; however, the intensity of the higher mass electron line in Fig. 7 diminishes sharply with applied [111] stress due to the valley splitting effect.

B. Identification of the lines: $\vec{H}_0 \| T$

The deconvolution of the hole spectrum by uniaxial stress enables us, with the aid of the energy level diagrams in Figs. 3 and 4, to establish the identities of the quantum lines. To do this we recorded spectra as a function of T in steps of ~75 kg/cm^2 at large stresses ($T > 500$ kg/cm^2) and at even smaller intervals at low stresses where the lines shift quite rapidly. Data for $T \| [111]$ and $T \| [001]$ are shown in Figs. 9 and 10 and Fig. 11, respectively. Measurements were made at both 1.2 °K (circles) and 4.2 °K (points). At 4.2 °K the higher transitions, up to $n = 6 \rightarrow 7$, become observable. The solid curves represent fits (for $k_H = 0$ unless otherwise noted) calculated from Figs. 3 and 4. Although the fits in Figs. 9–11 are excellent, it should be emphasized that they are *not* used to determine the band parameters. These can be gotten much more accurately, as we shall presently see, from the fundamental transitions. The dashed curves follow experimental points in

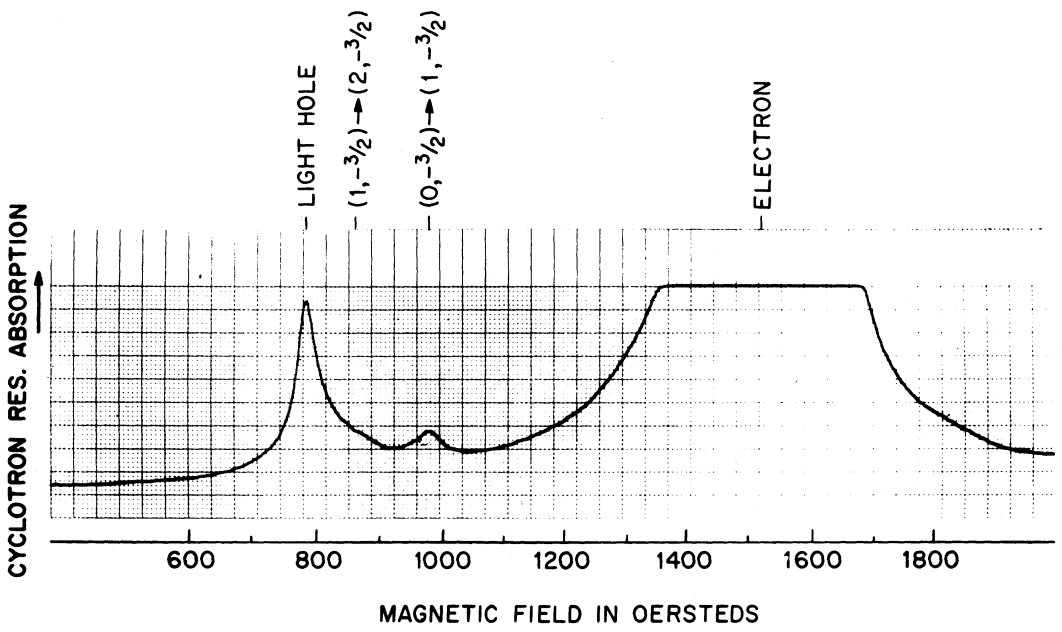

FIG. 8. Spectrum of $M_J = -\frac{3}{2}$ hole transitions taken at 50 kg/cm^2, $\Theta = 1.2$ °K and $\vec{H}_0$, $T \| [111]$. The spectrometer gain is approximately 5× greater than in Fig. 7.

instances where we have not attempted detailed calculations, e.g., for most transitions at $k_H \neq 0$. The transitions are labeled by N_n near zero stress and by (n, M_J) at large stress.

To facilitate the fitting of calculations to the experimental data in Figs. 9–11 we plot the data in terms of the strain parameter x_u or x_u' defined in Eq. (15). The conversion from sample loading (i.e., stress) to strain parameter depends on one "adjustable" parameter, namely, the uniaxial deformation potential (see Sec. IV C). In reading effective masses against this scale one should bear in mind that "constant x" does not imply constant stress; the constant-stress loci are hyperbolas, i.e., $x \propto m/m^*$, not "vertical" lines in these diagrams.

Having made line identifications at finite stress, we are able to track some of the lines to $T = 0$. Some light is shed thereby on the identities of the quantum lines of the unstressed crystal. Unfortunately, the procedure is not entirely definitive inasmuch as the spectrum near $T = 0$ is scrambled by the overlapping of many lines in addition to the complications introduced by k_H effects. For the most part the correspondences made will serve as a valuable, albeit qualitative, adjunct to the more elaborate analysis in Paper IV.

Included in Figs. 9 and 11 are data from transitions in the depopulated $M_J = -\frac{3}{2}$ states. As expected, these transitions are exceedingly weak and become undetectable for stresses greater than 250 kg/cm^2. (Consequently, they appear in Fig. 8 but not in Fig. 7.) We have devoted considerable effort to measuring these lines, for one of them, the fundamental transition $(0, -\frac{3}{2}) \rightarrow (1, -\frac{3}{2})$, is a crucial link in the determination of γ_1, γ_2, and γ_3.

We will now consider the cases $T \| [111]$ and $T \| [001]$ individually in more detail. A similar, comprehensive mapping of the spectrum for $T \| [110]$ has not been attempted. We anticipate the results to be qualitatively similar to the [111] and [001] cases (and very likely more complex at low stresses owing to the less stringent selection rules that result from the lower twofold symmetry).

1. $T \| [111]$

First let us consider the high-stress region. For $|x_u'| > 20$, we see in Fig. 9 that the lines of the quantum spectra fall into three series. As $|x_u'| \rightarrow \infty$, two series, $M_J = -\frac{1}{2}$ and $M_J = +\frac{1}{2}$, asymptotically converge to the fundamental transition $(0, -\frac{1}{2}) \rightarrow (1, -\frac{1}{2})$ while the third series, $M_J = -\frac{3}{2}$, converges to the fundamental transition $(0, -\frac{3}{2}) \rightarrow (1, -\frac{3}{2})$. We have been unable to detect any lines of the fourth series, $M_J = +\frac{3}{2}$, possibly because of strain broadening.

At large x_u' we observe an extra resonance[43] in the spectrum not attributable to any $k_H = 0$ transition in the $M_J = \pm\frac{1}{2}$ ladders. Its position is given by the data points in Fig. 9 tagged "k_H branch" alongside the $(0, -\frac{1}{2}) \rightarrow (1, -\frac{1}{2})$ transition. Experimentally we note its following characteristics: (i) It is first resolved near $x_u' \sim -30$ as a secondary

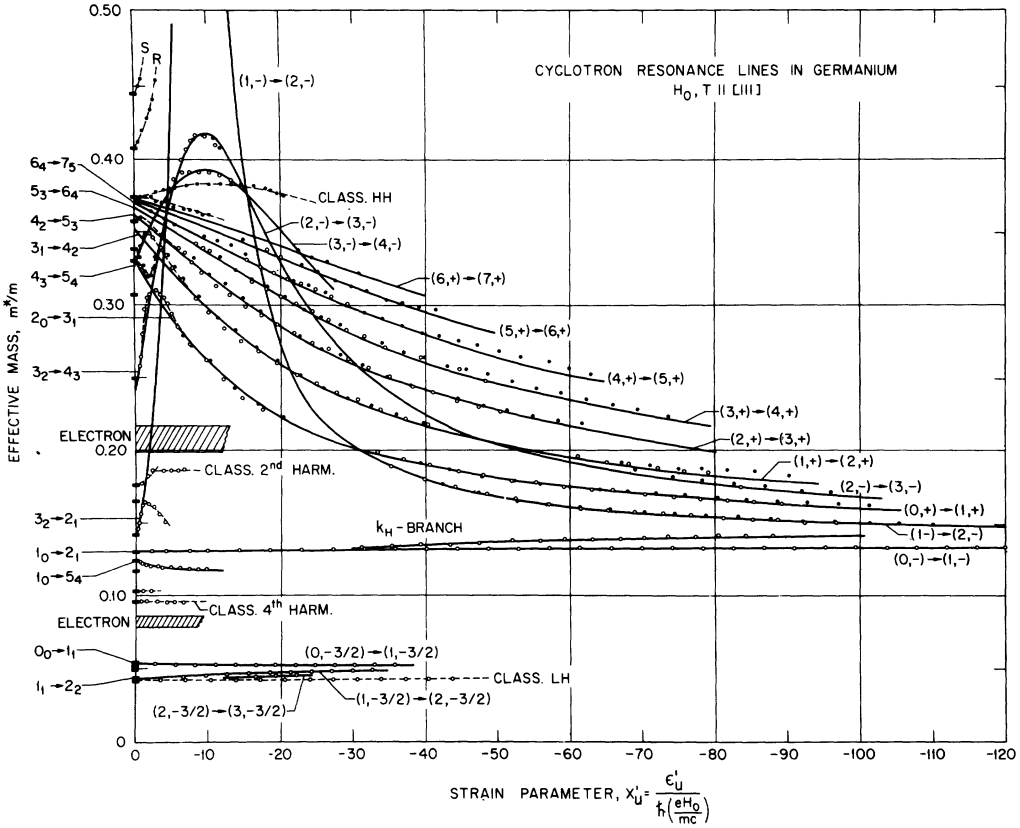

FIG. 9. Stress dependence of the hole cyclotron resonances for $\vec{H}_0$, $T \| [111]$. The runs were made at 53 GHz and at both 1.2°K (circles) and 4.2°K (points). The solid rectangles at the left border give the quantum line positions in unstrained Ge. The hatched areas indicate the part of the spectrum obscured by strong electron resonances. Transitions near $x'_u = 0$ are labeled by the N_n notation given in Fig. 1. At large x'_u we switch to the (n, M_J) scheme used in Fig. 4 (usually abbreviated for the $M_J = \pm\frac{1}{2}$ resonances by dropping the $\frac{1}{2}$). The solid curves were calculated. At large stresses a small empirical correction (~2% at maximum stress), estimated from the shift of the $(0,-) \to (1,-)$ transition, has been included in the solid curves to take into account the strain interaction with the $J = \frac{1}{2}$ band. The dashed curves drawn through data points serve as an aid to the eye.

shoulder on the high-field side of the $(0, -\frac{1}{2}) \to (1, -\frac{1}{2})$ ("primary") resonance. (ii) With increase in stress the secondary resonance shifts gradually away from the primary line towards higher m^*/m. (iii) At fixed temperature the intensity of the secondary resonance diminishes (weakly) with increasing stress. (iv) At fixed stress the intensity increases (roughly like the primary resonance) as the temperature is lowered from 4.2 to 1.2°K. We find that the anomalous resonance originates from a secondary critical point associated with the $(0, -\frac{1}{2}) \to (1, -\frac{1}{2})$ transition. To see this we refer to Fig. 12 where we have plotted m^*/m (calculated as a function of x'_u) vs $\zeta = k_H(eH_0/\hbar c)^{-1/2}$ for the $(0, -\frac{1}{2}) \to (1, -\frac{1}{2})$ transition. At $\zeta = 0$ lies the primary critical point which remains essentially fixed at $m^*/m = 0.130$ independent of x'_u. At $x'_u \sim -10$, a secondary critical point (a "maximum") begins to take shape near $\zeta = 0.4$. As $|x'_u|$ increases this critical point shifts to higher m^*/m and ζ, but not until $|x'_u| \gtrsim 30$ is it resolvable from the primary resonance (In Fig. 12 there also exists a second noncentral critical point, the sharp "minimum," but it does not contribute observable structure to the spectrum.) The ζ shift, through the dispersion of $E(\zeta)$, reduces the Boltzmann factor for the noncentral resonance, so its intensity gradually diminishes with increasing stress. To check this assignment we have computed line shapes (from the "spectral function" given in Paper I) which we find replicate the secondary as well as the primary resonances in the observed line shapes. Furthermore, in Fig. 9 the curve labeled "k_H branch" obtained from the computed secondary peaks closely fits the data. This confirms our identification.

Having thus assigned the "anomalous" line we have completed the identification of all lines ob-

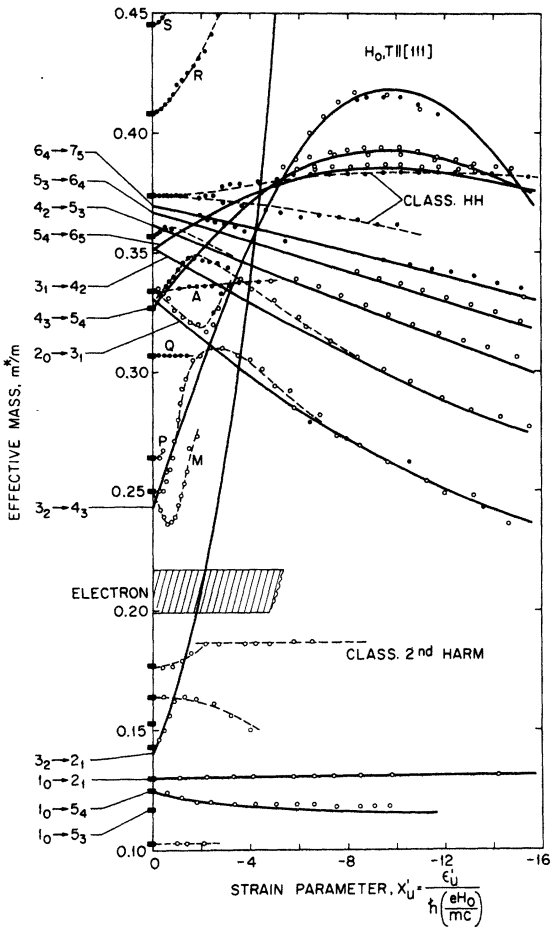

FIG. 10. Expanded plot of the low-stress region in Fig. 9 showing in greater detail the behavior of the quantum cyclotron resonances as the valence bands begin to decouple.

served at high stress. To check the converse statement—namely, that all predicted structure is accounted for—we have "synthesized" the entire quantum spectrum with k_H effects included by computing the "spectral function" for $x'_u = -100$. (Strictly speaking, this does not quite correspond to a physical situation; for, as we pointed out earlier, constant "x" is not equivalent to constant stress. It is, however, a good approximation for this case where all structure is clustered in one region of the spectrum.) The computed spectra match the spectra recorded at large stress, so we conclude that all transitions not seen are either too weak or too broad to be resolved as distinct lines.

For $|x'_u| < 20$, the stress dependence of the hole resonances plotted in Fig. 9 becomes rather complicated. An expanded view in Fig. 10 shows a part of this region in more detail. As $|x'_u|$ decreases to zero, the effective masses of the $M_J = +\frac{1}{2}$ line series increase monotonically; whereas the effective masses for the $M_J = -\frac{1}{2}$ series first increase rapidly and then pass over a maximum near $x'_u \approx -9$ as the energy levels "pinch" together (or cross). The rapidly shifting $M_J = -\frac{1}{2}$ lines are only observed in the immediate vicinity of $x'_u \approx -9$, where m^*/m is "stationary." As x'_u approaches 0, the data deviate from the computed ($k_H = 0$) curves to an increasing extent as k_H effects become pronounced. A number of the transitions in Fig. 10 exhibit curious behavior in the vicinity of $x'_u = -2$ due to level crossings. In particular, in Fig. 10 the transitions $2_0 \rightarrow 3_1$ and $3_2 \rightarrow 4_3$ appear to approach and repel one another as the 3_1 and 3_2 levels cross in Fig. 4. Although these levels seemingly cross without interaction in Fig. 4 ($k_H = 0$), actually both are $K = 3$ states and interact strongly when $k_H \neq 0$ (and the parity selection rule is broken). There is also evidence of level-crossing effects near $x'_u \sim -2$ among some higher transitions.

In addition to lines which can be followed continuously from low to high stress, there are a number of lines in Figs. 9 and 10 which exist only at low stress. Lines M, P, Q, A, R, and S appear in the spectrum at $x'_u = 0$ but rapidly diminish in intensity and disappear as the stress is turned up. They do not match with any of the solid curves which represent all low-lying transitions expected for $k_H = 0$. In Paper IV we show that these transitions are associated with noncentral critical points. We believe that as the bands become ellipsoidal under applied uniaxial stress these critical points at $k_H \neq 0$ shift to higher k_H (for one example, see Fig. 12) and "depopulate" causing the resonances to disappear. The data in Fig. 10 show clearly that the $m^*/m = 0.250$ resonance at zero stress is composed of an unresolved triplet of lines M, P, and $3_2 \rightarrow 4_3$ which split apart and are resolved when stress is applied. A triplet at $T = 0$ is predicted by our calculations in Paper IV. (Line P can be seen in certain samples of unstressed Ge, in particular when $\vec{H}_0$ is rotated a few degrees off the [111] axis, as a partially resolved shoulder at $m^*/m = 0.264$.)

We see in Figs. 9 and 10 that the classical cyclotron resonance lines—the heavy hole, the light hole, and the second and fourth harmonics of the heavy hole (the third harmonic is forbidden for $\vec{H}_0 \parallel [111]$)—persist even up to substantial uniaxial stresses ($T \sim 1000$ kg/cm^2 for the heavy hole). These resonances come from transitions between Landau levels deep in the bands which are not decoupled until T becomes very large. Under stress the heavy-hole resonance splits into two components; the upper and lower branches seem to follow the $M_J = -\frac{1}{2}$ and $+\frac{1}{2}$ series, respectively. The light hole resonance also shifts with T (not enough to be seen in Fig. 8) but does not split. As stress

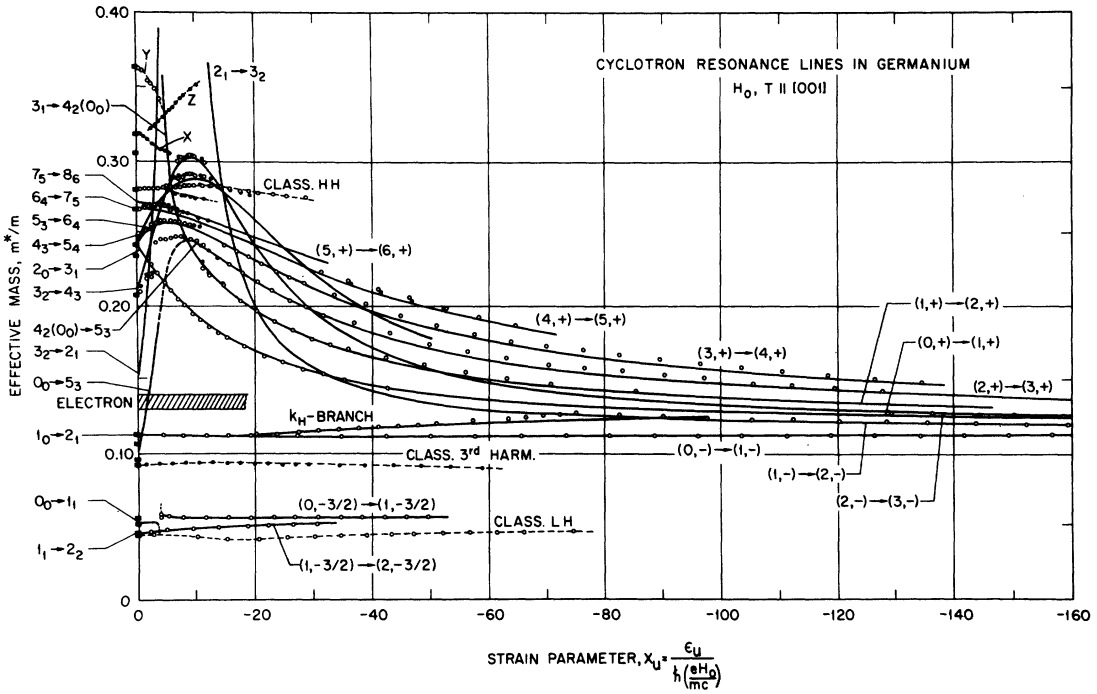

FIG. 11. Stress dependence of the hole cyclotron resonances for $\vec{H}_0$, $T \parallel [001]$. The remarks in the caption of Fig. 9 apply *mutatis mutandis*.

increases the light hole effective mass, initially $m^*/m = 0.0421$ at $T = 0$, first decreases to a minimum value of $m^*/m = 0.0416$ at $x_u' \approx -14$, and then increases toward the $M_J = \pm\frac{3}{2}$ series limit [the $(0, -\frac{3}{2}) \rightarrow (1, -\frac{3}{2})$ line].

The lines $1_0 \rightarrow 5_4$, $1_0 \rightarrow 5_3$, and $1_0 \rightarrow 2_1$ comprise the fundamental triplet [see Sec. IV D 2]. The transition $1_0 \rightarrow 5_4$ (the strongest member of the triplet at $x_u' = 0$) is forbidden at $k_H = 0$; the solid curves which fit these data in Figs. 9 and 10 were taken from the peaks of line profiles computed from the spectral function.

A few weak lines in Fig. 9 and 10 appear without labels; the uniaxial stress experiments provide little help in establishing their identifications. The resonances $m^*/m = 0.103$ and $m^*/m = 0.165$, 0.176 could be quantum fourth and second harmonics, respectively. The two quantum lines near the light hole at $m^*/m = 0.050$ and 0.052 and a line at $m^*/m = 0.153$ disappear as soon as stress is applied. More information about these lines is given in Paper IV.

2. $T \parallel [001]$

The behavior of the cyclotron resonance spectrum for $T \parallel [001]$ in Fig. 11 is rather similar to that just outlined for $T \parallel [111]$. Here we shall merely emphasize the more important points and call attention to the differences.

Overall the patterns of the three main line series $M_J = -\frac{1}{2}, +\frac{1}{2}$, and $-\frac{3}{2}$ in Fig. 11 closely duplicate those described for $T \parallel [111]$. In particular, we take note of the important "fixed" fundamental transitions $(0, -\frac{1}{2}) \rightarrow (1, -\frac{1}{2})$ and $(0, -\frac{3}{2}) \rightarrow (1, -\frac{3}{2})$, which mark the $\pm\frac{1}{2}$ and $\pm\frac{3}{2}$ series limits, respectively. Again a k_H branch accompanies the $(0, -\frac{1}{2}) \rightarrow (1, -\frac{1}{2})$ transition. The transitions $3_1 \rightarrow 4_2(0_0)$ and $4_2(0_0) \rightarrow 5_3$ behave anomalously near $x_u \sim -4$ due to the "level crossing" of the states 0_0 and 4_2 (see Fig. 3). [This is responsible for the switch in labels 0_0 to $4_2(0_0)$ in Fig. 11 which is intended to mean that the character of $4_2(0_0)$ is like 4_2 for $|x_u| > 4$ but passes continuously to 0_0 as x_u goes to zero.] This effect is also responsible for the "break" at $x_u \sim -4$ in the transition $0_0 \rightarrow 1_1$. As noted previously classical lines persist in the spectrum to moderately large stresses. The stress dependence of the light hole is quite marked; it decreases from $m^*/m = 0.0440$ at $x_u = 0$, reaches a minimum value $m^*/m = 0.0423$ near $x_u = -20$, and then increases toward the $M_J = \pm\frac{3}{2}$ series limit. Lines X, Y, and Z, apparently unrelated to any of the $(k_H = 0)$ calculated transitions, are believed to arise from non-central critical points. We are unable to measure the stress dependence of the lines at $m^*/m = 0.056$, 0.096, 0.241, and 0.305.

C. Deformation potentials: D_u and D_u'

Previously, we mentioned that the fitting of the curves in Figs. 9–11 for the $T \parallel [111]$ and $T \parallel [001]$

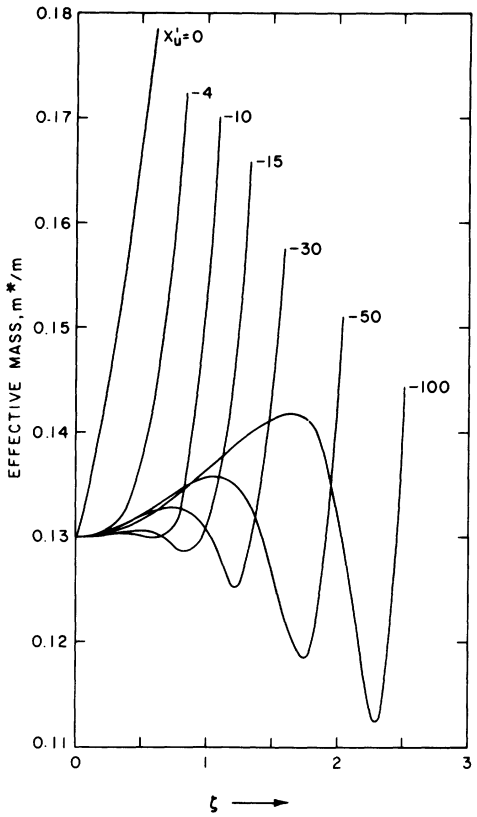

FIG. 12. Dispersion of the fundamental transition $(0, -\frac{1}{2}) \rightarrow (1, -\frac{1}{2})$ ($1_0 \rightarrow 2_1$ at zero stress) for $\vec{H}_0$, $T \| [111]$. The curves were calculated for various values of x'_u (and the same band parameters as Fig. 2). We express k_H in dimensionless form $\zeta = k_H(eH_0/\hbar c)^{-1/2}$.

cases involved one adjustable parameter each, a deformation potential. Our procedure for making the fit entails, first, converting the measured values of stress to units proportional to the strain parameter x_u or x'_u by dividing stress by H_0, the magnetic field at resonance (or, equivalently, by m^*/m). Next, by scaling the units, i.e., choosing the proportionality constants so the theoretical curves match the data, we determine the deformation potentials (in eV)

$$D_u = +3.32 \pm 0.20 \quad \text{for } T \| [001],$$
$$D'_u = +3.81 \pm 0.25 \quad \text{for } T \| [111] \tag{27}$$

(also listed in column 2 of Table II). That the signs of D_u and D'_u are both *positive* is assured by the over-all behavior of the quantum spectrum as a compressive stress is applied.[44] It is worth noting that this measurement of D_u and D'_u derives only from strain interactions *within* the $J = \frac{3}{2}$ multiplet and does not involve mass shifts which result from interactions with other bands. (In fact the gross shifts of the quantum lines considered here are nearly two orders of magnitude greater than the latter kind.) For comparison we include in Table II (column 3) values for D_u and D'_u measured by combined resonance experiments in Paper III (using a different and independently calibrated strain apparatus). We see that the two sets are nearly identical. A further check on the consistency of our results can be made. From Eq. (27) we obtain a value for the splitting anisotropy parameter

TABLE II. Valence-band uniaxial deformation potentials D_u and D'_u (in eV) and splitting-anisotropy parameter β for Ge.

	Cyclotron resonance (this work)	Combined resonance[a]	Calculated	Previous experiments
D_u	$+3.32 \pm 0.20$	3.21 ± 0.20	3.45[b]	3.2 ± 0.3,[c] 4.05 ± 0.45,[d] 3.14 ± 0.20[e]
			3.45[f]	3.6 ± 0.6,[g] 3.6 ± 0.3,[h] 3.9 ± 0.3[i]
D'_u	$+3.81 \pm 0.25$	3.91 ± 0.25	4.85[b]	6.1 ± 1.3,[c] 4.07 ± 0.43,[d] 4.00 ± 0.20[e]
			4.24[f]	3.03 ± 0.35,[g] 3.55 ± 0.35,[h] 4.07 ± 0.26[i]
β	$+0.69 \pm 0.01$			

[a] J. C. Hensel and K. Suzuki, Ref. 14.
[b] L. R. Saravia and D. Brust, Ref. 63.
[c] J. J. Hall, Ref. 58.
[d] A. M. Glass, Ref. 59.
[e] H. Fujiyasu, K. Murase, and E. Otsuka, Ref. 13(b).
[f] P. J. Melz, Ref. 64.
[g] I. Balslev, Ref. 60.
[h] I. Balslev, Ref. 61.
[i] F. H. Pollak and M. Cardona, Ref. 62.

$$\beta=\frac{\epsilon_u'}{\epsilon_u}=\frac{D_u'}{D_u}\frac{\frac{1}{2}s_{44}}{s_{11}-s_{12}}=0.69\pm0.05,$$

which coincides with the more exact result $\beta=0.69\pm0.01$ determined in Sec. IV F directly from the measured effective masses for $T\parallel[110]$.

D. Fundamental transitions

Let us now focus our attention on the fundamental transitions $(0,-\frac{1}{2})\rightarrow(1,-\frac{1}{2})$ and $(0,-\frac{3}{2})\rightarrow(1,-\frac{3}{2})$, which we shall use to determine γ_1, γ_2, and γ_3 and, additionally, D_w and D_w'. The sharpness of these resonances ($2\Delta H/H_0\lesssim 0.015$, where $2\Delta H$ is the full linewidth at one-half-maximum), unmatched by any others in the spectrum, plus the fact that their effective masses are nearly independent of strain interactions within $J=\frac{3}{2}$ and simply interpretable makes them uniquely suited for this purpose.

1. Dependence of the lines on stress

a. Determination of effective-mass band parameters γ_1, γ_2, and γ_3. In Figs. 13(a), 13(b), and 13(c) we plot on expanded scales the peak positions

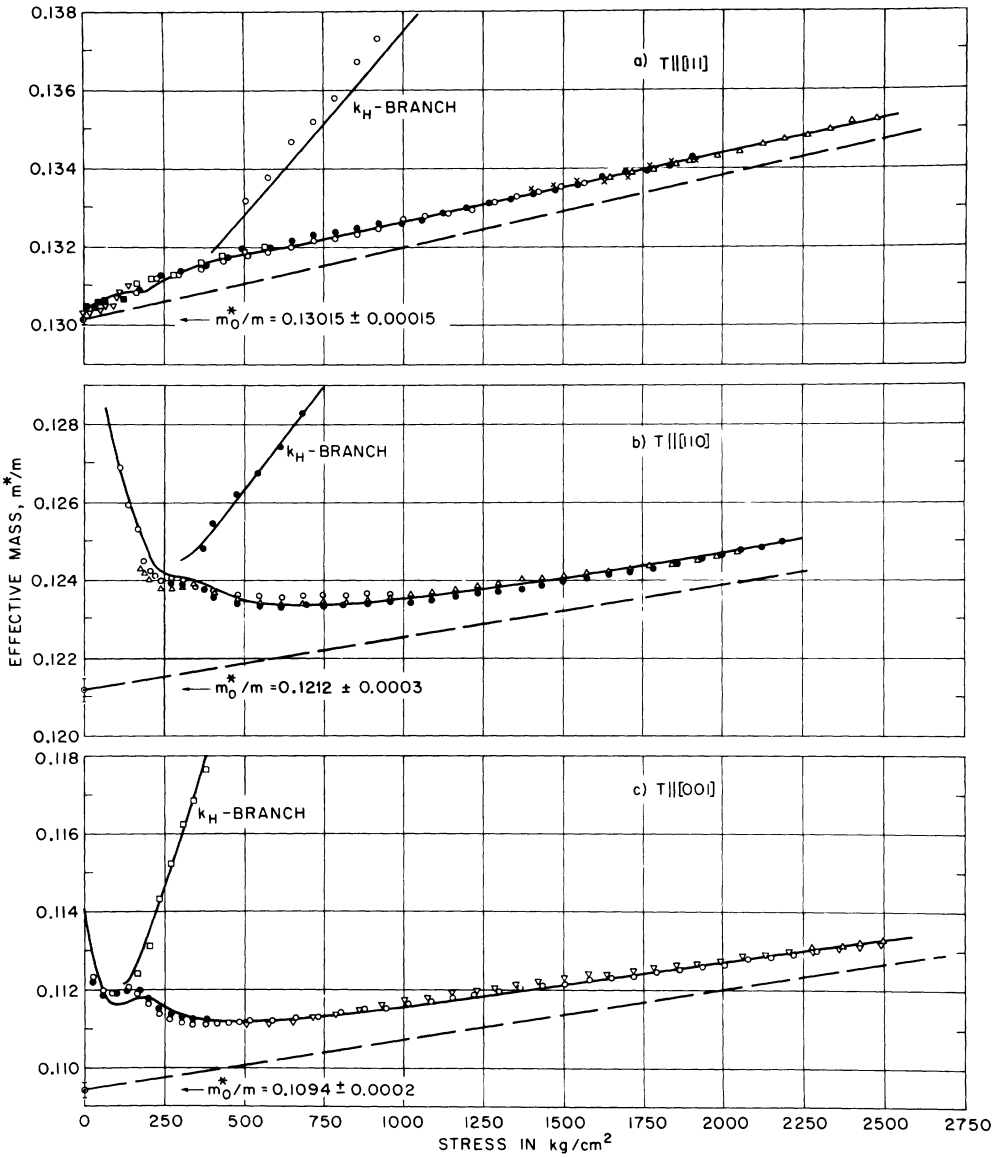

FIG. 13. Stress dependence of the $\vec{H}_0\parallel T$ fundamental transitions $(0,-\frac{1}{2})\rightarrow(1,-\frac{1}{2})$. The effective masses were measured at 1.2°K from the peaks of the resonances. The experimental uncertainties of m^*/m are approximately the height of the plotted points. Different runs are distinguished by distinctive symbols. The fits to the data determine m_0^*/m (given in the figure) and the linear mass-shift parameters α: (a) $T\parallel[111]$: $\alpha=-(10.5\pm0.7)\times10^{-5}$ cm^2/kg; (b) $T\parallel[110]$: $\alpha=-(9.4\pm1.1)\times10^{-5}$ cm^2/kg; (c) $T\parallel[001]$: $\alpha=-(10.8\pm0.8)\times10^{-5}$ cm^2/kg.

of the $M_J = -\frac{1}{2}$ fundamental transitions for $H_0 \parallel T$ with T along [111], [110], and [001], respectively. On the expanded scale we see that these resonances depend weakly on stress. This arises from two effects. First, they experience a linear shift because of the strain interactions between the $J=\frac{3}{2}$ and $J=\frac{1}{2}$ bands. (In order not to distort the linear form, we have plotted the data in Fig. 13 against T rather than x.) Second, the resonances shift slightly as the strain decouples the nearly "pure" $(0, -\frac{1}{2})$ and $(1, -\frac{1}{2})$ eigenstates from the other Landau states of $J=\frac{3}{2}$. This shift consists essentially of two parts: (a) a k_H-dependent part which varies as does k_H^2/T as $T \to \infty$, and (b) a warping part which varies as does $(\gamma_3 - \gamma_2)^2/T$ as $T \to \infty$. Part (a) causes a strain-dependent asymmetry in the line shape and concomitant shift of the resonance peak while part (b) gives rise to a strain dependence in the $k_H = 0$ effective masses (except for $\vec{H}_0 \parallel [111]$ whereupon it vanishes even at zero stress). As $T \to \infty$ both effects vanish as does $1/T$, and the effective mass asymptotically approaches m_0^*/m given by Eq. (16). In summary, the position of the resonance peak will be given by Eq. (25) augmented with *small* (stress-dependent) decoupling shift $\delta(T)$,

$$\frac{m}{m^*} = \frac{m}{m_0^*} - \alpha T + \delta(T) . \tag{28}$$

In the analysis[45] of experimental data in this section we do not assume any functional form for $\delta(T)$; instead we determine it numerically from the shift of the peaks of computed line profiles from their unperturbed position at m_0^*/m (computed). It should be noted that the demands on accuracy for $\delta(T)$ are not severe, since $\delta(T)$ is quite small [except close to $T=0$, $\delta(T) \lesssim 1\%$ of m/m_0^*]. The line shapes are calculated as a function of T from the spectral function using a trial set of band parameters (those estimated from the raw data in Figs. 13 and 14 would do). We obtained the best fits of the computed line shapes (including the k_H branch) to the resonances recorded at 1.2 °K by assuming $\tau \sim 3.2 \times 10^{-10}$ sec for the Lorentzian component lines and an effective temperature (see Sec. IV D) of $\Theta^* = 2.5$ °K. (The optimum value of τ depended slightly upon stress while the relative amplitude of the primary line to its k_H-branch was found to depend upon Θ^*.) This estimate of $\delta(T)$ is not very sensitive to the initial choice of values for the band parameters (nor to the value assumed for Θ^*). The entire analysis could be iterated, of course, for greater accuracy; but we found this unnecessary.

Substituting these estimates for $\delta(T)$, we fit the data with Eq. (28) and evaluate m_0^*/m and α. The fits obtained are shown by the solid curves in Fig. 13; the linear part of Eq. (28), which defines the $M_J = \pm\frac{1}{2}$ series limit, is represented by the dashed lines having slope $-(m_0^*/m)^2\alpha$ and intercept m_0^*/m.

Our analysis for $T \parallel [001]$ and $T \parallel [111]$ determines $m_\perp/m$, $\alpha_\perp$ and $m_\perp'/m$, $\alpha_\perp'$, respectively, for $M_J = -\frac{1}{2}$ which we list in Table III. The effective masses $m_\perp'$ and $m_\perp$ in Table III have been corrected for the magnetic shifts $\Delta(m^*/m) = -0.00015$ for $T \parallel [111]$ and $< 10^{-4}$ for $T \parallel [001]$, estimated from Eqs. (19) and (20). The experimental effective masses $m_\perp'$ and $m_\perp$ give

$$\gamma_1 - \gamma_3 = 7.692 \pm 0.010 , \tag{29}$$

$$\gamma_1 - \gamma_2 = 9.141 \pm 0.018 \tag{30}$$

from the relations in Table I.

The data for $T \parallel [110]$ $(\vec{H}_0 \parallel T)$ in Fig. 13 can be fully analyzed only in conjunction with measurements for the (two) "transverse" cases for $\vec{H}_0 \perp T$. We defer this to Secs. IV E and IV F.

The experimental data for the $M_J = -\frac{3}{2}$ fundamental transitions measured at 1.2 °K are shown on

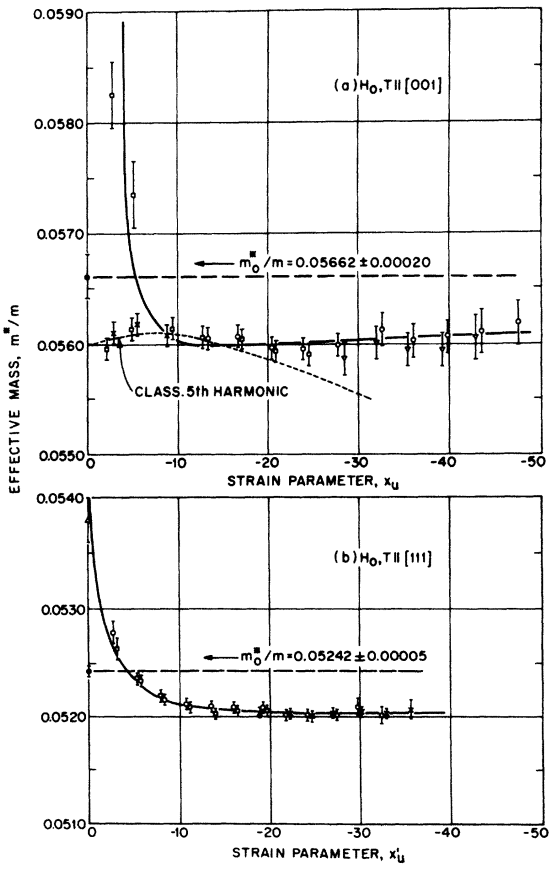

FIG. 14. Stress dependence of the $\vec{H}_0 \parallel T$ fundamental transitions $(0, -\frac{3}{2}) \to (1, -\frac{3}{2})$. The effective masses were measured at 1.2 °K from the peaks of the resonances. The fits to the data determine m_0^*/m (given in figure) and α ($\alpha \approx 0$ for both $T \parallel [111]$ and [001]).

TABLE III. Components of the effective-mass tensors (in units of the free-electron mass m) and the linear effective-mass shift parameters (in units of cm^2/kg) for Ge subjected to a uniaxial compressive stress along the principal crystallographic directions.

	$T \parallel [001]$	$T \parallel [111]$	$T \parallel [110]$
	$m_\perp = 0.1094 \pm 0.0002$	$m'_\perp = 0.13000 \pm 0.00015$	$m_1 = 0.117 \pm 0.001$
	$m_\parallel = 0.0458 \pm 0.0004$	$m'_\parallel = 0.0403 \pm 0.0003$	$m_2 = 0.126 \pm 0.001$
			$m_3 = 0.0420 \pm 0.0003$
$M_J = \pm\frac{1}{2}$			
	$\alpha_\perp = -(10.8 \pm 0.8) \times 10^{-5}$	$\alpha'_\perp = -(10.5 \pm 0.7) \times 10^{-5}$	$\alpha_1 = -(11.7 \pm 2.0) \times 10^{-5}$
	$\alpha_\parallel = +(24 \pm 5) \times 10^{-5}$	$\alpha'_\parallel = +(17 \pm 5) \times 10^{-5}$	$\alpha_2 = -(6.4 \pm 1.9) \times 10^{-5}$
			$\alpha_3 = +(25.9 \pm 5.5) \times 10^{-5}$
$M_J = \pm\frac{3}{2}$	$m_\perp = 0.05662 \pm 0.00020$	$m'_\perp = 0.05242 \pm 0.00005$	
	$\alpha_\perp \sim 0$	$\alpha'_\perp \approx 0$	

expanded scales in Figs. 14(a) and 14(b) for $\vec{H}_0$, $T \parallel [001]$ and $\vec{H}_0$, $T \parallel [111]$, respectively. The experimental uncertainties indicated by the error flags increase at higher stresses reflecting the worsening cyclotron-resonance signal-to-noise ratio as the $M_J = \pm\frac{3}{2}$ bands depopulate; accurate measurements of the $M_J = -\frac{3}{2}$ resonances became impossible for $T > 230$ kg/cm^2.

The first case we consider is $T \parallel [111]$ in Fig. 14(b). The analysis for the $M_J = -\frac{3}{2}$ transitions is similar to that discussed above for $M_J = -\frac{1}{2}$. Equation (28) again applies except we do not anticipate a contribution from the linear term αT inasmuch as the $M_J = -\frac{3}{2}$ states cannot admix with states in the $J = \frac{1}{2}$ band. Having computed $\delta(T)$ as before we fit the data with Eq. (28) to determine m_0^*/m and α. The fit is shown by the solid curve in Fig. 14(b); the dashed line is the series limit, given by the first two terms of Eq. (28). We see that the series limit has zero slope as expected, i.e., $\alpha \approx 0$. Also we note that (at large stresses) the $M_J = -\frac{3}{2}$ resonances approach the series limits from *below*—opposite to the $M_J = -\frac{1}{2}$ fundamental lines. The intercept of the series limit gives $m'_\perp/m\,(M_J = -\frac{3}{2}) = 0.05242 \pm 0.00005$ from which we get the relation

$$\gamma_1 + \gamma_3 = 19.077 \pm 0.018 \ , \tag{31}$$

with the help of Table I.

The excellent convergence of the $M_J = -\frac{3}{2}$ transition for $\vec{H}_0 \parallel [111]$ to the series limit in Fig. 14(b) warrants some comment. This behavior is unexpected *a priori* since the two participating Landau states $(0, -\frac{3}{2})$ and $(1, -\frac{3}{2})$ are not decoupled states. A clue can be found in Fig. 4 which shows that each lies *between* the pair of states which perturb it, $(0, +\frac{3}{2})$, $(2, -\frac{1}{2})$ and $(1, +\frac{3}{2})$, $(3, -\frac{1}{2})$, respectively, such that the interactions partially cancel one another. This cancellation is essentially responsible for the rapid convergence of $\delta(T)$ to zero as stress is applied and accounts for the nonmonotonic behavior of $\delta(T)$ near zero stress.

To be more definite it is instructive to derive by perturbation theory the decoupling shift $\delta(T)$ (we neglect the k_H-dependent part) for the $M_J = -\frac{3}{2}$ fundamental transition for $\vec{H}_0$, $T \parallel [111]$. Except for its rapid change near zero stress [cf. Fig. 14(b)], we find that $\delta(T)$ is elsewhere bounded, and at

$$-x'_u(\max) = (\gamma_1 - \gamma_3) + \tfrac{1}{2}\kappa + (\sqrt{3}/9\kappa)(\gamma_2 + 2\gamma_3)^2 + \tfrac{1}{2}\sqrt{3}\gamma_3 \tag{32}$$

$[x'_u(\max) \approx -27$ for Ge], it reaches an extremum (minimum effective mass) which fixes an upper bound

$$\delta_{\max} = +\tfrac{4}{3}(\gamma_2 - \gamma_3)^2 \{(2 + \sqrt{3}) \times [(2/9\kappa)(\gamma_2 + 2\gamma_3)^2 + \gamma_3]\}^{-1}, \tag{33}$$

for the shift of the inverse effective mass from m/m_0^* at $k_H = 0$. [Numerically Eq. (33) gives an effective mass shift of $-(m_0^*/m)^2\delta_{\max} = -1.73 \times 10^{-3}$, compared to the more "exact" result -1.71×10^{-3} from eigenvalues obtained on the computer.] The expression for the upper bound in Eq. (33) suggests that the convergence will be rapid whenever the warping $\gamma_3 - \gamma_2$ is small; so we conclude that the transition $(0, -\frac{3}{2}) \rightarrow (1, -\frac{3}{2})$ may have rather general applicability[46] for band parameter measurements.

Turning now to the $T \parallel [001]$ case in Fig. 14(a) we discover that unfortunately there is interference from a nearby transition, the classical fifth harmonic of the heavy hole, making an accurate determination of the position of the fundamental transition $(0, -\frac{3}{2}) \rightarrow (1, -\frac{3}{2})$ impossible. The expected location of the fifth harmonic is roughly indicated by the dashed curve in Fig. 14(a). Near $x_u \sim -5$ two lines can be seen; but elsewhere the fifth harmonic component is unresolved. An effort to correct the measurements for this contribution seems too uncertain to us to be worthwhile. Nevertheless, to get a rough idea of the effective masses, we fit the data with Eq. (28) [ignoring the fifth harmonic contribution to $\delta(T)$] and obtain $m_\perp/m\,(M_J = -\frac{3}{2}) = 0.05662 \pm 0.00020$ and $\alpha \sim 0$. This gives γ_1

$+\gamma_2 = 17.662 \pm 0.060$. Within its rather wide error limits this overlaps the value 17.624 ± 0.030 obtained from Eqs. (29)–(31) which assures us that the [001] data are not inconsistent with the rest.

Summarized below are the precision values of the valence band inverse mass parameters for Ge evaluated directly from Eqs. (29)–(31):

$$\gamma_1 = 13.38 \pm 0.02,$$
$$\gamma_2 = 4.24 \pm 0.03, \quad (34)$$
$$\gamma_3 = 5.69 \pm 0.02.$$

The signs of all three parameters are *positive*. In Sec. V A we shall compare these values with the results of previous cyclotron-resonance experiments.

b. Signs of γ_2, γ_3 and D_u *and* D_u'. In our discussion so far we have consistently taken positive signs for γ_2, γ_3 and D_u, D_u', this choice for the latter being equivalent to the order $\epsilon_{\pm 1/2} > \epsilon_{\pm 3/2}$ [Fig. 1(b)] for the strain-split valence-band states. It is worthwhile to pause at this point to outline the arguments which have led to these assignments.

By themselves the m_0^*/m values of the fundamental transitions just determined give only the magnitudes of γ_2 and γ_3; further experimental information is required if the signs are to be defined. First, the relative intensities at low temperatures of the "high-mass" and "low-mass" fundamental transitions can decide from which of the strain-split states each originates. For both $T \parallel [001]$ and [111] the low-mass fundamental transition derives from the band that depopulates with increasing compressive stress (see spectra in Figs. 7 and 8) which implies that $\gamma_2 D_u > 0$ and $\gamma_3 D_u' > 0$. Next, the existence of the linear effective-mass shift ($\alpha \neq 0$) of the stronger fundamental resonance (high mass) (and conversely the absence of a linear shift for the weaker transition) establishes the ordering $\epsilon_{\pm 1/2} > \epsilon_{\pm 3/2}$ or, equivalently, D_u, $D_u' > 0$. It follows that γ_2 and γ_3 are both *positive*. Another line of reasoning leads to the same conclusion. The nature of the quantum cyclotron-resonance spectra in Figs. 9–11 near and at zero stress is consistent only with the signs γ_2, $\gamma_3 > 0$. (Hence, D_u, $D_u' > 0$.) An entirely different quantum spectrum would obtain if either or both γ_2 and γ_3 were negative.

c. *Spin-dependent deformation potentials.* From the parameters $\alpha_\perp$ and $\alpha_\perp'$ summarized in Table III we can determine the "mixing" deformation potentials D_w and D_w', respectively. Using Eqs. (21) and (22) we obtain

$$\Gamma_2 D_w = 9.79 \pm 0.60 \text{ eV}, \quad (35)$$
$$\Gamma_3 D_w' = 16.0 \pm 1.0 \text{ eV} \quad (36)$$

based on the value[47] $\Lambda = 0.290 \pm 0.005$ eV for the spin-orbit splitting. Making the approximations $\Gamma_2 = \gamma_2$ and $\Gamma_3 = \gamma_3$ and using Eq. (34) we evaluate the deformation potentials

$$D_w = +2.31 \pm 0.17 \text{ eV}, \quad (37)$$
$$D_w' = +2.81 \pm 0.20 \text{ eV}. \quad (38)$$

As a cross check let us consider the "redundant" case[48] $T \parallel [110]$ for which the linear mass shifts are completely defined in terms of D_w and D_w'. Using the numbers in Eqs. (37) and (38) we calculate[48] the linear shift coefficient for $\vec{H}_0$, $T \parallel [110]$ to be $\alpha(110) = -(10.2 \pm 0.7) \times 10^{-5}$ cm^2/kg which is consistent with the experimental value $\alpha(110) = -(9.4 \pm 1.1) \times 10^{-5}$ cm^2/kg from the data in Fig. 13(b).

We note that D_w and D_w' are significantly smaller than the corresponding deformation potentials D_u and D_u' in Eq. (27). [In comparing these, we hasten to point out, the uncertainties of the differences are somewhat less than the absolute uncertainties of either, since we measured both on the same apparatus (and in some cases during the same run); so the most uncertain factor, the magnitude of the strain, is partly removed from the comparison.] As mentioned earlier this difference can be explained by the existence[49] of spin contributions to the deformation potentials. We can decompose D_u, D_u' and D_w, D_w' into spin-dependent and spin-independent components using the relations[50]

$$D_u = \tfrac{1}{2}D_2 + E_2, \quad D_w = \tfrac{1}{2}(D_2 - E_2),$$
$$D_u' = \tfrac{1}{2}D_3 + E_3, \quad D_w' = \tfrac{1}{2}(D_3 - E_3)$$

to get (in eV)

$$\tfrac{1}{2}D_2 = 2.65 \pm 0.18, \quad E_2 = 0.67 \pm 0.13, \quad (39)$$
$$\tfrac{1}{2}D_3 = 3.14 \pm 0.22, \quad E_3 = 0.67 \pm 0.15. \quad (40)$$

Further discussion follows in Sec. V B.

2. Fundamental triplet

It is well known that for $\vec{H}_0 \parallel [111]$ two low-lying Landau states in unstressed Ge, 1_0 and 2_1 in our nomenclature, decouple from the rest of the manifold at $k_H = 0$ and have the eigenvalues (in units of $\hbar e H_0/mc$)

$$\epsilon(n) = (\gamma_1 - \gamma_3)(n + \tfrac{1}{2}) - \tfrac{1}{2}\kappa - \tfrac{13}{8}q, \quad n = 0, 1. \quad (41)$$

Corresponding to the cyclotron resonance transition $1_0 \rightarrow 2_1$ ($n = 0 \rightarrow 1$), we would expect a line to appear in the spectrum at $m^*/m = (\gamma_1 - \gamma_3)^{-1}$; this coincides with the position of the *high-stress* fundamental transition $(0, -\tfrac{1}{2}) \rightarrow (1, -\tfrac{1}{2})$, which evolves from $1_0 \rightarrow 2_1$ as a [111] stress is applied (see Fig. 4). The simple connection between the line position and the quantity $\gamma_1 - \gamma_3$ would make the $1_0 \rightarrow 2_1$ transition useful for the determination of the band parameters. However, experimental efforts[4,25] in the past to locate and identify this line in Ge have proved to be unexpectedly difficult. The problem is simply this: At approximately the predicted posi-

tion of the resonance, $m^*/m = 0.133$, indeed a line does appear; but it is broad and very weak—little resembling the low-lying allowed transition sought. On the other hand, a much stronger transition is observed nearby; but its position, $m^*/m = 0.125$, cannot be reconciled with the known values of the band parameters.

We have resolved this quandary by studying the spectra for $\vec{H}_0 \| [111]$ as very small uniaxial stresses are applied. The results are illustrated in Fig. 15. In Fig. 15(a), a trace taken at zero stress, we see the prominent line at $m^*/m = 0.125$ mentioned above. Careful examination also reveals two additional very weak lines, one on either side, at $m^*/m = 0.117$ and 0.133. These three lines together comprise the "fundamental" triplet. In Fig. 15(b) we see the effects of a small uniaxial stress 30 kg/cm^2 applied along the [111] axis. The line originally at $m^*/m = 0.133$ has dramatically increased in amplitude and has shifted slightly to $m^*/m = 0.131$, precisely the location of the fundamental resonance; whereas the line originally at $m^*/m = 0.125$ has decreased in amplitude and has shifted to lower mass $m^*/m = 0.120$. We were unable to track the $m^*/m = 0.117$ line in Fig. 15(a) when stress was applied. In the trace in Fig. 15(c) taken at higher stress, 120 kg/cm^2, the upper line maintains its position at $m^*/m = 0.131$ as it becomes still narrower and stronger; the lower line continues to shift to $m^*/m = 0.118$ while becoming broader and weaker (it eventually vanishes as the stress is increased further). The positions of these lines are plotted as a function of x'_u in Fig. 10. From the evolution of the spectra in Fig. 15, we establish that the weak line at $m^*/m = 0.133$ in unstressed Ge is, in fact, the one which develops into the fundamental resonance under applied stress, thus identifying it as the line $1_0 \rightarrow 2_1$. But the questions remain, why is it so weak at zero stress and what is the origin of the other two lines?

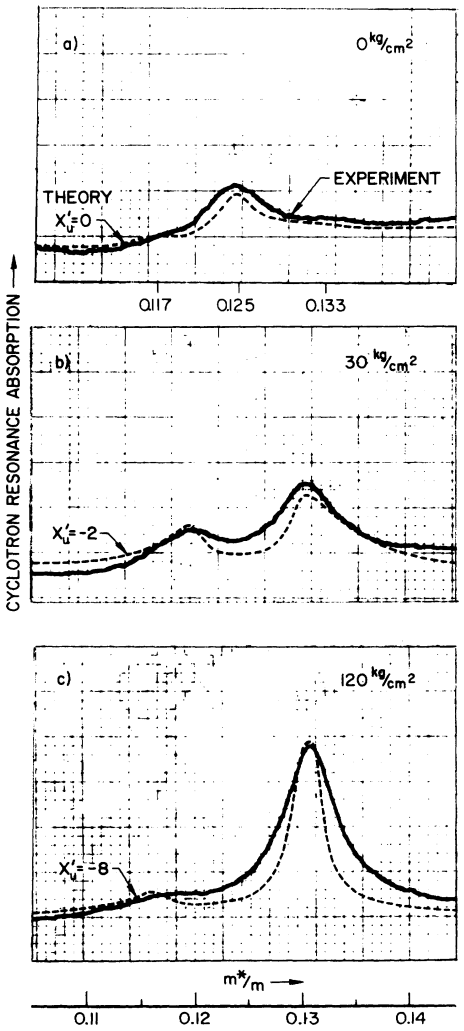

FIG. 15. Effect of uniaxial stress $T \| [111]$ on the $\vec{H}_0 \| [111]$ fundamental triplet $1_0 \rightarrow 2_1$, 5_4, 5_3. The experimental traces were taken at 49.95 GHz and 1.2°K. The effective masses of the three quantum resonances at $T = 0$ are listed under trace (a).

To answer this question let us examine the energy level diagram for $\vec{H}_0 \| [111]$ in Fig. 2. We note that the final state 2_1 of the transition $1_0 \rightarrow 2_1$ is nearly degenerate with two other states 5_3 and 5_4 of the same character $K = 2$. Owing to the decoupling peculiar to the $\vec{H}_0 \| [111]$ case, these states cannot admix for $k_H = 0$ and, consequently, the transition $1_0 \rightarrow 5_3$, 5_4 in Fig. 2 are forbidden. However, for $k_H \neq 0$ the strict selection rules are broken, and the three $K = 2$ states admix strongly. In this case all three $\Delta K = 1$ transitions $1_0 \rightarrow 2_1$, 5_3, 5_4 are allowed giving rise to the fundamental triplet.

The behavior of these transitions as a function of ζ is shown in Fig. 16 for three cases, $x'_u = 0$, -2, and -8, which correspond to the experimental traces in Fig. 15. For $x'_u = 0$ the transition $1_0 \rightarrow 2_1$ has at $\zeta = 0$ a "cusplike" critical point representing a very low joint density of states. The nature of the "dispersion" of m^*/m near $\zeta = 0$ would suggest that this cyclotron resonance should be broad, weak and k_H shifted to a higher effective mass, all of which fit our observations on the $m^*/m = 0.133$ line. The transition $1_0 \rightarrow 5_4$ (forbidden at $\zeta = 0$) has a high joint density of states in the region $\zeta = 0.2$ to 0.4 which is responsible for the line observed at $m^*/m = 0.125$. When uniaxial stress is applied, $x'_u = -2$ or -8, we see in Fig. 16 that the cusplike critical point of the $1_0 \rightarrow 2_1$ transition flattens resulting in a stronger and sharper line. At the same time the noncentral critical point for $1_0 \rightarrow 5_4$ shifts and loses strength (and eventually disappears) with increasing stress. The position of the transition $1_0 \rightarrow 5_3$ (not shown in Fig. 16) changes even more rapidly as a function of stress which explains our

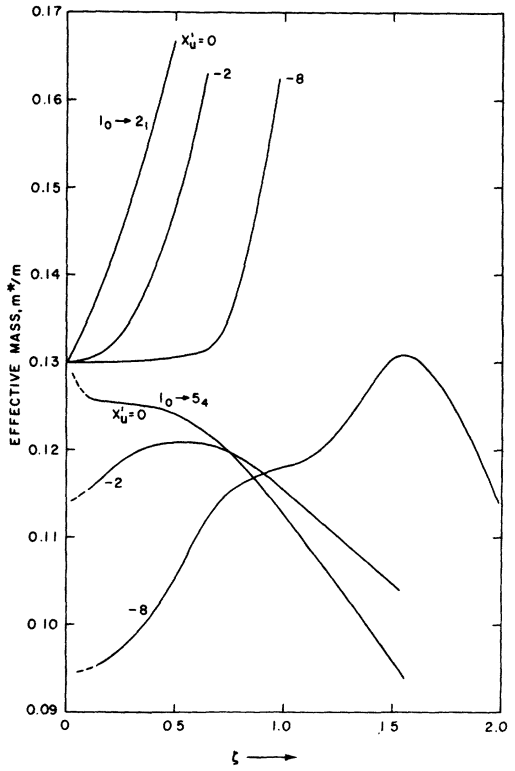

FIG. 16. Effects of a weak [111] uniaxial stress on the dispersion of two transitions $1_0 \rightarrow 2_1$ and $1_0 \rightarrow 5_4$ in the fundamental triplet (cf. Fig. 12).

inability to follow this line.

The above analysis is confirmed in detail by matching spectra calculated from the spectral function, shown by the dashed curves in Fig. 15, to the experimental resonances. The amplitudes of the theoretical curves were normalized to the peak of the $1_0 \rightarrow 2_1$ transition in Fig. 15(c). The calculated and experimental line shapes agree quite well (as does the line position given in Figs. 9 and 10). No attempt was made to include strain broadening which might account for some of the minor discrepancies in the fit.

E. Experimental results for $\vec{H}_0 \perp T$

Up until now our discussion has been restricted to measurements made in the geometry $\vec{H}_0 \parallel T$, which from the standpoint of simplicity of interpretation and sharpness of the observed spectra is unquestionably the optimum experimental arrangement. We have found it also worthwhile to investigate the spectra for the transverse geometry $\vec{H}_0 \perp T$, which can provide important checks on the values of the band parameters and deformation potentials, as well as assist in the determination of the strain anisotropy parameter β. We briefly summarize our results in this section.

For experiments with $\vec{H}_0 \perp T$ the apparatus pictured in Fig. 6 cannot be used because rotation of the magnet about the dewar axis to the "90°-position" results in the wrong electric field polarization $\vec{\mathcal{E}}_1 \parallel \vec{H}_0$ for cyclotron resonance. Instead our measurements were made on the apparatus designed for the combined resonance experiments in Paper III (where a more detailed description is given) in which the cavity electric fields were linearly polarized $\vec{\mathcal{E}}_1 \parallel T$; so that having set $\vec{H}_0 \perp T$ we automatically obtained the correct polarization $\vec{\mathcal{E}}_1 \perp \vec{H}_0$.

The notation (n, M_J) used so far to classify the (high stress) Landau states must be modified when we deal with $\vec{H}_0 \perp T$. A large stress decouples (at least for the uniaxial cases $T \parallel [001]$ and $T \parallel [111]$) the manifold $M_J = \pm\frac{3}{2}$ from the manifold $M_J = \pm\frac{1}{2}$, where M_J is the projection of $\vec{J}$ along T. In an orthogonal magnetic field the eigenstates within the $M_J = \pm\frac{1}{2}$ manifold are not the states with either $M_J = \frac{1}{2}$ or $-\frac{1}{2}$ but their linear combinations

$$(+) = (1/\sqrt{2})(|+\tfrac{1}{2}\rangle + |-\tfrac{1}{2}\rangle),$$
$$(-) = (1/\sqrt{2})(|+\tfrac{1}{2}\rangle - |-\tfrac{1}{2}\rangle). \tag{42}$$

It may easily be seen that of the two (if $\kappa > 0$), the (+) states lie "above" the (−) states (in the inverted scheme used for hole Landau levels). In this section we shall employ the labeling scheme $(n, \pm)$, where $\pm$ has the connotation suggested by Eq. (42) and n is the usual Landau quantum number. The $M_J = \pm\frac{3}{2}$ transitions have not been measured for $\vec{H}_0 \perp T$; and they are not discussed here.

The $\vec{H}_0 \perp T$ cyclotron resonance transitions $(0, -) \rightarrow (1, -)$ are plotted in Figs. 17 and 18 for $T \parallel [111]$, $T \parallel [001]$, and $T \parallel [110]$, respectively. These transitions, analogous to the fundamental transitions for $\vec{H}_0 \parallel T$, depend only weakly on stress and lie close to the series limits. These series limits [see Eq. (16)] depend upon the *longitudinal* components of the effective-mass tensor, the measurements of which, in principle, could give an independent set of values for γ_1, γ_2, and γ_3 (although, in fact, to somewhat lesser accuracy, for the $\vec{H}_0 \perp T$ resonances are found as a rule to be broader and more stress sensitive than those for $\vec{H}_0 \parallel T$).

We analyze the data in Figs. 17 and 18 using Eq. (28). Consistent with the lower level of precision involved here, we opt for a simpler, approximate method to estimate $\delta(T)$. We calculate[51] the Landau-level energy shifts from the second-order (k^4/T) projection of the $J = \frac{3}{2}$ Hamiltonian $\mathcal{H}_k + \mathcal{H}_e$ onto the 2×2 subspace of $(\pm)$; further, we neglect k_H effects and their contribution to the line shape. For a transition $(n, \pm) \rightarrow (n+1, \pm)$, the decoupling shift[51] $(k_H = 0)$ is given by

$$\delta(T) = (1/2|x|)[2A(n+1) \pm 2D], \tag{43}$$

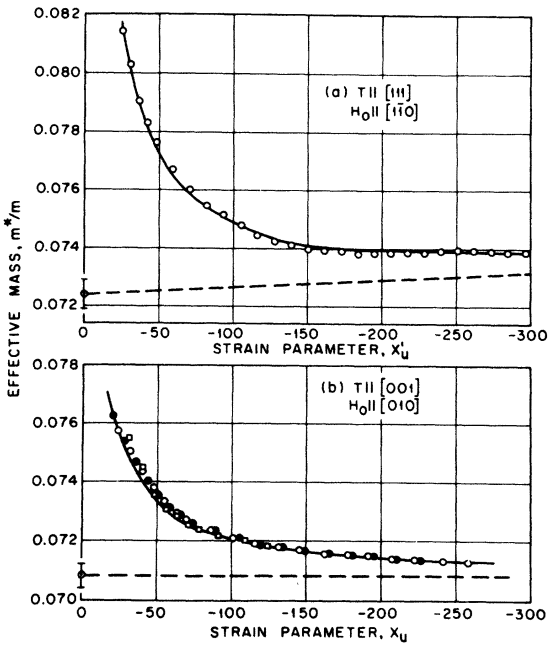

FIG. 17. Stress dependence of the $\vec{H}_0 \perp T$ fundamental transitions $(0, -) \rightarrow (1, -)$ with (a) $T \parallel [111]$ and (b) $T \parallel [001]$. The fits to the data determine m_0^*/m and α: (a) $T \parallel [111]$: $m_0^*/m = 0.0724 \pm 0.0004$, $\alpha = -(4.7 \pm 1.3) \times 10^{-5}$ cm^2/kg; (b) $T \parallel [001]$: $m_0^*/m = 0.0708 \pm 0.0004$, $\alpha = -(0.6 \pm 1.5) \times 10^{-5}$ cm^2/kg.

where x represents generically the strain parameters x_u, x_u', or x_u''. The x values of the data in Figs. 17 and 18 were *not* considered free to be adjusted by fitting but were fixed in terms of the stress by the values for D_u and D_u' in Eq. (27). Expressions for the coefficients A and D may be found in Table VIII of Paper I. Substituting Eq. (43) into Eq. (28) we fit the data as shown by the solid curves in Figs. 17 and 18. The dashed lines represent the series limits, the linear part of Eq. (28), from which we determine m_0^*/m (intercept at $x = 0$) and α (slope) as listed in the figure captions.

From the data in Fig. 17 for $T \parallel [001]$ and $T \parallel [111]$, we determined $m_\parallel/m$, $\alpha_\parallel$ and $m_\parallel'/m$, $\alpha_\parallel'$, respectively, using Eqs. (16), (25), and (26) and the values for $m_\perp/m$, $m_\perp'/m$, $\alpha_\perp$, and $\alpha_\perp'$ measured in Sec. IV D 1. Similarly, the data for $T \parallel [110]$ in Fig. 13(b) and in Fig. 18 were analyzed[48] together to give m_1/m, m_2/m, and m_3/m and α_1, α_2, and α_3. The results thus obtained are listed in Table III.

The $\vec{H}_0 \perp T$ experiments are "redundant" in the sense that together with the $\vec{H}_0 \parallel T$ measurements they "overdetermine" the band parameters and deformation potentials. The extra relationships which result from this redundancy are useful for checking the over-all consistency of our work.

First, consider the band parameters. Using the $\vec{H}_0 \parallel T$ values of γ_1, γ_2, and γ_3 [Eq. (34)] we can calculate the $\vec{H}_0 \perp T$ cyclotron resonance effective masses:

$$\begin{aligned}(m_\parallel m_\perp/m^2)^{1/2}(\text{calc}) &= 0.07075 \pm 0.00015 \\ &\quad \text{for } T \parallel [001], \\ (m_\parallel' m_\perp'/m^2)^{1/2}(\text{calc}) &= 0.07247 \pm 0.00015 \\ &\quad \text{for } T \parallel [111].\end{aligned} \tag{44}$$

These are in very close agreement with the measured values given in the caption of Fig. 17. (We treat the $T \parallel [110]$ effective masses in Sec. IV F.)

Next, we consider the deformation potentials as represented by the linear-shift components. From the $\vec{H}_0 \parallel T$ experimental values for $\alpha_\perp$ and $\alpha_\perp'$ in Table III we can use the relations $\alpha_\parallel = -2\alpha_\perp$ and $\alpha_\parallel' = -2\alpha_\perp'$ to calculate the parallel components relevant to $\vec{H}_0 \perp T$ experiments:

$$T \parallel [001]: \quad \alpha_\parallel(\text{calc}) = +(21.6 \pm 1.6) \times 10^{-5} \text{ cm}^2/\text{kg},$$

$$T \parallel [111]: \quad \alpha_\parallel'(\text{calc}) = +(21.0 \pm 1.4) \times 10^{-5} \text{ cm}^2/\text{kg}.$$

In addition, using Eq. (I.144), we obtain

$$T \parallel [110]: \quad \alpha_1(\text{calc}) = -(14.0 \pm 1.4) \times 10^{-5} \text{ cm}^2/\text{kg},$$

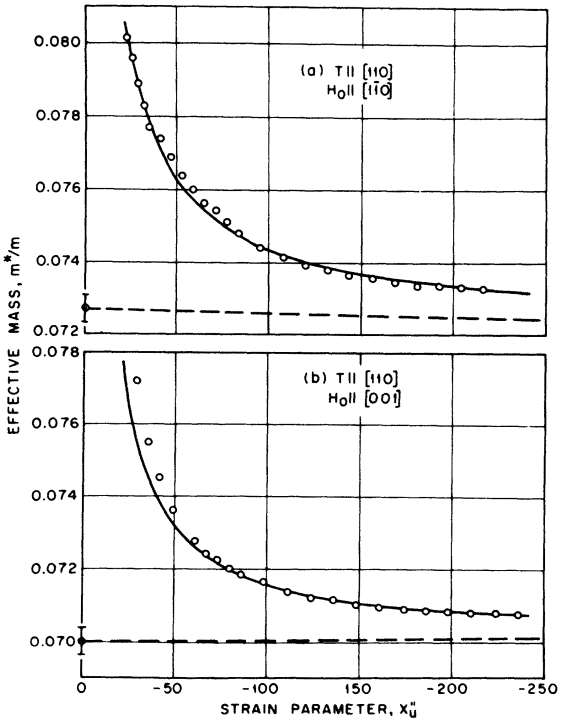

FIG. 18. Stress dependence of the $\vec{H}_0 \perp T$ fundamental transitions $(0, -) \rightarrow (1, -)$ with $T \parallel [110]$. The fits to the data determine m_0^*/m and α: (a) $\vec{H}_0 \parallel [1\bar{1}0]$: $m_0^*/m = 0.0727 \pm 0.0004$, $\alpha = +(2 \pm 2) \times 10^{-5}$ cm^2/kg; (b) $\vec{H}_0 \parallel [001]$: $m_0^*/m = 0.0700 \pm 0.0004$, $\alpha = -(2 \pm 2) \times 10^{-5}$ cm^2/kg.

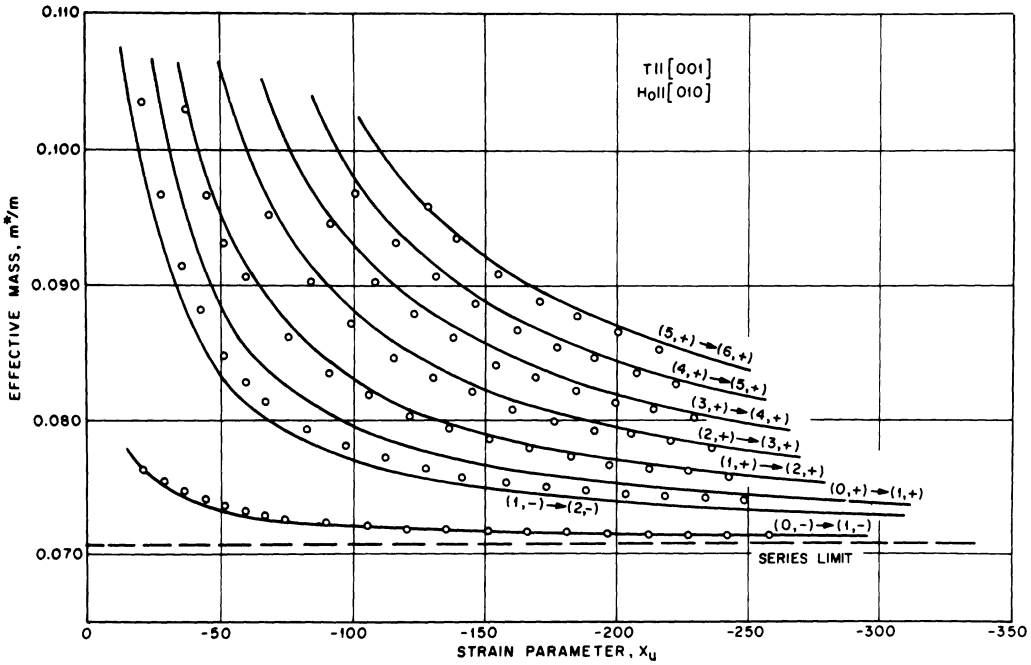

FIG. 19. Stress dependence of the $\vec{H}_0 \perp T$ resonance series with $T \parallel [001]$. We sealed the x_u values of the data from the stress using $D_u = 3.32$ eV.

$$\alpha_2(\text{calc}) = -(7.1 \pm 0.5) \times 10^{-5} \text{ cm}^2/\text{kg},$$

$$\alpha_3(\text{calc}) = +(21.2 \pm 1.5) \times 10^{-5} \text{ cm}^2/\text{kg}.$$

These numbers are all in reasonable agreement with the measured parameters given in Table III. In passing it should be pointed out that the sum rule[23]

$$\sum_{i=1,2,3} \alpha_i = 0$$

obeyed if the linear shifts originate exclusively from within the Γ_{25}^+ manifold, is roughly satisfied by the experimental α's in Table III for each of the three directions of T:

$$T \parallel [001]: \sum_i \alpha_i = +2.4 \pm 5.0,$$

$$T \parallel [111]: \sum_i \alpha_i = -4.0 \pm 5.0,$$

$$T \parallel [110]: \sum_i \alpha_i = +7.8 \pm 6.0$$

(in units of 10^{-5} cm^2/kg); in all three cases, the residuals[52] are quite small compared to $\sum_i |\alpha_i| \sim 40$, which reflects the total intraband contribution.

So far, only the lowest $n = 0 \rightarrow 1$ transitions for $\vec{H}_0 \perp T$ have been discussed; however, we have also measured some of the higher transitions for $T \parallel [001]$ and $T \parallel [111]$ the data for which are shown in Figs. 19 and 20, respectively. The calculated line positions (solid curves) are determined by adding the effective mass shifts $-(m_0^*/m)^2 \delta(T)$ calculated from Eq. (43) to the series limits (dashed lines) taken from Fig. 17. Theory predicts that all resonances with the exception of the "lowest" transition, (0, −) → (1, −), occur as close doublets, i.e., (1, −) → (2, −) lies close to (0, +) → (1, +), etc. On a few occasions, two peaks were actually resolved. Usually, however, we were unable to distinguish the individual resonances; so the data points in Figs. 19 and 20 represent the composite peaks of each unresolved pair. In the case of the lowest doublet, (1, −) → (2, −) and (0, +) → (1, +), we see that the calculated curves in both Figs. 19 and 20 straddle the data points as expected. For the sake of clarity the higher transitions are only fitted by a single curve; accordingly in Fig. 19 the curve labeled (1, +) → (2, +) in fact represents the mean of (1, +) → (2, +) plus (2, −) → (3, −) and so on. In Fig. 20 the curves shown, (1, +) → (2, +), etc., represent the single *stronger* member of the doublet as labeled. The fit of the data in Figs. 19 and 20 even at low x values by approximation (43) for $\delta(T)$ is surprisingly good. This suggests the possibility that the second-order projection formulas having the virtue of simplicity [see Eqs. (I. 125) and (I. 127)] may be generally useful for analyzing cyclotron resonance "stressed" spectra. It should be pointed out that the close match of the observed stress dependence of the resonances with the curves calculated by Eq. (43) also confirms the ($\vec{H}_0 \parallel T$) values of the deformation potentials D_u and D_u' in Eq. (27) upon which the x values in Figs.

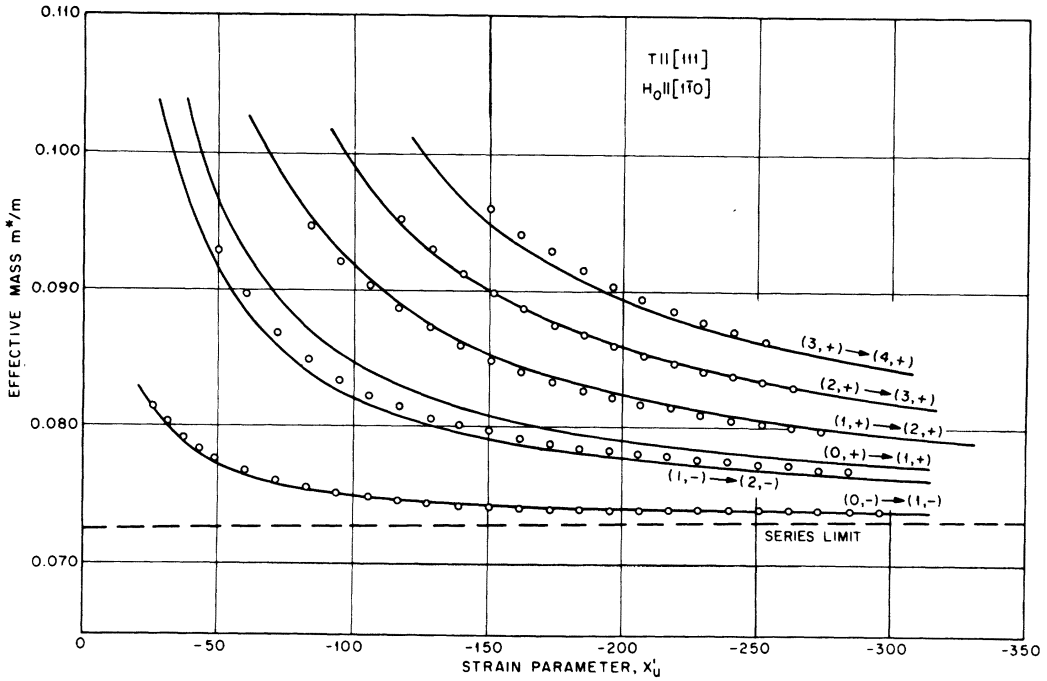

FIG. 20. Stress dependence of the $\vec{H}_0 \perp T$ resonance series with $T \| [111]$. We scaled the x'_u values of the data from the stress using $D'_u = +3.81$ eV.

17–20 are based without adjustment. (This is noteworthy in view of the fact the measurements for $\vec{H}_0 \perp T$ and $\vec{H}_0 \| T$ were made using different independently calibrated sets of apparatus.)

F. Determination of β

From the effective masses measured for $T \| [110]$ we can determine the splitting anisotropy parameter β. Using our "standard" values of γ_1, γ_2 and γ_3 in Eq. (34) we can calculate (see Table I) the effective masses m_1/m, m_2/m and m_3/m for $T \| [110]$ as a function of $|\beta|$. The results are plotted in Fig. 21 in the form $\sqrt{(m_1 m_2/m^2)}$, $\sqrt{(m_1 m_3/m^2)}$, $\sqrt{(m_2 m_3/m^2)}$, which can be directly compared with the measured data. On the same plot the experimental points taken from Figs. 13 and 18 and projected onto the calculated curves fix the value

$$|\beta| = 0.69 \pm 0.01 . \tag{45}$$

Since D_u and $D'_u > 0$, it follows that $\beta > 0$. The ratio of the deformation potentials is, therefore, $D'_u/D_u = 1.15 \pm 0.02$. As a further check on the effective mass measurements, we note that in Fig. 21 all three experimental effective masses are consistent with a single value of $|\beta|$, an unlikely coincidence if the measurements were appreciably in error.

V. DISCUSSION

A. Effective-mass band parameters

Prior to stress experiments,[12,13] the only direct measurements of the inverse-mass parameters γ_1, γ_2, and γ_3 reported for Ge were obtained from the *classical* light- and heavy-hole cyclotron resonances in unstressed crystals. Unfortunately this method suffers, in principle, from three rather serious drawbacks: (i) The signs of γ_2 and γ_3 cannot be ascertained. (ii) The apparent cyclotron resonance peak positions may be shifted by unresolved quantum effects which can be present since the classical condition, $\hbar\omega \ll k\Theta$, is never strictly satisfied in experiments. (iii) The cyclotron resonance lines are broadened and shifted in a complicated fashion by the k_H dependence of the effective masses. Such effects are usually very difficult to correct for accurately.

To a large degree these problems are overcome by our measurements on the fundamental "quantum" transitions which are more precise (sharper resonance lines), less subject to systematic errors (smaller line shifts) and, importantly, give the signs of γ_2 and γ_3. (In passing we should mention that the positive signs found for γ_2 and γ_3 are consistent with the current picture of the Ge band structure.[53])

In Table IV we compare quantum and "classical" values[3,24,54,55] for γ_1, γ_2, and γ_3. Offhand the numbers seem to be in reasonable accord; nonetheless, at the level of precision now realized some systematic discrepancies between the two kinds of experiments show up (compare column 2 with 3).

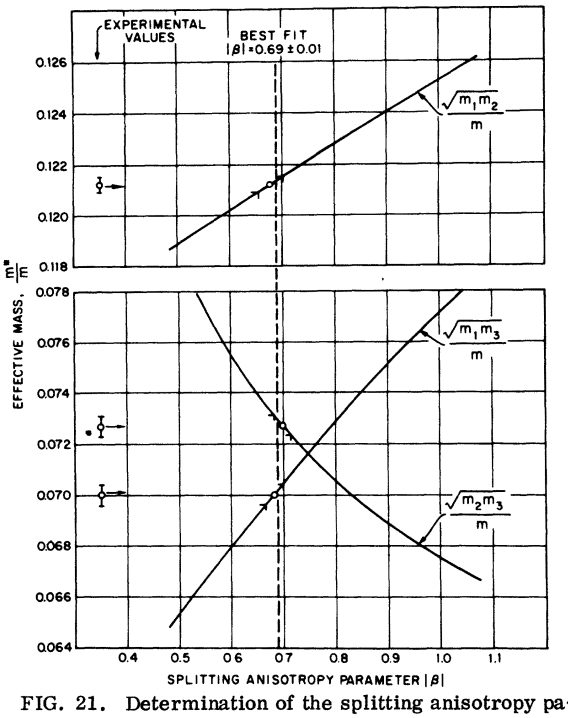

FIG. 21. Determination of the splitting anisotropy parameter β from the $T \parallel [110]$ fundamental transitions. The curves were calculated (see Table I) from the values of γ_1, γ_2, and γ_3 in Eq. (34).

The most serious difference, more than five standard deviations, is seen in the γ_1's. We believe the classical measurements to be at fault for the reasons described in (ii) and (iii). These difficulties [especially (ii)] could well have been anticipated inasmuch as experimental conditions in the past, typically 24 GHz and 1.3 °K (i.e., $\hbar\omega \sim k\Theta$), fell considerably short of being truly "classical."

In order to verify that this actually is the problem we have repeated the experiments (see the Appendix) at 9 GHz (and 1.2 °K), closer to the classical regime than reached heretofore. We observe at 9 GHz that the classical resonances (especially the light hole) are indeed slightly shifted to lower effective masses which tends to mitigate the disagreement, in particular for γ_1. After correcting line shapes (see Appendix) to compensate for the remaining shifts, we obtain the following classical values for the Ge valence-band parameters: γ_1 (classical) = 13.40 ± 0.03, γ_2(classical) = 4.26 ± 0.05, γ_3(classical) = 5.69 ± 0.03, which are in excellent agreement with the quantum parameters in Eq. (34). We conclude that the quantum (stress) and classical measurements of γ_1, γ_2, and γ_3 can, in fact, be brought into harmony, but only after the line shapes of the classical hole resonances are understood.

We might add that the complex quantum spectra in unstressed Ge (as we shall see presently in Paper IV) can be fitted quite precisely with calculated spectra based on these same values of γ_1, γ_2, and γ_3 given in Eq. (34)—further evidence that this set of parameters now stands on rather solid footing.

From stress experiments at 35 GHz Fujiyasu *et al.*[13(b)] obtained the band parameters in column 7 of Table IV, but low resolution and an inadequate analysis make their accuracy suspect. The questionable interpretation of early quantum experiments[4-6] (without stress) cause us to doubt the meaningfulness of the quoted parameters and we omit them from our comparison.

B. Deformation potentials

From cyclotron-resonance experiments in uniaxially stressed Ge we can deduce the valence-band (uniaxial) deformation potentials from two effects, namely, the band splitting within the $J = \frac{3}{2}$ manifold and the strain interactions between the $J = \frac{1}{2}$ and $J = \frac{3}{2}$ manifolds. Unexpectedly, our experiments in Ge show that a sizable disparity exists between the two [compare Eqs. (37) and (38) with Eq. (27)] We attribute the differences[49] to spin-dependent terms[56] in the strain Hamiltonian of sym-

TABLE IV. Comparison of inverse-mass band parameters for Ge measured by different cyclotron resonance experiments. The signs of γ_2 and γ_3 in columns 3–6 (classical work) are indeterminate.

	Present work (quantum)	LF[a]	FYM[b]	DKK[c]	DZL[d]	FMO[e]
γ_1	13.38 ± 0.02	13.27 ± 0.03	13.21	13.2 ± 0.1	13.1 ± 0.4	13.50 ± 0.05
γ_2	4.24 ± 0.03	±(4.32 ± 0.06)	±(4.28)	±(4.45 ± 0.03)	±(4.15 ± 0.3)	4.40 ± 0.05
γ_3	5.69 ± 0.02	±(5.60 ± 0.03)	±(5.56)	±(5.40 ± 0.05)	±(5.50 ± 0.3)	5.87 ± 0.04

[a] B. W. Levinger and D. R. Frankl, Ref. 24.
[b] Values quoted by R. R. Goodman (Ref. 7) from analysis of measurements of R. C. Fletcher, W. A. Yager, and F. R. Merritt, Ref. 3.
[c] G. Dresselhaus, A. F. Kip, and C. Kittel, Ref. 54.
[d] R. N. Dexter, H. J. Zeiger, and B. Lax, Ref. 55.
[e] H. Fujiyasu, K. Murase, and E. Otsuka, Ref. 13(b).

metry $I_x\sigma_x\epsilon_{xx}$, $(I_x\sigma_y+I_y\sigma_x)\epsilon_{xy}$, etc. (Here, $\vec{I}$ is the vector angular momentum operator for $I=1$; and $\vec{\sigma}$ is the Pauli spin operator.) The projections of these spin-terms onto the $J=\frac{3}{2}$ subspace are isomorphic to the projections of the more familiar spin-independent terms[23] $I_x^2\epsilon_{xx}$, $(I_xI_y+I_yI_x)\epsilon_{xy}$, etc.; therefore, the two can be lumped together in the $J=\frac{3}{2}$ space with a single coefficient $D_u=\frac{1}{2}D_2+E_2$ or $D_u'=\frac{1}{2}D_3+E_3$ identical to the Kleiner-Roth uniaxial deformation potentials as originally defined [see Eq. (6)]. On the other hand, the projections are different in the 2×4 "cross space" connecting $J=\frac{3}{2}$ and $J=\frac{1}{2}$ producing an analogous but independent set of "mixing" deformation potentials $D_w=\frac{1}{2}(D_2-E_2)$ and $D_w'=\frac{1}{2}(D_3-E_3)$. Measurements in either subspace alone are not sufficient to permit a decomposition into spin-dependent (E_2 and E_3) and spin-independent (D_2 and D_3) parts.

Previous strain experiments of diverse kinds have all basically measured the same quantity, the $J=\frac{3}{2}$ band splitting which determines only D_u and D_u'.[57] These results[13,58-62] are tabulated in column 5 of Table II for comparison with our values in column 2. Although the values in column 5 exhibit some scatter, their trend falls reasonably in line with our results. The only other cyclotron-resonance measurements of D_u and D_u' by Fujiyasu *et al.*[13(b)] agree quite well with ours.

Recently, Saravia and Brust[63] and Melz[64] have calculated the valence-band deformation potentials (D_u and D_u') for Ge using the pseudopotential method. Their results are also included in Table II.

No other measurements in Ge have been reported for the mixing deformation potentials D_w and D_w', nor the components D_2, D_3, E_2, and E_3 derived therefrom. On one point, however, we can make a tenuous but interesting connection with other experiments. Lawaetz[65] in a recent study of the systematics of the valence-band deformation potentials has found evidence suggesting a correlation between values of the spin-independent deformation potentials for different semiconductors of the same ionicity. If this is true, we would then expect a close match between the respective deformation potentials in the two purely covalent semiconductors Si and Ge. Our most recent measurements[66] for Si give tentatively $D_w\approx+2.3$ eV and $D_w'\approx+3.0$ eV. Assuming spin effects are negligible[67] in Si, we can write $\frac{1}{2}D_2\approx D_w=2.3$ eV and $\frac{1}{2}D_3\approx D_w'=3.0$ eV, which we see are not very different from the Ge values in Eqs. (39) and (40), respectively.

So far, the theory of the phenomenological spin-dependent deformation potentials E_2 and E_3 has not been completely worked out. From perturbation theory we find that the following three kinds of terms (see Paper I) contribute to E_2 and E_3:

(i) $\langle\Gamma_{25}^+|\vec{\sigma}\cdot(\overleftrightarrow{\epsilon}\cdot\nabla V\times\vec{p}+\nabla V\times\overleftrightarrow{\epsilon}\cdot\vec{p})|\Gamma_{25}^+\rangle$,

(ii) $\langle\Gamma_{25}^+|\vec{\sigma}\cdot\nabla(\epsilon_{\mu\nu}V_{\mu\nu})\times\vec{p}|\Gamma_{25}^+\rangle$,

(iii) $\sum_l(\langle\Gamma_{25}^+|\mathcal{H}_{so}|l\rangle\langle l|\mathcal{H}_e|\Gamma_{25}^+\rangle$
$+\langle\Gamma_{25}^+|\mathcal{H}_e|l\rangle\langle l|\mathcal{H}_{so}|\Gamma_{25}^+\rangle)/(E_0-E_l)$,

where V is the periodic crystal potential and

$$V_{\mu\nu}=\frac{\partial V[(1+\overleftrightarrow{\epsilon})\cdot\vec{x}]}{\partial\epsilon_{\mu\nu}}.$$

The first is the "kinetic" term which derives simply from the scaling process in applying the Pikus-Bir[17] transformation to the coordinates and is readily evaluated giving $\frac{1}{3}\Delta$. The second term is less transparent; it depends upon the change of crystal potential V with strain $V_{\mu\nu}$, which must be determined in a self-consistent way—a difficult and unsolved problem. The third, and presumably least important term, is a second-order contribution containing matrix elements of the spin-orbit interaction $\mathcal{H}_{so}$ and strain interaction $\mathcal{H}_e$ which connect the valence states Γ_{25}^+ with the relatively remote even-parity conduction-band states $l=\Gamma_{12}^+$, Γ_{15}^+, and Γ_{25}^+.

With the theory for E_2 and E_3 incomplete, we can only consider the partial result given by the kinetic term; in other words we are forced to assume $V_{\mu\nu}=0$, an approximation which is equivalent to using the deformable-ion model. In this approximation $E_2=E_3=\frac{1}{3}\Delta\sim0.1$ eV. Comparing this with the experimental results $E_2=E_3\sim0.7$ eV, we see that the kinetic term alone is too small to account for our observations although it has the correct sign. The disagreement is not surprising, for it has been shown before[68] in Si that the deformable-ion model gives poor estimates for valence-band deformation potentials (D_u and D_u').

The same three terms also give rise to a change[11] in spin-orbit energy Δ from the dilatational component of strain $\epsilon_{xx}+\epsilon_{yy}+\epsilon_{zz}$. This change in Δ is often written

$$\delta\Delta/\Delta=-\eta\delta a/a,$$

where a is the lattice constant and η is a dimensionless coefficient expressible in terms of the dilatational spin-dependent deformation potential $E_1=-\frac{1}{9}\eta\Delta$ defined in Paper I. Theoretical estimates of η have been made by Brust and Liu,[69] $\eta=4$ (at L); Cerdiera *et al.*,[70] $\eta=1.7$; Melz and Ortenburger,[71] $\eta=1.8$; and Wepfer *et al.*,[72] $\eta=0.2$. It is interesting to compare these with the deformable ion value $\eta=2$ we get from the kinetic term[11] ($E_1=-\frac{2}{9}\Delta=0.06$ eV). An experimental value of $\eta=0.8\pm0.8$ has been reported.[71] Although evidence is still meager and not unanimous, it seems clear that within the valence bands, spin-dependent strain energy shifts due to dilatation (E_1) are considerably weaker than those of a uniaxial kind (E_2 and E_3).

C. Hole scattering times

As a byproduct of our cyclotron-resonance experiments we obtain some information about the hole scattering times. The line shapes of the hole resonances are almost completely determined by k_H broadening; however, in a few instances, notably the fundamental resonances, k_H effects are sufficiently small so that the relaxation-time broadening mechanism is seen. We have not attempted a comprehensive or systematic study; rather we summarize some typical kinds of measurements which might serve as a basis for further work.

(a) From the linewidth of the sharpest quantum resonance observed, the $(0, -\frac{1}{2}) \rightarrow (1, -\frac{1}{2})$ fundamental transition for $\vec{H}_0 \parallel [111]$, we measure the hole scattering time at 1.2 °K and 52.9 GHz,

$$\tau = (5.1 \pm 0.6) \times 10^{-10} \text{ sec} \qquad (46)$$

($\omega\tau = 170$), using the relation $\omega\tau = H_0/\Delta H$, where ΔH is the half-width measured at half-maximum. [ΔH is taken from the "leading" edge (low-field side) which is the narrower side of the slightly k_H-broadened line.] This lowest transition in the Landau ladder should have the longest scattering (relaxation) time, if $\tau(\epsilon)$ is assumed to be a decreasing function of energy ϵ.

(b) We unfortunately do not have measurements of the fundamental transitions at frequencies widely enough separated from 53 GHz to determine the dependence of τ on ω. However, we can get a rough idea by analyzing the linewidths of the *classical* light-hole resonances, for which data ($\vec{H}_0 \parallel [111]$ and $\Theta \approx 1.3$ °K) are available at 8.9 (see Appendix), 24,[73] and 53 GHz (see Paper IV):

$\tau = 1.1 \times 10^{-9}$ sec ($\omega\tau = 60$) at 8.9 GHz,

$\tau = 4.7 \times 10^{-10}$ sec ($\omega\tau = 70$) at 24 GHz,

$\tau = 2.7 \times 10^{-10}$ sec ($\omega\tau = 90$) at 53 GHz.

We note that there is a marked decrease in τ with increasing ω; such that, the value of $\omega\tau$ changes relatively little.

(c) The temperature dependence of τ can be inferred from a measurement [cf. Ref. 13(b)]

$$\tau \approx 2.9 \times 10^{-10} \text{ sec } (\omega\tau \approx 95)$$

at 4.2 °K and 53 GHz estimated from the linewidth of the $(0, -\frac{1}{2}) \rightarrow (1, -\frac{1}{2})$ transition for $\vec{H}_0 \parallel [111]$. (A similar value, $\tau = 2.7 \times 10^{-10}$ sec, was adopted in Paper IV in computing a fit for the unstressed quantum spectra for Ge at 4.0 °K). Comparing this result with Eq. (46) we observe that the temperature dependence for τ is much weaker than the typical $\Theta^{-3/2}$ dependence characteristic of a *classical* acoustic phonon scattering process.[19]

In summing up we would mention that the properties of the hole scattering time noted above, τ approximately inversely proportional to ω and only weakly dependent on temperature,[74] are characteristic of *quantum* acoustic phonon scattering. It was first pointed out by Meyer[27] that the usual concepts of "classical" transport theory are inadequate as a description of the cyclotron resonance scattering times when $\hbar\omega/k\Theta \gtrsim 1$, at which point the cyclotron radius becomes comparable to the wavelength of the relevant scattered phonons. At very "low" temperatures (a limit approached in our experiments) he found that the linewidth of the *quantum* transition $n = 0 \rightarrow 1$ becomes independent of temperature, as all phonon excitations are frozen out, but increases linearly with magnetic field (frequency) reflecting the increase in the density of states.

Measurements of scattering times from the cyclotron resonance linewidths could enable one, in principle, to determine[75] the dilatational deformation potential D_d which, in contrast to the uniaxial components D_u and D'_u, is not obtainable from the stress-induced line shifts in the hole spectrum (nor can it be isolated from interband optical experiments).

D. Hole thermalization

The long hole scattering times in Ge are responsible for a phenomenon which shows up unexpectedly in our experiments, namely, that below ~2.5 °K a significant fraction of the optically excited holes fail to thermalize. This becomes evident when we attempt to fit experimental resonance traces taken at, say, 1.2 °K with computed line shapes (more striking are the effects on the relative intensities in the quantum spectra in Paper IV); in order to fit the data we find it necessary to assume that the holes are "hot,"[76] i.e., at ~2.5 °K. On the other hand, at 4.2 °K all experimental results are consistent with the holes being in equilibrium with the lattice.

These observations suggest that in cooling from 4 to 1 °K at some point the hole lifetime τ_t and thermalization time τ_s become comparable. The hole lifetime is determined by the trapping of holes on ionized shallow acceptors, a process which according to the "cascade theory"[77] has a strong temperature dependence[78] $\tau_t \sim \Theta^3$. But τ_s, which is essentially the lattice scattering time, is roughly independent of Θ (if anything, it is a decreasing function of Θ). Thus, at sufficiently low temperatures we would expect that $\tau_t \sim \tau_s$ whereupon the holes would be unable to relax in energy to the lattice temperature. We assume that this non-equilibrium situation can be described by a Boltzmann distribution with an effective temperature $\Theta^* > \Theta_{\text{lattice}}$. For our samples ($N_A \sim 4 \times 10^{12}$ cm^{-3}) we estimate[79] that this critical condition, $\tau_t \sim \tau_s \sim 10^{-9}$ sec, will be reached near 2 °K.

The "heating" effect may be aggravated in many

of our samples by their high degree of compensation, i.e. nearly all acceptors are ionized and, hence, free to act as fast hole traps.

Following this extremely fast capture of a hole by an acceptor, a plausible next step[80] in the recombination chain could be the capture of an exciton by the neutral trap with a subsequent three particle Auger recombination emitting an energetic hole into the valence band to repeat the cycle. Despite the fact that this (and/or competing processes) may be relatively slow compared to the initial fast capture, there is little likelihood that the recombination process will be "bottlenecked" by a "saturation" of the traps inasmuch as the carrier density $\sim 10^9$ cm^{-3} (see Sec. III C) is several orders of magnitude less than the trap density. (As to experimental evidence bearing on this question we fail to note any marked change in thermalization with even an order of magnitude increase in light intensity.)

VI. CONCLUDING REMARKS

High-resolution cyclotron-resonance studies have been presented which provide a comprehensive picture of the structure of the valence bands in Ge and their behavior under uniaxial stress. Perhaps even more importantly these results underscore the potentialities of the uniaxial stress technique as a powerful spectroscopic tool for the analysis of quantum spectra from cyclotron resonance in degenerate bands. Indeed, at present it is possibly the only way complex spectra of this kind can be sorted out. We see that the application of stress affords, first, unambiguous identification of many lines in the spectra and, second, a direct means to measure a number of important parameters: namely, the hole effective-mass band parameters, the valence-band deformation potentials and hole scattering times—all of which are relevant to other work. In particular, we should emphasize that a clear-cut procedure is indicated whereby the effective-mass parameters γ_1, γ_2, and γ_3 can be determined in a precise but elementary way from measurements of only a few key easily identified lines of the (stressed) spectra—the fundamental lines, $n = 0 \rightarrow 1$, $M_J = -\frac{1}{2}$, and $-\frac{3}{2}$—thus obviating the necessity to measure and analyze the remaining (and more complex) parts of the spectra. We have outlined the complete analysis of the spectra in some detail in anticipation that it might serve as a model for future studies in other cubic, tetrahedrally coordinated semiconductors most of which have degenerate valence-band structures like those found in Ge.

Future experimenters should consider the use of uniaxial tension as a complement to the uniaxial compression employed in our work. In such experiments the $M_J = \pm\frac{3}{2}$ Landau levels would lie lowest (see Figs. 3 and 4); and the $(0, -\frac{3}{2}) \rightarrow (1, -\frac{3}{2})$ fundamental transitions would consequently show up as strong resonances easily followed over a large range of stress, thus facilitating measurements of the band parameters. Since the $M_J = \pm\frac{3}{2}$ resonances (for $\vec{H}_0 \parallel T$) fall at magnetic fields much lower than the $M_J = \pm\frac{1}{2}$ resonances, the stress in tension needed to achieve a given degree of decoupling (the same x value) would be much less than in compression.

In review it is appropriate to point out briefly the merits of quantum cyclotron resonance as a technique for measuring valence-band deformation potentials. First, band mixing and band splitting produce different and easily distinguished first order effects in the spectra which can be measured directly to determine deformation potentials of the *two* types, D_w, D'_w and D_u, D'_u, respectively. Second, cyclotron resonance transitions, unlike optical transitions, are strictly intraband effects, so external states, interactions, or excitations—e.g., excitons, phonons, other bands, impurity states, etc.—whose systematic behavior with strain is difficult to assess, are not introduced. The analysis for the deformation potentials is based entirely on valence-band effective-mass Hamiltonians checked self-consistently by the cyclotron resonance experiments themselves. Third, the inherent high-resolution obtainable in the quantum spectra permits measurements of deformation potentials to be carried out at low stresses, which precludes the appearance of nonlinear effects to any appreciable degree.

We should not close without drawing attention to the very close agreement which exists throughout this work between experimental results and the calculations. The significance of this is emphasized when one considers that the calculations based on a minimal set of band parameters (five to be exact) account for a wide variety of observations ranging from the positions of a multitude of cyclotron resonance lines to even such subtle features as the line shapes and line intensities. In view of this highly satisfactory situation we conclude that the effective mass formalism of Luttinger and Kohn, upon which our calculations are based, provides a remarkably accurate description of the structure of the degenerate valence bands of Ge and the motion of holes therein with a magnetic field applied. More striking evidence on this point follows in Paper IV.

ACKNOWLEDGMENTS

The successful execution of this work has benefited from the contributions of many people, to all of whom we wish to express our gratitude. In particular, we single out P. Lawaetz, A. R. Hutson, and E. O. Kane with whom we have had many useful discussions. We wish especially to thank

the latter two for critically reading the manuscript. Helpful advice provided by D. W. Berreman on computational questions is greatly appreciated. We are indebted to S. H. Koenig and J. J. Hall for providing ultrapure crystals of Ge on which most of our measurements were made. D. H. Sweet prepared samples and assisted with the measurements. Our experimental work owes much to the precision machine work of G. Broecker who constructed the microwave cavities and the strain apparatus.

APPENDIX: CLASSICAL CYCLOTRON RESONANCES OF HOLES IN Ge

We pointed out in Sec. V A that small discrepancies are found when the values of the effective-mass parameters γ_1, γ_2, and γ_3 from our quantum cyclotron-resonance experiments are compared with the results from classical cyclotron-resonance experiments. We attribute these differences to systematic shifts of the classical hole resonances by quantum and k_H effects. Our goal in this Appendix is, first, to confirm directly the existence of these shifts by remeasuring the classical resonances much closer to the limit $\hbar\omega \ll k\Theta$ than reached heretofore; and, second, to outline how corrections can be made for these line shifts to extrapolate to the true, limiting values of the hole effective masses. (All measurements and formulas in this section refer to the unstressed crystal.) The corrected values of the effective masses ultimately enable us to reconcile the classical and quantum determinations of γ_1, γ_2, and γ_3.

A. Measurements of light- and heavy-hole effective masses

Our experiments were done on a balanced bridge (rectangular TE_{101}) cavity spectrometer operating at 9 GHz, the essential features of which have been described earlier.[81] The measurements were made with the microwave power (10^{-7}–10^{-8} W) and light intensity both reduced to levels where the hole cyclotron resonances ceased to narrow further. A single (flat, rectangular) sample, cut in the (110) plane from Ge crystal *nWLP*-33, was used in all runs; by rotating the magnet about the Dewar axis we could set $\vec{H}_0$ along each of the three crystallographic axes [001], [111], and [110]. (Only for $\vec{H}_0 \parallel [111]$ were $\vec{H}_0$ and the microwave electric field $\vec{\mathcal{E}}_1$ orthogonal.) By observing the splitting of the electron cyclotron-resonance lines the orientation of $\vec{H}_0$ could be made *in situ* to within 0.1° of the desired crystal axis. To take advantage of narrower resonance lines most measurements were made at 1.3 °K rather than 4.2 °K; we found that the shift of the hole resonances which resulted from lowering Θ was almost insignificant (the failure of the holes to thermalize at the lower temperature may be partly responsible).

A complete listing of classical hole cyclotron resonance lines we observed is given in Table V. For $\vec{H}_0 \parallel [110]$ (see Fig. 22) we observed the classical line at $m^*/m = 0.263$ reported by Fletcher *et al.* (4.2 °K spectrum)[3] and identified by Bagguley and Stradling[82] as arising from a noncentral critical point at $k_H/k_H(\max) = 0.60$. (The quantum analog of this resonance is described in Paper IV.) The heavy-hole resonance for $\vec{H}_0 \parallel [110]$ is unfortunately totally obscured by a much stronger electron line; however, we may estimate its effective mass, $m^*/m = 0.368 \pm 0.001$, rather accurately from the position of the sharp third-harmonic resonance seen in Fig. 22.

B. Corrections for cyclotron-resonance lineshifts

In Table VI we list the effective masses of the light- and heavy-hole resonances measured at different microwave frequencies. One notes that the effective masses are slightly frequency dependent, decreasing by roughly 1% as the frequency is reduced from 53 to 9 GHz. Clearly, if we are to achieve a precision of the order of or better than

TABLE V. Hole cyclotron resonances in Ge observed at 8964 MHz and 1.3 °K. The effective mass values (in units of m) were measured from the peaks of the resonances. Included here are the harmonics of the heavy-hole resonances as well as a classical k_H line and its third harmonic observed for $\vec{H}_0 \parallel [110]$. The nominally forbidden second harmonic of the heavy hole for $\vec{H}_0 \parallel [110]$ appears in our spectrum owing to the presence of a longitudinal component $\vec{\mathcal{E}}_1 \cdot \vec{H}_0$ of the microwave electric field. The fourth harmonic was not detected in any of the orientations.

Line	$\vec{H}_0 \parallel [001]$	$\vec{H}_0 \parallel [111]$	$\vec{H}_0 \parallel [110]$
light hole	0.0431 ± 0.0001	0.04160 ± 0.00005	0.04201 ± 0.00005
fifth harmonic	0.056 ± 0.001	not observed	not observed
third harmonic	0.0931 ± 0.0005	forbidden	0.1225 ± 0.0003
second harmonic	forbidden	$\sim 0.18 \pm 0.01$	0.182 ± 0.002
heavy hole	0.279 ± 0.001	0.374 ± 0.001	···
k_H line	···	···	0.263 ± 0.003
third harmonic of k_H line	···	···	0.090 ± 0.005

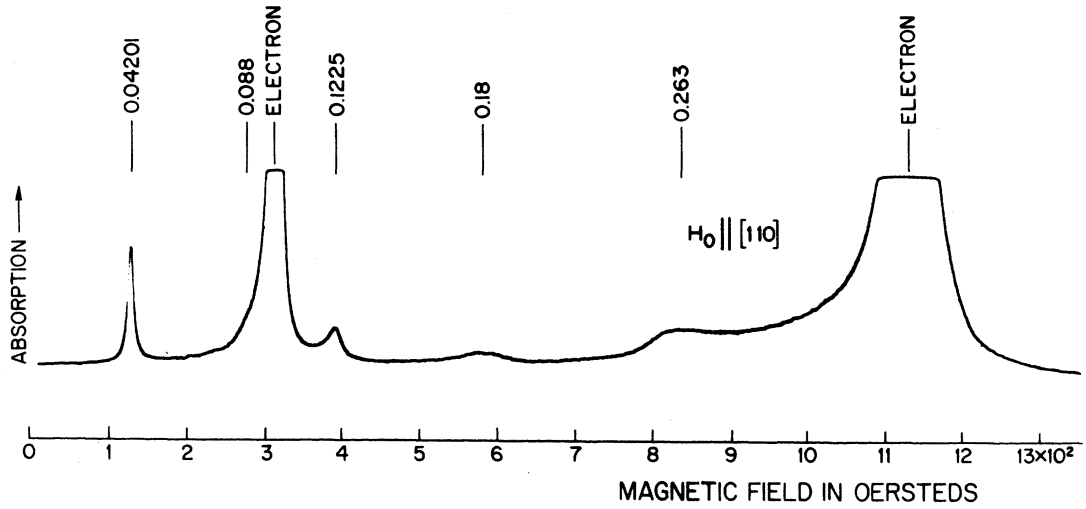

FIG. 22. "Classical" cyclotron resonance spectrum of Ge for $\vec{H}_0 \| [110]$ measured at 1.3°K and 8970 MHz.

1% in determining the band parameters from classical cyclotron-resonance data, we must examine rather carefully the question of line shifts for the hole resonances.

Although the effective masses measured at 9 GHz closely approach the classical limiting values, matters could be improved still further if we could estimate from a linebroadening theory the shifts that remain. Unfortunately, there is no simple theory that predicts the line shape from combined k_H- and quantum-line-broadening processes.[26] We can, however, obtain the line shape by direct numerical computation of the spectral function based on estimated or "trial" values for the five band parameters which appear in $\mathcal{H}_k$ in Eq. (1). Assuming a Lorentzian shape for each component line [whose position is specified by the inverse effective mass $\omega(n, k_H) = m/m^*(n, k_H)$] we sum the transitions from, say, $n = 0$ to n_{max} and integrate over k_H to generate a partial line shape (up to $n = n_{max}$). We choose n_{max} large enough so that this partial line shape contains most of the quantum and k_H effects. If necessary the weak remaining contributions to the resonance from transitions $n > n_{max}$ can be easily included if it is assumed that these lines have converged to the classical limit and, therefore, can be approximated by adding to the above partial line shape a single Lorentzian (of the appropriate intensity) at the position $\omega(n = \infty)$. The difference $\Delta\omega$ in the peak position of the calculated line shape thus gotten and the calculated limiting position, $\omega(n = \infty)$, gives the "correction" to be used in in-

TABLE VI. Light- and heavy-hole cyclotron resonances as a function of microwave frequency. Except where stated otherwise the measurements were made at ~1.3°K. At 53 GHz the heavy-hole lines are no longer well defined as they have begun to break up into quantum resonances.

Line	9 GHz[a]	24 GHz[b]	53 GHz[c]
light hole			
[001]	0.0431 ± 0.0001	0.04368 ± 0.00008	0.0440 ± 0.0001
[111]	0.04160 ± 0.00005	0.04187 ± 0.00005	0.0421 ± 0.0001
[110]	0.04201 ± 0.00005	0.04236 ± 0.00005	0.0426 ± 0.0001
heavy hole			
[001]	0.279 ± 0.001	0.2825 ± 0.0006	...
[111]	0.374 ± 0.001	0.377 ± 0.002	...
[110]	0.368 ± 0.001	0.368[d]	...

[a]Present work.
[b]Levinger and Frankl, Ref. 24.
[c]Present work (Paper IV).
[d]Fletcher, Yager, and Merritt, Ref. 3. Data taken at 4.2°K. No uncertainties quoted.

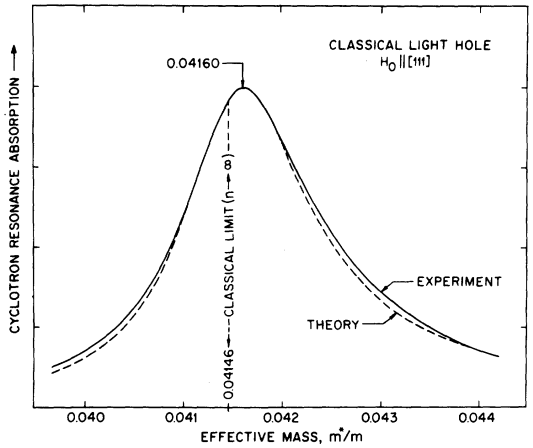

FIG. 23. Comparison of the experimental and calculated line shapes for the classical light-hole cyclotron resonance in Ge for $\vec{H}_0 \| [111]$. The resonance was recorded at 1.3 °K and 8978 MHz. The theoretical line shape was calculated for $\Theta^* = 2.0$ °K, $\nu = 9$ GHz, and $\tau = 1.08 \times 10^{-9}$ sec ($\omega\tau = 61$) from a superposition of (k_H-broadened) quantum lines as discussed in the text. The calculated line-shift correction puts the "classical" limit ($n \to \infty$) for the light-hole mass at $m^*/m = 0.04146 \pm 0.00008$.

terpreting the experimental resonance. In spite of the fact that the peak position depends sensitively upon the choice of "trial" parameters in $\mathcal{H}_k$, the difference $\Delta\omega$ does not.

In Figs. 23 and 24 we fitted calculated line shapes to the light- and heavy-hole resonances, respectively, for $\vec{H}_0 \| [111]$. The secular determinants were truncated at dimension 69×69, which gave $n_{max} = 14$. The width of the component lines is defined by the scattering time $\tau = 1.08 \times 10^{-9}$ sec ($\omega\tau = 61$). Although the Ge sample was at 1.3 °K, we had to assume in the calculations an effective hole temperature of $\Theta^* \sim 2.0$ °K, the value found to give the best fit of line shape to the "quantum" bump[83] on the low-field side of the heavy hole resonance in Fig. 24. For $\vec{H}_0 \| [111]$ the *peak positions* (but not necessarily the shape) of the light- and heavy-hole resonances are actually rather insensitive to Θ^* because the contributions to the asymmetric line shape from both k_H and quantum effects fall on the *same* side of the resonance; consequently, at a higher temperature, for instance, the reduction in the quantum contribution would be partially compensated by an increased k_H-contribution. We see that the experimental and computed line shapes in Figs. 23 and 24 agree reasonably well. Discrepancies on the "wings" of the line shapes, most evident in Fig. 24, are believed to result from the truncations of n and k_H in the diagonalization. The "trial" parameters used in calculating the line shape were, in fact, the "actual" values from Eq. (34), so not surprisingly the calculated and experimental line *positions* coincided without adjustment. From the locations of the $n \to \infty$ classical limits in these figures we obtain the effective masses listed in Table VII.

In the same way it is possible to reanalyze earlier experiments[3,24] done at 24 GHz. We did this for one case with $\vec{H}_0 \| [111]$ and found that the corrected effective masses agreed closely with our results in Table VII.

For $\vec{H}_0 \| [001]$ and $\vec{H}_0 \| [110]$, $\omega(n, k_H)$ converges much more slowly to $\omega(\infty, k_H)$ than for $\vec{H}_0 \| [111]$; so even with the largest (80×80) secular determinants we diagonalized, we were unable to obtain an accurate line shape. Instead we simply estimated the corrections from the asymmetry of the experimental line shapes. Since the corrections for the 9-GHz experiments are quite small, $\lesssim \frac{1}{2}\%$, such an estimate is probably adequate. The corrected effective mass values for [001] and [110] are given in Table VII.

C. Determination of γ_1, γ_2, and γ_3

We can now evaluate γ_1, γ_2, and γ_3 from the corrected classical-hole effective masses. In lieu of making the customary series expansions of the Shockley integral[84] for the ($k_H = 0$) "tube" mass, we have derived alternative expansions for m^* by diagonalizing the Luttinger Hamiltonian $\mathcal{H}_k$ in Eq. (1) in the limit $n \to \infty$. We restrict ourselves to $k_H = 0$; and having chosen the eigenfunctions of the "spherical" Hamiltonian ($\gamma_2 = \gamma_3$) as a basis, we

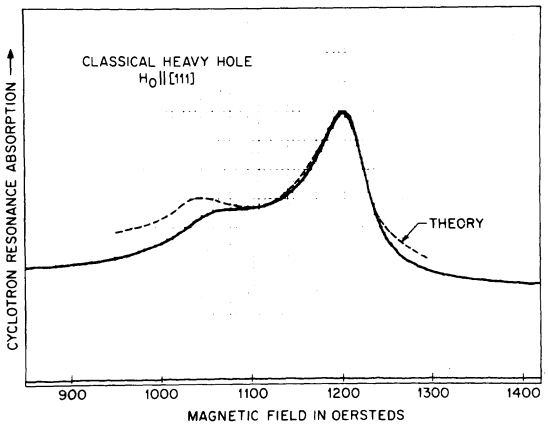

FIG. 24. Comparison of the experimental and calculated line shapes for the classical heavy-hole cyclotron resonance in Ge for $\vec{H}_0 \| [111]$. The trace was taken at 1.3 °K and 8964 MHz. The theoretical line shape was calculated as in Fig. 23. The cyclotron-resonance peak lies at $m^*/m = 0.374 \pm 0.001$. The "bump" at $m^*/m = 0.335$ (see Ref. 83) and "background" absorption at lower magnetic fields are k_H effects. Both are reproduced by the calculations. The calculated line-shift correction puts the "classical" limit ($n \to \infty$) for the heavy-hole mass at $m^*/m = 0.3762 \pm 0.0010$.

TABLE VII. Corrected values of light- and heavy-hole effective masses (in units of m) for Ge. The data in Table V were corrected for k_H and quantum line shifts as discussed in the text.

$\vec{H}_0$	[001]	[111]	[110]
light hole	0.04342 ± 0.00015	0.04146 ± 0.00008	0.04191 ± 0.00010
heavy hole	0.279 ± 0.001	0.3762 ± 0.0010	0.368 ± 0.001

treat by second-order perturbation theory the off-diagonal matrix elements containing all terms in $(\gamma_3 - \gamma_2)$. For $\vec{H}_0 \parallel [111]$ (because the $k_H = 0$ cyclotron orbits are circular) the results by either technique are trivial; both expansions reduce to a single, identical term. However, for $\vec{H}_0$ along [001] or [110] the expansions we have developed converge more rapidly than the Shockley integral series despite the fact that both employ the same expansion parameter $(\gamma_3 - \gamma_2)^2$. The more rapid convergence results from our choice of a zeroth order effective mass which closely approximates the actual effective mass rather than the [111] effective mass $m^*(111)$ appearing in the Shockley expansion, which may be a poor starting point if the anisotropy of $m^*(\theta)$ is appreciable. It is sufficient for our needs to go only to the second term [of order $(\gamma_3 - \gamma_2)^2$] in the [001] and [110] expansions.

The results of these expansions are outlined below. For any direction of $\vec{H}_0$ the dimensionless inverse effective mass $\omega = m/m^*$ can be written

$$\omega_\pm = \gamma_1 \pm 2\Gamma + \Delta_\pm \tag{47}$$

(the upper and lower signs refer to light and heavy holes, respectively), with Γ and $\Delta_\pm$ given in Table VIII. The expression for the second-order corrections $\Delta_\pm(110)$ for $\vec{H}_0 \parallel [110]$ is unfortunately so cumbersome that it would not be useful to present it here; instead we merely quote their numerical values in the following analysis. It is convenient for the determination of γ_1, γ_2, and γ_3 to invert the relationships in Eq. (47), whereby we obtain

$$\begin{aligned} \gamma_1 &= \tfrac{1}{2}(\omega_+ + \omega_-)(1 - \delta_+), \\ \Gamma &= \tfrac{1}{4}(\omega_+ - \omega_-)(1 - \delta_-), \end{aligned} \tag{48}$$

with

$$\delta_+ = (\Delta_+ + \Delta_-)/2\gamma_1 \quad \text{and} \quad \delta_- = (\Delta_+ - \Delta_-)/4\Gamma\,. \tag{49}$$

Let us now analyze the results for $\vec{H}_0$ along [111], [001], and [110]:

1. $\vec{H}_0 \parallel [111]$

The values of the inverse effective masses

$$\begin{aligned} \omega_+(111) &= 24.120 \pm 0.047, \\ \omega_-(111) &= 2.658 \pm 0.007 \end{aligned} \tag{50}$$

from data in Table VII give the following:

$$\gamma_1 = 13.39 \pm 0.03, \tag{51}$$

$$(\gamma_2^2 + 3\gamma_3^2)^{1/2} = 10.73 \pm 0.03, \tag{52}$$

with the help of Eq. (48) ($\delta_+ = \delta_- = 0$). From the [111] measurements alone we cannot determine γ_2 and γ_3 separately; to do this requires an additional measurement either for [001] or [110] both of which follow.

2. $\vec{H}_0 \parallel [001]$

The analysis of the [001] inverse effective masses (from the data in Table VII)

$$\begin{aligned} \omega_+(001) &= 23.031 \pm 0.080, \\ \omega_-(001) &= 3.584 \pm 0.013 \end{aligned} \tag{53}$$

is straightforward if we first estimate the small corrections $\delta_+ = -0.0072$ and $\delta_- = 0.0124$. Substituting these numbers into Eq. (48), we obtain

$$\gamma_1 = 13.40 \pm 0.05\,, \tag{54}$$

$$\tfrac{1}{2}(7\gamma_2^2 + 3\gamma_3^2 + 6\gamma_2\gamma_3)^{1/2} = 9.60 \pm 0.05\,. \tag{55}$$

3. $\vec{H}_0 \parallel [110]$

From the experimental inverse effective masses (Table VII)

TABLE VIII. Anisotropic components of the inverse effective mass [Eq. (47)] for classical-hole cyclotron resonances.

$\vec{H}_0$	Γ	$\Delta_\pm$
[001]	$\frac{1}{4}(7\gamma_2^2 + 3\gamma_3^2 + 6\gamma_2\gamma_3)^{1/2}$	$\frac{9}{512}\frac{(\gamma_2^2 - \gamma_3^2)^2}{(\pm\Gamma)^3}\left(\frac{4\Gamma^2 + \gamma_2^2}{4\Gamma^2 - \gamma_2^2} \mp \frac{4\Gamma}{\gamma_1 \pm 2\Gamma}\right)$
[111]	$\frac{1}{2}(\gamma_2^2 + 3\gamma_3^2)^{1/2}$	0
[110]	$\frac{1}{16}(31\gamma_2^2 + 111\gamma_3^2 + 114\gamma_2\gamma_3)^{1/2}$	not given

$$\omega_+(110) = 23.861 \pm 0.057,$$
$$\omega_-(110) = 2.717 \pm 0.007, \quad (56)$$

[and the "corrections" $\delta_+(110) = -0.010$, $\delta_-(110) = 0.016$] and using Eq. (48), we obtain

$$\gamma_1 = 13.42 \pm 0.05, \quad (57)$$

$$\tfrac{1}{8}(31\gamma_2^2 + 111\gamma_3^2 + 114\gamma_2\gamma_3)^{1/2} = 10.41 \pm 0.05. \quad (58)$$

As an alternative method one could derive the corrections δ_+ and δ_- by direct numerical integration of the Shockley integral for $k_H = 0$ on a computer using an assumed set of parameters γ_1, γ_2, and γ_3. We have actually tried this and obtain the values $\delta_+(001) = -0.0072$, $\delta_-(001) = +0.0127$, $\delta_+(110) = -0.0105$, and $\delta_-(110) = +0.0141$ from the computer which are in excellent agreement with the perturbation estimates. The direct method is easily extended to practically arbitrary precision.

As the final step, we collect results. First, we determine a mean value for γ_1 from Eqs. (51), (54), and (57),

$$\gamma_1(\text{classical}) = 13.40 \pm 0.03. \quad (59)$$

Second, the simplest way, we find, to determine γ_2 and γ_3 independently is by plotting Eqs. (52), (55), and (58) as shown in Fig. 25. The intersection of the three curves in the figure then fixes the values

$$\gamma_2(\text{classical}) = 4.26 \pm 0.05, \quad (60)$$

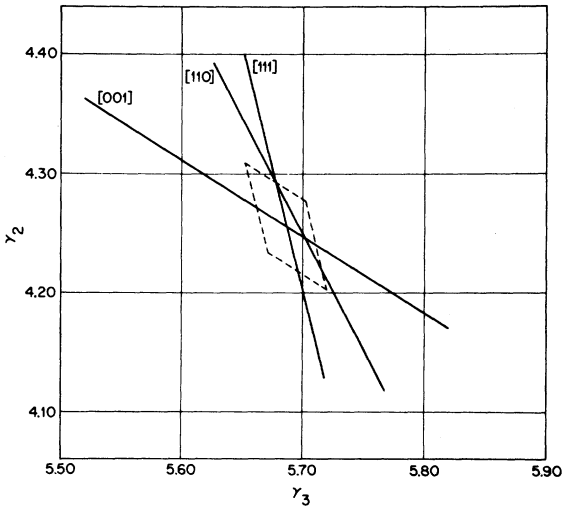

FIG. 25. Classical determination of the effective-mass band parameters γ_2 and γ_3 from the simultaneous solution of Eqs. (52) ($\vec{H}_0 \| [111]$), (55) ($\vec{H}_0 \| [001]$), and (58) ($\vec{H}_0 \| [110]$), The experimental uncertainties for [111] and [001] are indicated by the dashed lines.

$$\gamma_3(\text{classical}) = 5.69 \pm 0.03.$$

Within their error limits the results for [111], [001], and [110] are consistent, as evidenced by, first, the smallness of the deviations of the three independent values of γ_1 from the mean in Eq. (59) and, second, the near coincidence of the intersections of the curves in Fig. 25. We believe, therefore, that systematic errors resulting from k_H and quantum effects in the classical resonances have been reduced to a level less than the uncertainties of measurement.

---

*Present address: Osaka University, Toyonaka, Japan, where part of this work was completed.

[1]J. M. Luttinger and W. Kohn, Phys. Rev. 97, 869 (1955).
[2]J. M. Luttinger, Phys. Rev. 102, 1030 (1956).
[3]R. C. Fletcher, W. A. Yager, and F. R. Merritt, Phys. Rev. 100, 747 (1955).
[4]J. C. Hensel, *Proceedings of the International Conference on the Physics of Semiconductors, Exeter*, 1962 (The Institute of Physics and Physical Society, London, 1962), p. 281.
[5]J. J. Stickler, H. J. Zeiger, and G. S. Heller, Phys. Rev. 127, 1077 (1962).
[6]W. Mercouroff, Phys. Status Solidi 2, 282 (1962).
[7]R. R. Goodman, Phys. Rev. 122, 397 (1961).
[8]V. Evtuhov, Phys. Rev. 125, 1869 (1962); and in Ref. 4, p. 590.
[9]M. Okazaki, J. Phys. Soc. Jap. 17, 1865 (1962).
[10]A brief summary of our spectroscopic studies on the valence bands of Ge has been given earlier: J. C. Hensel and K. Suzuki, *Proceedings of the Tenth International Conference on the Physics of Semiconductors, Cambridge*, 1970, edited by S. P. Keller, J. C. Hensel and F. Stern, CONF-700801 (U. S. AEC Div. of Tech. Information, Springfield, Va., 1970), p. 541.
[11]K. Suzuki and J. C. Hensel, preceding paper, Phys. Rev. B 9, 4184 (1974), hereinafter referred to as Paper I. References herein to equations in Paper I are identified by a "I" preceding the equation number.
[12]J. C. Hensel, Solid State Commun. 4, 231 (1966).
[13](a) E. Otsuka, K. Murase, and H. Fujiyasu, Phys. Lett. 21, 284 (1966); (b) H. Fujiyasu, K. Murase, and E. Otsuka, J. Phys. Soc. Jap. 29, 685 (1970).
[14]J. C. Hensel and K. Suzuki (unpublished), hereinafter referred to as Paper III. A preliminary account of part of this work has been given earlier: J. C. Hensel, Phys. Rev. Lett. 21, 983 (1968); and J. C. Hensel and K. Suzuki, Phys. Rev. Lett. 22, 838 (1969).
[15]J. C. Hensel and K. Suzuki (unpublished), hereinafter referred to as Paper IV. A partial account of this work appears in J. C. Hensel and K. Suzuki, *Proceedings of the Third Materials Research Symposium: Electronic Density of States, Gaithersburg, Maryland*, 1969, edited by L. H. Bennett, Natl. Bur. Stds. Special Publ. No. 323 (U. S. GPO, Washington, D. C., 1971), p. 431. See also Ref. 10.

[16]See, for example, E. O. Kane, *Semiconductors and Semimetals* (Academic, New York, 1966), Vol. 1, p. 75.

[17]G. E. Pikus and G. L. Bir, Fiz. Tverd. Tela 1, 154 (1959) [Sov. Phys.-Solid State 1, 136 (1959)]; Fiz. Tverd. Tela 1, 1642 (1959) [Sov. Phys.-Solid State 1, 1502 (1959)]; Fiz. Tverd. Tela 3, 1001 (1961) [Sov. Phys.-Solid State 3, 730 (1961)].

[18]W. H. Kleiner and L. M. Roth, Phys. Rev. Lett. 2, 334 (1959).

[19]J. C. Hensel and G. Feher, Phys. Rev. 129, 1041 (1963).

[20]J. C. Hensel and K. Suzuki, Bull. Am. Phys. Soc. 14, 113 (1969); K. Suzuki and J. C. Hensel, 14, 113 (1969).

[21]J. C. Hensel (unpublished results).

[22]T. R. Loree, M. H. Halloran, and R. N. Dexter, Bull. Am. Phys. Soc. 6, 426 (1961).

[23]H. Hasegawa, Phys. Rev. 129, 1029 (1963).

[24]B. W. Levinger and D. R. Frankl, J. Phys. Chem. Solids 20, 281 (1961).

[25]Reference 5. See also G. S. Heller, J. J. Stickler, and H. J. Zeiger, *Proceedings of the XIth Colloque Ampere, Eindhoven*, 1962 (North-Holland, Amsterdam, 1963), p. 521.

[26]The phenomenon of k_H broadening may be visualized from an elementary standpoint by considering the following simple example. Suppose that a cyclotron resonance transition $n \rightarrow n'$ takes place between a pair of Landau states, labeled n and n', whose energy dependence on k_H obeys a parabolic law $A_n \hbar^2 k_H^2$, but such that $A_n \neq A_{n'}$. For this case the transition energy is a function of k_H, and we obtain a skewed cyclotron resonance peak having the form

$$\mathcal{L}(\omega,\ \omega_0) - \Omega\tau \frac{d}{d(\omega\tau)} \mathcal{L}(\omega,\ \omega_0),$$

where $\mathcal{L}(\omega,\ \omega_0)$ is the usual Lorentzian function whose center frequency is ω_0 and whose width is defined by the inverse relaxation time τ^{-1}. The expansion parameter $\Omega\tau$ contains a "frequency" Ω defined by

$$\Omega = (k \mathfrak{S}/\hbar)\,[(A_n' - A_n)/A_n]\ .$$

The second or "dispersive" term in the above line-shape expression puts an asymmetric tail on the otherwise symmetric function $\mathcal{L}(\omega,\ \omega_0)$, and the side of the line on which the tail falls is governed by the sign of Ω, i.e., whether A_n is greater or less than A_n'. The foregoing expansion is valid for $\Omega\tau \ll 1$, in other words, when the k_H broadening is much less than the Lorentzian width. These considerations as well as the case $\Omega\tau \gg 1$ will be discussed in a later paper, J. C. Hensel (unpublished).

[27]H. J. G. Meyer, Phys. Lett. 2, 259 (1962). Also see J. C. Hensel, Phys. Lett. 4, 38 (1963); and R. Ito, M. Fukai and I. Imai, J. Phys. Soc. Jap. Suppl. 21, 357 (1966).

[28]The parameters γ_1, γ_2, and γ_3 are related to the set A, B, and N of Dresselhaus, Kip, and Kittel (Ref. 54) as follows: $\gamma_1 = -A$, $\gamma_2 = -\frac{1}{2}B$, and $\gamma_3 = -\frac{1}{6}N$.

[29]The possibility that anomalies in the Landau levels can arise from k_H effects was first pointed out by R. F. Wallis and H. J. Bowlden, Phys. Rev. 118, 456 (1960). See also Refs. 8 and 9.

[30]See Appendix A of Paper I.

[31]Strictly speaking, the anisotropic q term in Eq. (1) is also a type of warping, although it is small and seldom of consequence. Henceforth, by "warping" we shall mean only the kind due to $\gamma_2 \neq \gamma_3$.

[32]More precisely the dimensions of the secular matrices were [001], 4 times 20×20; [111], 3 times 23×23; [110], 2 times 40×40.

[33]This identification by n is only strictly accurate for the "parent" states, the eigenstates of the axial Hamiltonian. However, in passing to the actual case in Ge only two states, 3_0 and 3_2, become sufficiently mixed so that the correspondence is lost.

[34]This selection rule subsumes the set ($\vec{\mathcal{E}}_1 \perp \vec{H}_0$) given by H. Kamimura, Phys. Rev. 129, 614 (1963).

[35]Reference 18. The Kleiner-Roth notation is related to Pikus and Bir's by $D_d = +a$, $D_u = -\frac{3}{2}b$, and $D_u' = -\frac{1}{2}\sqrt{3}d$. (See Ref. 26 of Paper I.)

[36]This property would presumably break down if the "warping" were to mix the zero stress eigenstates to a substantially greater degree.

[37]For full details, see Sec. VI of Paper I.

[38]The strain shifts for the quantum transitions are calculated in Paper I by projecting the strain decoupled ($T \rightarrow \infty$) $M_J = \pm\frac{1}{2}$ substates from the full Γ_8^+ Hamiltonian. It should be pointed out that these results are valid at *finite* stress for the fundamental transitions connecting the "pure" $M_J = -\frac{1}{2}$ states (0, $-\frac{1}{2}$) and (1, $-\frac{1}{2}$).

[39]This apparatus is a scaled-down and refined model patterned after the X band "parallel squeezer" used in earlier work. See Ref. 19. For further details see D. K. Wilson and G. Feher, Phys. Rev. 124, 1068 (1961).

[40]Our earlier calibration, Ref. 12, determined only from the calculations of the mechanical advantage of the apparatus, was incorrect (~30% too low) owing to a trivial error in misreading one of the mechanical dimensions.

[41]H. J. McSkimin, J. Appl. Phys. 24, 988 (1953).

[42]See S. H. Koenig, J. Phys. Chem. Solids 8, 227 (1958). We are grateful to Dr. Koenig for supplying us with a portion of crystal *nWLP*-33.

[43]The observation of this resonance has been reported earlier (Ref. 12) but no definite assignment was proposed.

[44]Offhand, it might seem that this argument is begging the question, if we admit the possibility of γ_2 and/or γ_3 being negative. For cyclotron resonance under large uniaxial stress, this would lead to the kind of sign ambiguity in the deformation potentials discussed in Ref. 19 which can only be resolved by considering interactions with states external to the $J = \frac{3}{2}$ manifold. However, the *quantum* spectra near and at zero stress uniquely fix the signs of γ_2 and γ_3 as *positive*. See Sec. IV D (1 *b*).

[45]Superficially, the present procedure bears considerable resemblance to that used earlier in Ref. 19 to analyze the classical-hole resonances in uniaxially stressed Si. The important difference here is that the shift $\delta(T)$, first, is small and, second, can be rather accurately calculated; whereas, in Ref. 19 it was large and could only be estimated empirically on the assumption that it obeyed a stress dependence γ/T.

[46]As further evidence of the generality of this statement, we offer a simple proof that the properties of the $M_J = -\frac{3}{2}$ fundamental transition—namely, its being stress invariant and coincident with the $M_J = \pm\frac{3}{2}$ series limit—hold *rigorously* independent of warping for $\kappa = 0$, near which the validity of Eq. (33) might be questioned. We consider the 3×3 matrix Hamiltonian ($k_H = 0$, $n = 0$, 1)

for $\vec{H}_0$, $T \parallel [111]$ which has the form [see Eq. (62) of Ref. 2]

$$M_J = \begin{array}{c} \begin{matrix} +\frac{3}{2} & -\frac{1}{2} & -\frac{3}{2} \end{matrix} \\ \begin{pmatrix} A+x'_u & U & -q/\sqrt{2} \\ U & B-x'_u & V \\ -q/\sqrt{2} & V & C+x'_u \end{pmatrix} \end{array} .$$

If we set $\kappa = 0$ (and $q = 0$), then $A = C$ (the $\pm\frac{3}{2}$ basis states become degenerate); and we find now that the secular equation factors exactly yielding a trivial eigenvalue

$$\epsilon(n) = A + x'_u = (\gamma_1 + \gamma_3)(n + \tfrac{1}{2}) + x'_u, \quad n = 0, 1,$$

which depends linearly on stress. The transition $n = 0 \rightarrow 1$ is, therefore, stress invariant and lies at $m^*/m = (\gamma_1 + \gamma_3)^{-1}$, the $\pm\frac{3}{2}$ series limit. This argument is not essentially altered if we permit κ to become finite (but small); for then it merely contributes a constant term $-\frac{3}{2}\kappa$ to $\epsilon(n)$ (if the warping is small, i.e., $V^2 \ll U^2$).

[47]Measured at 4°K by M. V. Hobden, J. Phys. Chem. Solids 23, 821 (1962). R. L. Aggarwal [Phys. Rev. B 2, 446 (1970)] obtained the value $\Lambda = 0.296 \pm 0.002$ eV at ~30°K.

[48]For $T \parallel [110]$ the connection between α and α_1, α_2, and α_3 has been worked out in Appendix D of Ref. 19. We take this opportunity to correct an error in Eq. (D8) of this reference. In all three formulas comprising Eq. (D8), $\cos^2\varphi$ and $\sin^2\varphi$ should be interchanged. Expressions relating α_1, α_2, and α_3 to the deformation potentials are given in Eq. (I. 144).

[49]In ascribing the anomalous effective-mass shift to spin-dependent deformation potentials, we must not overlook the possibility of other strain effects which could perturb the cyclotron resonance line position, an obvious one being the change of the effective-mass parameters γ_1, γ_2, and γ_3 themselves, due to energy shifts in the conduction states under applied uniaxial stress. We expect the most significant contribution of this kind to come from the nearest state Γ_2^- at $E_0 \sim 0.9$ eV. We estimate that the *increase* of the direct gap E_0 with stress contributes $\sim +0.1$ eV to the values measured for D_w and D'_w. This shift is of the *opposite* sign and much smaller than that from the spin-dependent components E_2 and E_3. (See Sec. VII of Paper I.) The results given in Eqs. (39) and (40) are uncorrected for these "interband" shifts.

[50]Refer to Eqs. (I.32) and (I.129).

[51]See Sec. V B of Paper I.

[52]See also Eq. (I.155) and succeeding discussion in Paper I.

[53]For example, see F. Herman, R. L. Kortum, C. D. Kuglin, and R. A. Short, *Quantum Theory of Atoms, Molecules, and the Solid State* (Academic, New York, 1966), p. 381.

[54]G. Dresselhaus, A. F. Kip, and C. Kittel, Phys. Rev. 98, 368 (1955).

[55]R. N. Dexter, H. J. Zeiger, and B. Lax, Phys. Rev. 104, 637 (1956).

[56]That strain can affect the spin-orbit interaction seems to have been pointed out first by Pikus and Bir, Ref. 17. The existence of these strain-dependent spin terms was also recognized by H. Hasegawa, Ref. 23.

[57]One exception is the nonlinearity which appears in the strain-splitting of the $J = \frac{3}{2}$ band at large stresses, from which, in principle, one would deduce the strain matrix elements connecting $J = \frac{3}{2}$ and $J = \frac{1}{2}$ and, hence, D_w and D'_w. [Reference 67. Also M. Cardona (private communication)].

[58]J. J. Hall, Phys. Rev. 128, 68 (1962).

[59]A. M. Glass, Can. J. Phys. 43, 12 (1965).

[60]I. Balslev, Phys. Rev. 143, 636 (1966); and Phys. Lett. A 24, 113 (1967).

[61]I. Balslev, Solid State Commun. 5, 315 (1967).

[62]F. H. Pollak and M. Cardona, Phys. Rev. 172, 816 (1968).

[63]L. R. Saravia and D. Brust, Phys. Rev. 178, 1240 (1969).

[64]P. J. Melz, J. Phys. Chem. Solids 32, 209 (1971).

[65]P. Lawaetz (unpublished work).

[66]J. C. Hensel (unpublished). These values of D_w and D'_w measured from quantum resonances in Si differ only slightly from our earlier ones quoted in Ref. 19.

[67]Measurements by L. Laude, F. H. Pollak, and M. Cardona, Phys. Rev. B 3, 2623 (1970) confirm that E_2 and E_3 are quite small in Si.

[68]L. Kleinman, Phys. Rev. 128, 2614 (1962).

[69]D. Brust and L. Liu, Solid State Commun. 4, 193 (1966).

[70]F. Cerdeira, J. S. DeWitt, U. Rössler, and M. Cardona, Phys. Status Solidi 41, 735 (1970).

[71]P. J. Melz and I. B. Ortenburger, Phys. Rev. B 3, 3257 (1971).

[72]G. G. Wepfer, T. C. Collins, and R. N. Euwema, Phys. Rev. B 4, 1296 (1971).

[73]See Refs. 3 and 24. In both references the value quoted, $\omega\tau = 50$, was taken directly from the linewidth of the light-hole resonance. A computer synthesis of the line shape to match this linewidth (see Appendix), however, requires a larger value, $\omega\tau \approx 70$, for the *component* Lorentzian lines.

[74]The interpretation of the temperature dependence of τ for holes in Ge is further complicated by the fact that for $\Theta < 2.5$°K the holes are not in thermal equilibrium with the lattice. Thus, even if the scattering process were classical, the usual $\frac{3}{2}$ power law would not strictly apply. Instead, if equipartition holds, the appropriate relation might be $\tau \propto \Theta\epsilon^{1/2}$, where ϵ is the hole energy.

[75]H. Fujiyasu, K. Murase, and E. Otsuka, Phys. Lett. A 27, 597 (1968). Also see Ref. 13(b).

[76]Carrier heating effects are probably responsible for the anomalous line broadening which frustrated our earlier attempts (Ref. 21) to measure the valence-band inverse-mass parameters under classical conditions (1.2°K and 9 GHz) in uniaxially stressed Ge. The classical-hole linewidths at finite stress depend upon the Hasegawa line-broadening process (Ref. 23), an inhomogeneous broadening arising from band non-parabolicity (k^4 terms), which is dependent upon the effective *hole* temperature Θ^*. Classical experiments can be particularly susceptible to carrier heating because the scattering times are long. In silicon, by comparison, the holes are able to thermalize rather effectively (see Ref. 19) essentially because trapping into the more tightly bound Si acceptor states in slower.

[77]M. Lax, Phys. Rev. 119, 1502 (1960).

[78]The strong dependence on Θ comes from the trapping cross section $\sigma \propto \Theta^{-7/2}$ [see M. Lax, J. Phys. Chem. Solids 8, 52 (1959)]. From σ we obtain $\tau_t = (\sigma\bar{v}N_A)^{-1}$, where $\bar{v}$ is the rms hole velocity which depends weakly on temperature as $\Theta^{1/2}$. Hence, $\tau_t \propto \Theta^3$.

[79]See Ref. 78. The value of σ at ~2°K was extrapolated from the experimental results (3–7°K) of S. Koenig, R.

D. Brown, and W. Schillinger, Phys. Rev. 128, 1668 (1962). We assume for the purposes of this rough estimate that the trapping cross section for holes in Ge is the same as that for electrons.
[80]Suggested by P. J. Dean (private communication).
[81]G. Feher, Bell System Tech. J. 26, 449 (1957).
[82]D. M. S. Bagguley and R. A. Stradling, Proc. Phys. Soc. Lond. 78, 1078 (1961).
[83]This is undoubtedly the "extra" [111] resonance which appears in the 4.2 °K data of R. C. Fletcher *et al.*, Ref. 3.
[84]W. Shockley, Phys. Rev. 79, 191 (1950). Also see Ref. 54.